Tesis Doctoral

Manipulación diestra en ambientes desconocidos : un modelo bio-inspirado

Matuk Herrera, Rosana Isabel

2008

UNIVERSIDAD DE BUENOS AIRES
Facultad de Ciencias Exactas y Naturales
Departamento de Computación

MANIPULACION DIESTRA EN AMBIENTES DESCONOCIDOS

UN MODELO BIO-INSPIRADO

Tesis presentada para optar al título de Doctor de la Universidad de Buenos Aires en el área Ciencias de la Computación

Rosana Isabel Matuk Herrera

Director de tesis: Prof. Enrique Carlos Segura
Consejero de estudios: Prof. Juan Miguel Santos

Buenos Aires, 2008

Manipulación Diestra en Ambientes Desconocidos
Un Modelo Bio-inspirado

En la actualidad, la manipulación robótica diestra y autónoma en ambientes desconocidos aún nos eluye. Niños de pocos años pueden levantar y manipular objetos no familiares con mayor destreza que los robots actuales. En consecuencia, los investigadores en robótica coinciden cada vez más que ideas de la biología pueden resultar beneficiosas en el diseño de mejores modelos para los robots.

En este trabajo de tesis se presentan un modelo de control y algoritmos para cada una de las fases de manipulación, que están fuertemente inspirados en estudios neurofisiológicos sobre manipulación diestra humana. El control de las fuerzas de presa y carga en cada fase es dirigido por señales que simulan las respuestas aferentes humanas durante un proceso de manipulación. El objetivo del modelo es manipular objetos desconocidos con estabilidad de la presa y comportamiento similar al humano.

Se utilizaron elementos finitos para simular computacionalmente dos dedos opuestos que toman objetos desconocidos, y un dedo presionando objetos. Los dos componentes esenciales del modelo de control propuesto fueron simulados y testeados exitosamente: la estimación del coeficiente de fricción entre el objeto y los dedos, y la detección del deslizamiento incipiente.

Palabras Claves: Manipulación Diestra, Redes Neuronales, Robótica en Ambientes Desconocidos, Modelos Bio-inspirados, Estimación de la Fricción, Detección del Deslizamiento Incipiente

Dexterous Manipulation in Unknown Environments
A Bio-inspired Model

At present, autonomous, robotic dexterous manipulation in unknown environments still eludes us. Few years old children lift and manipulate unfamiliar objects more dexterously than today's robots. Thus, robotics researchers increasingly agree that ideas from biology can strongly benefit the design of autonomous robots.

Inspired by neurophysiological studies about human dexterous manipulation, a control model and algorithms for each one of the manipulation phases are presented. The control of the grip and load forces at each phase is driven by signals that simulate the human afferent responses during a manipulation. The control model goal is to manipulate unfamiliar objects with grasp stability and human-like behavior.

Finite element analysis was used to simulate computationally two opposed fingers taking unknown objects, and a finger pressing objects. The two crucial components of the control model were simulated and tested successfully: the estimation of the coefficient of friction between the object and the fingers, and the detection of the incipient slipping.

Keywords: Dexterous Manipulation, Neural Networks, Robotics in Unknown Environments, Bio-inspired Models, Friction Estimation, Incipient Slipping Detection

Acknowledgments

First of all, it is my pleasure to thank my supervisor Enrique Carlos Segura, without whom this thesis would not exist.

I also want to thank my advisor Juan Miguel Santos, for his excellent predisposition to help me along these years of doctoral studies.

A special thank is for Anna Theorin (f. Israelsson), Lars Rådman, Benoni Edin and Roland Johansson, for kindly providing the software code of their afferent simulator program.

I wish to thank Fabio Leoni, for some initial discussions about this work.

I would like to express my deep gratitude to the Departamento de Computación, Facultad de Ciencias Exactas y Naturales, Universidad de Buenos Aires, for the support I had in developing my thesis. I would also like to acknowledge the Dipartimento di Informatica, Università di Pisa, and the Scuola Superiore Sant'Anna, Pisa, for hosting me during my research stay in Italy.

A huge thank is for Isabel Méndez Díaz and Irene Loiseau for their encouragement, and for asking me so many times when I would finish the thesis.

I would like to thank the referees of the thesis, Ezequiel Di Paolo, Roberto Perazzo and Silvano Zanutto for having devoted part of their time to help me improve the work.

I wish to thank Fernando Alvarez and Guillermo Alfaro, for their helpful technical support.

I also want to thank my roommates Clara, Martín, Luciano, and Rodrigo for being cheerful, and for being always creating a very funny atmosphere at the office.

An international thank is for my italian friend Eleonora, for so many e-mails with "in bocca al lupo" for the thesis.

I wish to thank my colleagues and friends Marta Mejail, Daniel Acevedo, Rocío Romero Zaliz, Aída Interlandi, Julio Jacobo Berlles, Leticia Seijas, María Elena Buemi, Paula Zabala, Silvana Picchi, Mercedes Sánchez,

Alessandro Urpi, Paulina Abre, Mariana Coppolecchia, for their friendship and their words of encouragement.

Last, but absolutely not least, I thank my family for their continuous support.

To my parents

Ἀναξαγόρας μεν οῦν φησι δια το χειρας εχειν φρονιμωτατον ειναι τον ζωων ανθροπον : ευλογον δε δια το φρονιμωτατον ειναι χειρας λαμβανειν [1]

ARISTOTLE, *De partibus animalium*

[1] "Anaxagoras says that because of having hands, man grew the most intelligent among animals. [I think] it is correct to say that because of his intelligence he has hands" (as cited by Bicchi (2000)).

CONTENTS

CHAPTER 1

INTRODUCTION

Within a year of birth, a human infant is clearly more dexterous than today's robots. Robotics researchers increasingly agree that ideas from biology can strongly benefit the design of autonomous robots. Biological organisms have evolved to perform and survive in a world characterized by rapid changes, high uncertainty, indefinite richness, and limited availability of information. Industrial robots, in contrast, operate in highly controlled environments with no or very little uncertainty. Although many challenges remain, concepts from biologically inspired (bio-inspired) robotics will eventually enable researchers to engineer machines for the real world that possess at least some of the desirable properties of biological organisms, such as adaptivity, robustness, versatility, and agility (Pfeifer et al., 2007).

1.1 Motivation

Although industrial robots have been used for years to manipulate objects in highly constrained domains, the problem of manipulating unknown objects in a realistic environment is still largely unsolved. Industrial robots can achieve their task robustly because they exist in a rigidly controlled environment. In unknown environments, humans manipulate objects more dexterously than today's robots. The control system of the human hand created by nature is the product of uncountable genetic mutations and natural selection processes happened in thousands of years. Therefore, the encounter between roboticists and neurophysiologists may give fruitful results to both communities. Neurophysiological researchers can prove

hypothesis of models of human behavior in robots. Robotics researchers can take inspiration on neurophysiological studies to improve the design of robots and control systems.

1.2 Objectives

The aim of this thesis is to take inspiration in neurophysiological studies about the human dexterous manipulation, to design a computational control system for the dexterous manipulation in unknown environments. Thus, the control of the grip and load forces at each phase must be driven by signals that simulate the responses of the human tactile afferent. Typically, when robots manipulate objects, they must do so with a predetermined grasp force. By contrast, humans are skilled at manipulating objects with grasp forces maintained only slightly above the minimum required to prevent slipping. The term grasp stability entails both the prevention of accidental slips and the prevention of excessive fingertip forces. The control model goal is to manipulate unfamiliar objects with grasp stability and human-like behavior. To achieve this goal, a control model and algorithms, emulating each one of the human manipulation phases need to be designed.

The friction estimation and the incipient slip detection occupy a central place in the human dexterous manipulation. To maintain grasp stability, the normal:tangential force ratio must exceed a critical value, called the slip ratio, which corresponds to the inverse coefficient of friction between the object and the hand. Human tactile afferents provide the central nervous system with signals related to the frictional conditions already at the initial touch. The initial adjustment to the new friction often is insufficient and further "secondary" adjustments will occur later in the lift. Responses originated from small slips localized to only a part of the skin area in contact with the object and in the absence of detectable vibrations events, are often followed by small force ratio changes (Westling and Johansson, 1987). Such incipient slips, also trigger appropriate grip force adjustments for grasp stability when an object is held in the air. Thus, a particular emphasis has been put in this thesis, on the initial friction estimation and the incipient slip detection.

1.3 Context

In the 1970s, tactile sensing for robotic applications emerged as its own field of research. Research kept increasing during the next decade, and in controlled environments there has been great progress. Lee in 2000 (Lee, 2000) pointed out that in structured environments, we are able to come very far without tactile information. Hence, he foresees that tactile sensing will be most useful in unstructured environments where object properties and/or the environment is not fully known (Tegin and Wikander, 2005).

The human tactile system has not been so extensively studied as the human visual and auditive systems. Further neurophysiological research is needed to reveal more deeply how tactile sensors in the fingertips encode direction of fingertip forces, the shape of surfaces contacted by the fingertips, the friction coefficient, the slips during manipulation, the torque load. The model proposed in this work is strongly based on neurophysiological studies of the human dexterous manipulation. A main contribution of this work, is that the proposed model summarizes these neurophysiological studies from a computer science and algorithmic perspective.

As humans grasp and lift objects, they make use of dynamic receptors in the skin that respond to small, localized slips that are precursors to gross sliding of the object (Johansson and Westling, 1990). These dynamic tactile sensors enable them to gain a better estimate of the friction conditions at the contacts. It is therefore desirable to provide robots with a counterpart to the human ability to obtain continuous and accurate updates of the friction coefficient. Although it is evident that humans benefit from the ability to continually adjust their grasp forces based on incipient slip sensing, comparatively little has been done to provide such capabilities for robots.

Simulations were used to validate the proposed model. The finite-element model used in the simulations are a 3-D extension of the plane (2-D) finger model of Maeno et al. (Maeno et al., 2004). However, instead of estimating the friction coefficient based on the shear strain as in Maeno's work, it is estimated based on simulated human afferent signals. Israelsson Israelsson (2002) designed a computational simulator of the responses of the afferents from the glabrous skin during human manipulation. Thus, to simulate the afferent responses, software code provided by Anna Theorin (f. Israelsson), Lars Rådman, Benoni Edin and Roland Johansson of Umeå University was adapted.

1.4 Impact

For a versatile robot in an uncertain environment, tactile sensing will open up new possibilities. Recently we have seen some impressive humanoids, but if they cannot be made to interact with their surrounding, they will be of little use. Combining these humanoids with advanced grasping and manipulation capabilities, has for long been a dream that opens up possibilities limited only by imagination. Such robots could be used pretty much anywhere in which it can be cumbersome or dangerous to use humans (Tegin and Wikander, 2005). Also, the computational modeling of the dexterous manipulation process, could give new insights on the understanding of the human manipulation process, and could help to design better prothesis for handicapped people.

1.5 Thesis organization

This thesis is organized as it follows:

Chapter 2 surveys some neurophysiological studies about the human dexterous manipulation.

Chapter 3 explores the state of the art about the simulation of the human afferent signals, the friction coefficient and incipient slip detection, and the slip correction.

Chapter 4 presents the control model. It presents the general design of the control model and algorithms for each one of the manipulation phases.

Chapter 5 shows simulated experiments using the finite element method. The two crucial components of the control model were simulated and tested successfully: the estimation of the friction coefficient and the detection of the incipient slipping.

Chapter 6 draws the conclusions.

CHAPTER 2
HUMAN DEXTEROUS MANIPULATION

Human dexterous manipulation is the product of the human sensory, mechanical, and control systems. There are about 17000 mechanoreceptors in each hand. The regulation of the grip and load forces is driven by the responses of these mechanoreceptors. In this chapter, we present a survey of the neurophysiological studies about human dexterous manipulation.

2.1 Precision grip

When reaching for an object, the selected pattern of grasp is determined not only by the shape and the size of the object but also by the intended activity (Jeannerod, 1997). For example, a rod can be held with a *precision grip*, if the desired action is to write; or a *power grip*, if it is going to be used as a tool. In every day activities, precision grip is more frequently used as it offers the possibility of fine manipulative actions, i.e. movement of the object relative to the fingers within the hand (Elliott and Junge, 1984). In this grasp configuration the thumb is abducted and rotated so that its pulpar surface is diametrically opposed to the pulpar surface of the other fingers.

2.2 Grasp stability

Lifting small objects with the fingers is something we do daily without much mental effort. Still it is difficult to program a robot to do the same thing (Cutkosky, 1985; Murray et al., 1994; Spong et al., 1993).

The difficulty arises from the mechanical demands of the task (Fagergren, 2003). Though the vertical force (load force) required to lift an object is completely determined by the weight of the object, the grip force is more tricky since it depends on the force of friction (Johansson and Westling, 1984c) as well as the shape (Jenmalm and Johansson, 1997) of the finger-object contact area. Grasp stability, i.e., the prevention of accidental slips as well as of excessive fingertip forces, requires tuned grip force. In order to avoid a slip between the fingers and the object, the grip force (GF) has to be greater than the slip limit, i.e., the load force (LF) divided by the coefficient of friction (μ): GF $\geq$ LF/μ. Ideally, the grip force could be tuned in parallel with the load force, so whatever the load force is, the grip force changes accordingly. But even a small external perturbation to the load could then cause a slip. Therefore, the grasp stability would increase if the grip force had a small force offset (F_o), thus creating a safety margin to the slip limit: GF $\geq$ F_o + LF/μ. This grasp stability strategy is similar to what human grip experiments reveal (Johansson and Westling, 1984a,c).

The friction coefficient determines the ratio between the grip and the lift force required to prevent slips. Unfortunately, the friction is a difficult parameter to estimate since it depends on several factors, such as the amount of sweat from the fingertips and the relative motion between the fingertips and the contact area, and therefore changes over time. Hence, the ability to adequately tune the grip force relies on the tactile information from local micro-slips creeps at the periphery of the finger-object contact area (Smith, 1993). These micro-slips are a precursor to the unwanted gross slip, and make it possible to sense the slip limit before it is reached. This sensory mechanism is an important key to the efficient grasp stability in humans, and has so far no counterpart in robotics (Fagergren, 2003).

Many manipulatory tasks require application of torques tangential to the grasp surfaces. Tangential torques typically develop when we tilt or otherwise rotate grasped objects whose center of mass does not lie on the grip axis, e.g., the axis between the centers of the grip surfaces of the tips of the thumb and a finger during a precision grip. These destabilizing torques tend to rotate the object around the grip axis and may thus cause rotational slips. The grip forces required to prevent rotational slips approximately increase linearly with the torque load with a slope that depends on the friction of the grasp (Kinoshita et al., 1997). Furthermore, the minimum grip forces required to prevent slips depend strongly on the curvatures of the grasped surfaces (Goodwin et al., 1998).

Thus, to manipulate an object with grasp stability, human subjects tune

the fingertip forces and torques to the requirements imposed by the objects' shape, friction coefficient, weight and distribution of mass (Goodwin et al., 1998; Jenmalm and Johansson, 1997; Johansson and Westling, 1984a,c, 1988a; Johansson et al., 1999).

2.3 Receptors in the glabrous skin of the human hand

The human tactile system is dependent of several kinds of somatosensory receptors. To drastically simplify, all of the human specialized sensory receptors forms three groups based on their different functions: (1) nociceptors, (2) thermoreceptors and (3) mechanoreceptors. The nociceptors are specific for potential tissue damaging stimuli, thermoreceptors for temperature and mechanoreceptors are specifically tuned to mechanical stimuli. These three groups differ not only in their morphology but also, and more importantly, in their sensitivity to different kinds of physical stimuli (Purves et al., 1997).

The most common type of afferent in the glabrous skin of the human hand is the FA I type (43% of the tactile sensors), followed by the SA I (25%), the SA II (19%) and the FA II (13%) types (Johansson and Vallbo, 1979). All together, there are approximately 17,000 mechanoreceptors in the glabrous skin of each hand. The type II afferents are uniformly distributed from the wrist to the tips of the fingers, except regions close to the nails, which are densely innervated by SA II afferents. The type I afferents show pronounced distribution gradient and are most frequent on the tips of the fingers.

The mechanoreceptors have low thresholds to mechanical stimuli, their afferents (i.e., nerve axons who send signals to the central nervous system) have high conduction velocities. The SA I and SA II units are referred to as *slowly adapting afferents*, which means that they show a sustained discharge in the presence of ongoing stimuli (see Fig. 2.1). In contrast, the *fast adapting afferents* (FA I and FA II) fire rapidly when a stimulus is presented (or removed) and then fall silent when the stimulation cease to change (Johansson, 1978). FA units thus primarily signal the change in a skin deformation whereas SA units in addition respond to the amplitude of the deformation. Each type of afferent is associated with a particular type of corpuscular ending that can be identified by their microanatomy.

The *Meissner corpuscle* (FA I units) is located at the interface between the

epidermis and the dermis, directly at the top of the epidermal ridges (Johansson, 1996a; Johnson, 2001). This receptor is the most common of the mechanoreceptors in the human hand with about 150 receptors per cm^2 at the fingertip. Located at the same ridges lie the *Merkel's disks* (SA I units), which also are particularly dense in the fingertip, with about 100 receptors per cm^2. Deep down in the dermis, but also in ligaments and tendons, there is a third kind of mechanoreceptor, the *Ruffini* ending (SA II units). The last receptor type, the *Pacinian corpuscle* (FA II units), is located furthest down; deep in the subcutaneous fat tissue and is the least frequently found receptor in the human hand.

The skin area where responses can be evoked from a receptor is called its *receptive field* (RF). The RFs of FA I and SA I units typically have sharply delineated borders and show several small zones of maximal sensitivity (Johansson, 1978, 1996a; Johnson, 2001). In contrast, the SA II and FA II have large RFs but only one zone of maximal sensitivity and a gentle increase of threshold further and further away from this zone (Israelsson, 2002).

The differences in RF properties between type I and type II units can partly be explained by the location of their receptors within the skin: type I units are close to the skin surface whereas type II units are found deeper in the skin (Johansson, 1978, 1996a; Johnson, 2001). Moreover, whereas each type II afferents innervates a single corpuscular ending, type I afferents divide in several branches to innervate several corpuscles (Israelsson, 2002).

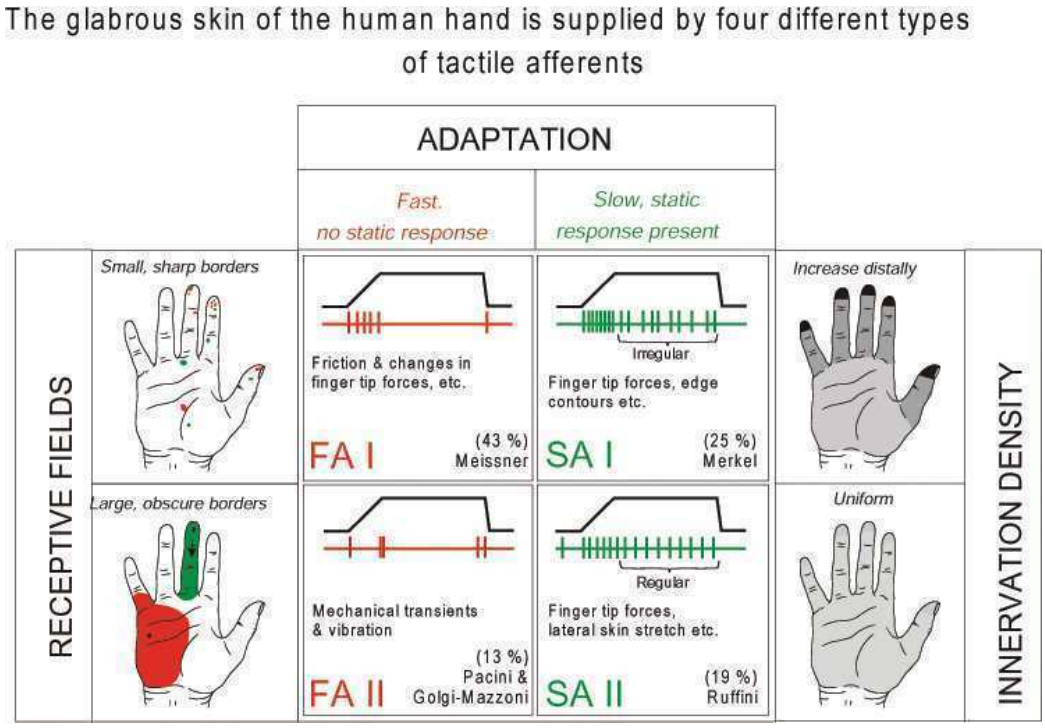

FIG. 2.1: Tactile afferents in the human glabrous skin. FA I and SA I show RFs with small sharp borders whereas the RFs of FA II and SA II show large obscure borders. SA afferents adapt slowly to mechanical stimuli whereas FA adapts fast (Johansson, 1996a).

The FA I units' zones of maximal sensitivity are located within a circle or an oval covering five to ten papillary ridges (Johansson, 1978, 1996a; Johnson, 2001). Their axons terminate at sites that are highly correlated to the maximum sensitivity zones. FA I units have the smallest RFs, about 3-5 mm^2. Since FA I units respond uniformly across the RF they cannot show a good spatial resolution, i.e., their branches contribute equally to each stimulus and there is no branch that dominate (Israelsson, 2002).

The SA I contains fewer highly sensitive zones than the FA I unit. Their axons branch over an area of about 5 mm^2 and innervate a large but unknown number of Merkel cells (>100). When a smaller area than the RF becomes activated by some spatial detail, the branch that terminates within that area becomes dominant (Johansson, 1978). Since these areas overlap, a population of SA I units have high spatial resolution. Accordingly, humans can discriminate details of 0.5 mm (Israelsson, 2002).

FA II units have the largest RFs of the four units. Their RFs may include the whole hand and their threshold becomes lower when the vibrations are parallel to the skin surface. The FA II unit is a perfect illustration of the importance of the microanatomy of the mechanoreceptors. The lamellae of the onion shaped FA II structure have the effect of a band-pass filter, which explains their high sensitivity to specific frequencies (Israelsson, 2002; Johnson, 2001).

The response properties of SA II units are also well correlated with their microanatomy. They can be divided into three groups (Johansson, 1978; Johnson, 2001): those that are found in the palm increase their discharge rate in response to stretches along a preferred axis, which is determined by the location of the cell. A second group responds in one direction of stretch only and is mostly found in the phalanges. Units of the third type are located close to nails and show the highest discharge rates when pressure is applied to the free edge of the nail (Israelsson, 2002).

2.4 Phases of a manipulation task

All humans lift objects in a similar manner. They transport and shape their hand to achieve the best possible structure and the appropriate closure of the fingers around an object. This first step is largely determined by the initial view of the object and its properties before the movement onset. In contrast, visual signals have less importance during the subsequent phases of object manipulation (Johansson, 1996a). Once the finger-

tips have reached the object, an episode of lifting and lowering an object from and to a table top involves (Johansson, 1996b; Johansson and Westling, 1984c, 1987; Wing, 1996):

1. *Preload phase:* using the fingers to apply force perpendicular to the object's surface at the points of contact of the fingers with the object. At this phase the grip force is increased but not the load force. This period lasts 80 ± 40 ms.

2. *Load phase:* is characterized by a parallel increase in the grip and load forces.

3. *Transitional phase:* it begins when the load force has overcome the weight of the object and therefore the object starts to move. This phase ends when the object arrives into the desired vertical position. In this period, grip force reaches its maximum value during a transient overshoot of its steady state.

4. *Static (hold) phase:* where the object is held in the air by fairly constant grip and load forces.

5. *Controlled lowering phase:* by reducing load forces below the value needed to counteract gravity. This reduction of load force allows the object's position to slowly approach the tabletop.

6. *Release phase*: after the contact with the table there is a short delay before a rapid parallel decrease of grip and load forces due to the release of the object.

As seen in fig. 2.2, short-lasting, specific patterns of sensory activity seem to trigger the transition between the different phases of a task (Johansson, 1996a; Johansson and Edin, 1992).

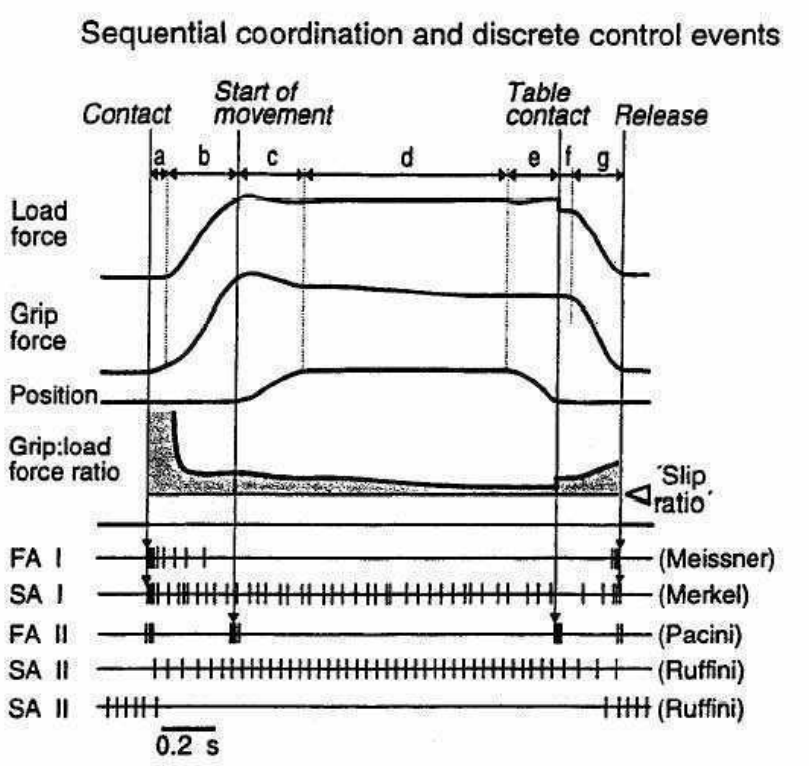

FIG. 2.2: Schematic illustration of the lifting task. After contact with the object the grip force increases by a short period while the grip is established (a–preload phase) before the command is released for a parallel increase in grip and load force during isometric conditions (b–load phase). This parallel increase continues until the start of movement when the load force overcomes the force of gravity. The object is lifted to the intended position (c) by wrist and/or elbow flexion, and a static (-hold-) phase is reached (d). After the replacement of the object (e) and table contact occurs there is a short delay (f) before the two forces decline in parallel (g–unload phase) until the object is released (Johansson, 1996a).

2.5 Parallel coordination of the forces

Grasp stability is primarily obtained by the parallel change (increase and decrease) in the grip and load forces applied to each contact surface (Edin et al., 1992; Johansson and Westling, 1984b). This parallel change in grip and load forces represents a control strategy, i.e., by linking these forces together it offers a considerable flexibility when lifting objects of different weights. With a heavy object, the load forces reaches high values before the weight is counterbalanced and the object is lifted, while the corresponding increase in grip force ensures appropriate grip forces. The force ratio is higher than the slip ratio by a certain safety margin (Fig. 2.3). The safety margin for rough materials required to prevent slips is 40% of the slip ratio in adults (Forssberg et al., 1995).

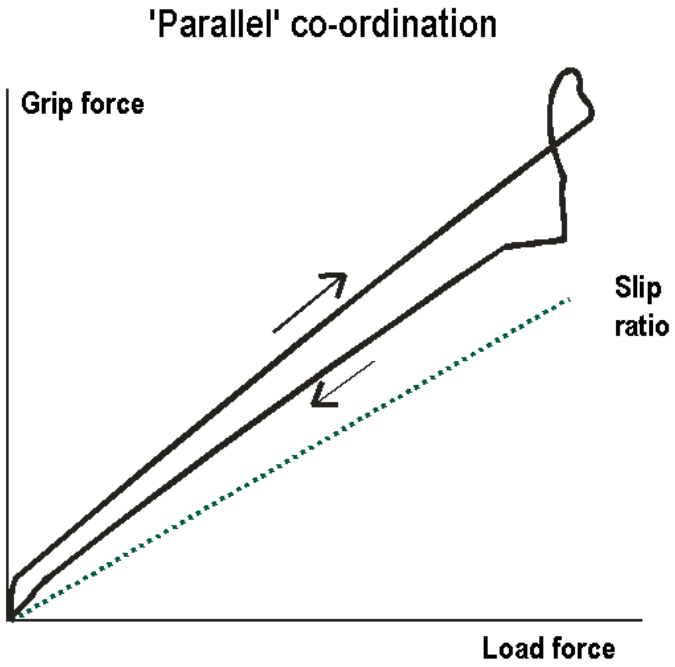

FIG. 2.3: Parallel coordination of the forces during manipulation. Dashed line indicates the minimum grip:load force ratio to prevent slips. (Johansson, 1996a)

2.6 Models of human force control

One way to use digital sensors to adjust the force output to object properties would be to engage them in closed feedback loops. But such loops imply large time delays. These time delays arise from, e.g. impulse conduction in peripheral nerves, conduction and processing time in the CNS, and, not least, the inherent sluggishness of muscles. In humans, these factors add up to at least 100 ms for the generation of a significant force response. Despite these control issues, subjects rely on feedback control in certain types of manipulative tasks. This occurs in reactive tasks when we restrain 'active' objects that impose unpredictable loads tangential to the grip surfaces, e.g. when we hold a dog's leash (Johansson, 1998).

Because of long time delays with feedback control, the systems involved in human object-manipulation seem to be controlled by a feed-forward sensory control system that is called *anticipatory parameter control* (APC) (Johansson, 1996b; Johansson and Edin, 1993; Johansson and Cole, 1992). Anticipatory parameter control refers to the use of visual and somatosensory inputs for object identification, in conjunction with internal models, to tailor fingertip forces for the properties of the object manipulated prior to the execution of the motor commands. This control strategy implies that the system uses previous experience with an object or with similar objects to adjust the motor commands parametrically in advance. As such, APC can be viewed as a system that operates on fairly long time scales. In contrast, by using the discrete mechanical events in the afferent signal, the *sensory discrete-event drive control* (DSC) results in changes of the motor output whenever a mismatch between the expected and the actual outcome of the sensory inflow occurs (Johansson and Edin, 1993). Hence, DSC can be considered to operate on a shorter time scale.

Johansson (Johansson, 1996b) proposed a conceptual model for the application of grip forces and load forces in a lifting task. Briefly, vision provides information on object position, object size, and object shape. This information is used to activate controllers for transporting the hand towards the object while the fingers are being preshaped. Based on visual estimates of weight and friction, a set of tactile responses is predicted to guide planning for the application of initial grip force to the object. Tactile perceptions of weight and texture are fed back and compared to the predicted weight and texture. The mismatch is used to update memory representations of weight and texture for a specific object appearance. This memory is assumed to be retrieved on later occasions to guide anticipatory application of forces (Gordon et al., 1993). If a declining grip force

results in slip, a resulting slip alert signal in hand mechanoreceptors triggers a reactive increase in grip force.

2.7 Previous lift memory

The initial forces applied to an object reflect the requirements of the previous lifts. The frictional conditions in the preceding lift with an object are reflected in the development of the grip forces immediately after the object is touched (Edin et al., 1992; Forssberg et al., 1995; Johansson and Westling, 1984b). Likewise, the adaptation of force development to an object's weight during the load phase must rely on memory representations of the object's weight acquired during previous lifts because explicit information about object's weight is not available until lift-off (Gordon et al., 1991, 1993; Johansson and Westling, 1988b). Thus, one must hypothesize that there exist sensorimotor memories that represent both important physical properties of the objects to be manipulated and the appropriate magnitude parameters of the motor commands (Johansson, 1996b).

2.8 Weight and friction adaptation

The *weight* of the object principally modifies the duration of the loading and unloading phases and the force rates during these phases. The heavier the object, the more extended the phases of parallel force increase and the higher the force rates. However, the ratio between the two forces is not influenced (Johansson and Westling, 1990). [1]

When grasping and lifting familiar objects that we can identify either visually or haptically, the force development is via APC tailored to the weight of the object before sensory information related to weight becomes available at lift-off (Johansson and Westling, 1988a). As we have all experienced, however, our predictions of objects' weight may sometimes be erroneous. In such cases, the lifting movement may be either jerky or slow. If the object is lighter than anticipated, the force drive will be too strong when the lift-off takes place. Although burst responses in FA II afferents evoked by the unexpectedly early lift- off, trigger an abrupt termination of the force drive, this occurs too late (due to control loop delays) to avoid

[1] Note the difference between force ratio (i.e., the ratio between the grip and load forces), and force rate (i.e., the amount of applied force reached).

an excessively high lift. Conversely, if the object is heavier than expected, people will initially increase load force to a level that is not sufficient to produce lift-off and no sensory event will be evoked to confirm lift- off. Importantly, this absence of a sensory event at the expected lift-off now causes the release of a 'new' set of motor commands. These generate a slow discontinuous force increase, until terminated by a neural event at the true lift-off. Thus, corroborating the DESC policy, control actions are taken as soon there is a mismatch between an expected sensory event and the actual sensory input. Moreover, once an error occurs, the internal model of the object is updated to capture the new weight for use in subsequent interactions with the object, i.e., single trial learning (Birznieks, 2003).

The *friction* between an object and a digit determines the relationship between the normal (grip) and tangential (load) forces that can be applied without slip. Thus, the proportional relationship between the employed grip and load forces during self- paced manipulative tasks is functional only if the normal-to-tangential force ratio is appropriately set for the friction between the skin and object. To prevent slip, this ratio must exceed a minimum normal-to-tangential force ratio determined by the friction. We know that the friction between objects and the fingers may vary widely in everyday situations. For example, objects have different surface structures, they may be wet, and the sweating rates of the fingers vary over time (Cadoret and AM, 1996; Johansson and Westling, 1984b). Nevertheless, people automatically adjust the balance between the grip and load forces to the frictional conditions such that a relatively small but adequate safety margin at each engaged digit is obtained, i.e., the more slippery the object the higher the employed grip force at any given load force (Burstedt et al., 1997; Cole and Johansson, 1993; Edin et al., 1992; Johansson and Westling, 1984a,c). Furthermore, it is clear that this adaptation is made to the friction per se, rather than on the basis of different texture properties of the surface materials (Cadoret and AM, 1996; Jenmalm, 1998, 2000; Johansson and Westling, 1984b).

Thus, with weight variations, the parallel change in grip and load forces ensures grasp stability when lifting objects regardless of weight, i.e., with a heavier object both the grip and load forces reach higher values before the weight is counterbalanced than with a lighter one. With frictional variations, the balance between the grip and load force is a motor output parameter that is set to the current frictional limits (fig. 2.4).

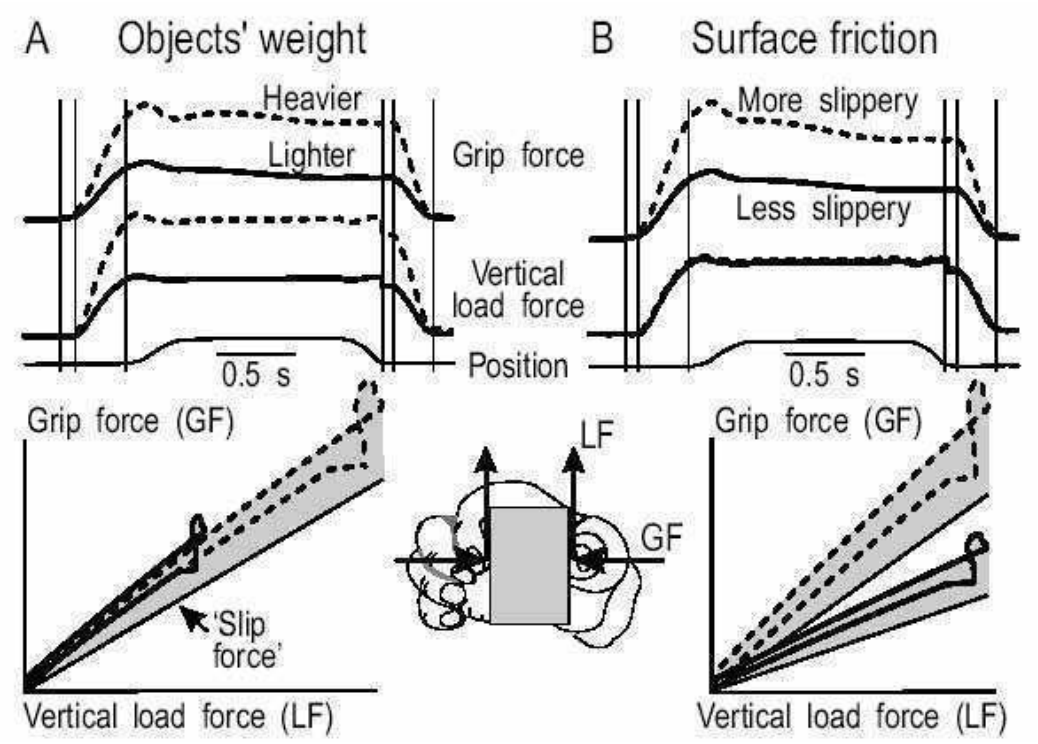

FIG. 2.4: Principles for parametric adjustments of motor output to object weight (A) and friction in relation to the skin (B). Subject lifts an instrumented test object from a table, holds it in the air and then replaces it, using the precision grip. Upper graphs show the horizontally orientated grip force ('GF'), the vertically orientated load force ('LF') and the object's vertical position as a function of time. The lower graphs show the grip force as a function of the load force in a phase-plane plot for the same trials. Thin lines indicate the minimum grip-to-load force ratio to prevent slips ('slip force') and the safety margin against slips is indicated by shading. Note that with weight variations, the parallel change in grip and load forces ensures grasp stability when lifting objects regardless of weight, i.e., with a heavier object both the grip and load forces reach higher values before the weight is counterbalanced than they do with a lighter one (A). With frictional variations, the balance between the grip and load force is a motor output parameter that is set to the frictional limit (B). Adapted from Johansson and Westling (1988a) (A), and Johansson and Westling (1984c) (B) (Jenmalm, 2000).

Adjustment to friction and independent control of fingertip forces

With equal frictional conditions at the two grip surfaces in precision grip lifting, the fingertip forces are about equal at the two digits, i.e., similar vertical lifting forces and grip forces are used (Fig. 2.5A). With different friction at the two digits, the digit contacting the most slippery surface exerts less vertical lifting force than the digit in contact with the less slippery surface (Fig. 2.5B-C). When gripping an object, a new frictional condition influences the development of the tangential forces about 0.1s after contact, i.e., well before the start of the vertical movement (Fig. 2.5B). Likewise, after about 0.1 s after contact the rate of increase of the grip force is influenced by the average friction of the grasped surfaces. Thus, an updating of the force coordination to the changes in frictional condition took place. As illustrated in Fig. 2.5C, this 'new' coordination is used already when the forces initially develop in the subsequent trial with the same object, indicating that the relationship between the two forces is controlled on the basis of a memory trace. Importantly, the safety margin employed at a particular digit is largely determined by the frictional conditions encountered by that digit and barely influenced by the surface condition at the other digit (Johansson and Westling, 1987).

In case of insufficient initial adjustments to the frictional condition, slips may occur when the object has been lifted, primarily at one digit (Fig. 2.5D). The tangential force at that digit suddenly decreases while it increased at the other digit. Such transient redistribution of the tangential force caused by slips is always followed by a grip force increase triggered by slip event. The net outcome is an increased safety margin at the slipping digit but a virtually unaffected safety margin at the other digit (see Fig. 2.5D). That is, the overall safety margin is restored preventing further slips. The resultant new force co-ordination following slips is in each instance maintained throughout the lifting trial and is used as a default coordination for subsequent trials with the same object, again indicating that the force coordination is controlled on the basis of a memory trace (APC). In this situation, the slip updated the relevant memory mechanisms (Johansson and Westling, 1987).

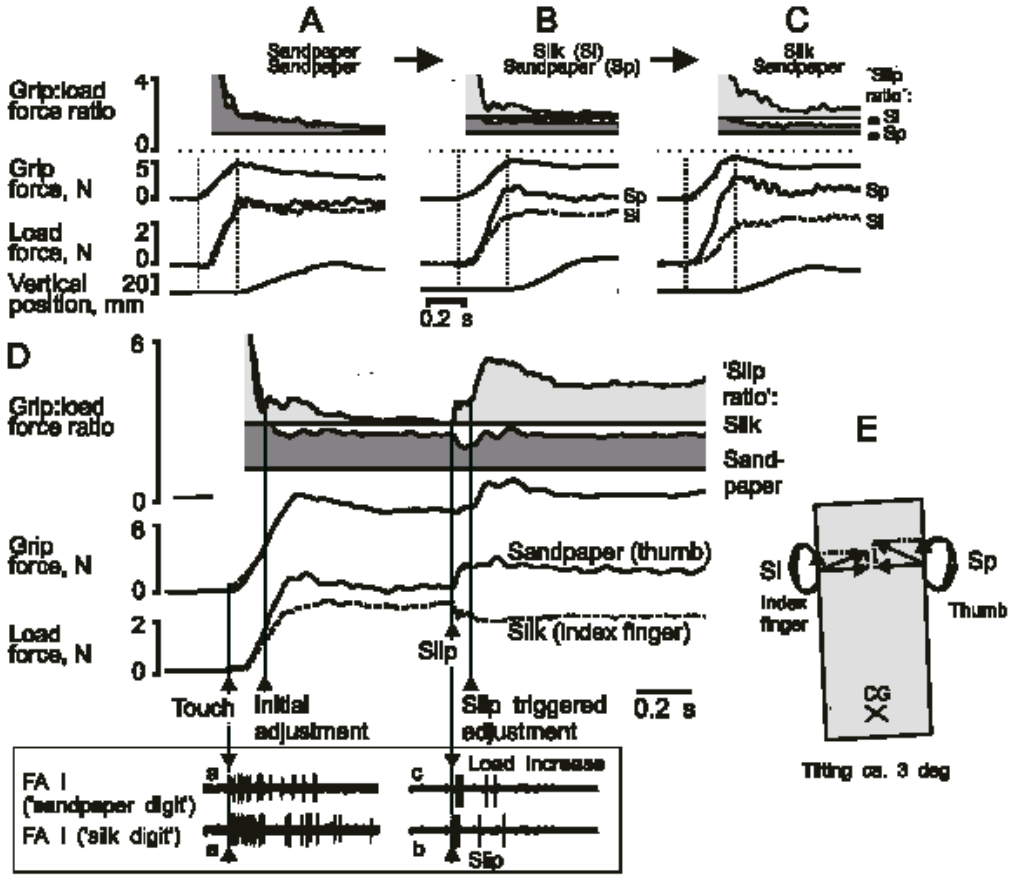

FIG. 2.5: Adjustments of fingertip forces to the local frictional condition in a lifting task performed with a precision grip (Johansson and Westling, 1987).

When the digits contacted different surface materials the requirement for stable contact at each finger is that

$N_1 \geq T_1/\mu_1$ and $N_2 \geq T_2/\mu_2$ (1)

where N, T and stands for normal force, tangential force and coefficient of friction (inverse of slip ratio) at digit "1" and digit "2" respectively. That the load (L) is the sum of the two tangential forces ($L = T_1 + T_2$) implies that for stable contact

$L \leq N_1 * \mu_1 + N_2 * \mu_2$ (2)

In case of identical normal forces ($N_1 = N_2 = N$),

$L \leq N * (\mu_1 + \mu_2)$ (3)

Rearranging this equation we get that grasp stability requires

$N \geq L/(\mu_1 + \mu_2)$ (4)

Thus, if the normal forces are constrained to be similar at the two digits, only information about the total load force and average friction at the two contact sites is required to specify the minimum normal force to prevent loss of the object (Birznieks, 2003).

Afferent responses at initial contact

When gripping an object, there are initial contact responses present in the SA-I and FA-II afferents, and most distinct in the FA-I afferents (see inset in Fig. 2.5) (Westling and Johansson, 1987). The CNS apparently utilizes such contact responses to confirm that adequate contact has been established between the fingertips and an object before releasing the muscle commands, leading to further manipulation (Johansson and Westling, 1984c).

The initial responses in the FA-I afferents are also considered responsible for the initial adjustment to a new frictional condition because they are influenced by the surface material (see inset in Fig. 2.5) (Westling and Johansson, 1987). The more slippery the material, the higher the discharge rate, of the initial response of the FA I unit. Usually the impulse rates increased but the durations of the impulse bursts decreased. The initial adjustment to the new friction often is insufficient and further "secondary" adjustments will occur later in the lift. The estimation of the friction between the skin and the object most likely depends on afferent signals related to small localized slip events within the contact area when an object is initially contacted. Such localized slips are explained by the unequal

distribution of normal and tangential forces over the areas of contact that occur due to the elastic properties and curvature of the fingertip (Westling and Johansson, 1987). Thus, tactile afferents provide the central nervous system with signals related to the frictional conditions already at the initial touch.

If an object surface changes between lifts but the friction visually appears to be the same, subjects use grip forces appropriate for the last lift (Johansson, 1996a; Johansson and Westling, 1987; Westling and Johansson, 1987). Adjustments to a new frictional condition can be observed as early as 100 ms after the initial contact with the object, but also later during the lift. Tactile afferents show differential responses to, for instance, friction, prior to any force adjustment, and this suggests that they provide the information necessary to change the force output (Johansson and Westling, 1987; Westling and Johansson, 1987).

2.9 Slips during manipulation

To prevent slips the human system uses a pretty small safety margin, i.e., the ratio between grip and load forces (grip:load force ratio), which have to exceed a certain value. There have been experiments where subjects have been asked to slowly separate their fingers while holding an object, and it was found that it is very difficult to voluntarily reduce the grip:load force ratio when the system is able to detect small slips (Johansson and Westling, 1987).

The contact area between the finger and an object may be divided into two subareas: one *stick area*, where the ratio between the normal and the tangential forces are above a certain numerical value (the slip ratio), and one *slip area*, where the ratio is lower. Slips are most likely to occur at the edges of the contact area because this is where the normal forces are lowest (Maeno et al., 2000).

When subjects lift an object with two parallel vertical surfaces and a slip occurs during the load phase, there is a stepwise decrease of the load force on the slipping digit. Conversely, on the non-slipping digit, there is an increase in the load force, i.e., the total load force is not changed but is redistributed between the engaged digits. About 74 ± 9 ms after the onset of the slip there is a change in the force ratio; the upward movement stops (tangential forces become constant) and the normal forces increase (Johansson, 1996a; Johansson and Westling, 1987; Westling and Johansson,

1987). This helps the subject to fasten the grip so that he or she will not drop the manipulated object. Most slips during the object manipulations occur without the subjects or anyone else for that matter, even noticing them. Contrary to what one might expect, such unnoticeable slips actually occur within no more than 10 to 30% of the total contact area (Johansson and Westling, 1987; Westling and Johansson, 1987). Once 75% or more of the contact area slips, a total slip is bound to occur.

Thus, slip events during the load phase trigger changes in both the load (change in load force distribution) and grip (increase) force rates. During the static phase, however, the correction is a fast increase in the grip force. This phase dependence is functional, since gravity restrains the response alternatives preventing efficient load force adjustments during the static phase (Johansson, 1996b). These control signals clearly demonstrated a phase dependent control, where similar tactile input signals trigger different grip and load force responses in different phases of the lift.

Afferent responses to slips

The intensity of the afferent slip responses ranged from a single impulse to brief bursts with peak frequencies up to ca. 300 imp/s. Slip responses occurred in every kind of mechanoreceptor except for SA II units (Johansson and Westling, 1987; Westling and Johansson, 1987). Responses to slips are evoked in FA-I, FA-II and SA-I afferents (see inset in Fig. 2.5); each of the three types thus appears capable to signal the occurrence of such slips. In contrast, responses originated from small slips localized to only a part of the skin area in contact with the object and in the absence of detectable vibrations events, are only observed in the FA-I and SA-I units and are often followed by small force ratio changes (Westling and Johansson, 1987). Such slips, called *localized frictional slips*, also trigger appropriate grip force adjustments for grasp stability when an object is held in the air. While recording from FA I and SA I units, sometimes there was a pronounced increase in the firing rate just before the slip responses occurred. This kind of "incipient slip response" was associated with 7% and 15 % of the slip events observed from the accelerometer signal while recording from these two unit types, respectively.

The afferent slip responses in the highly vibration sensitive FA II units, might have been evoked by the high frequency vibration in the object/hand caused by the overall slips. This would be consistent with the finding that the FA II units rarely exhibited localized slip responses.

Strong burst responses in the FA II units caused by transients other than those evoked by slips did not trigger upgradings of the force ratio. Thus, by exclusion, signals in the type I units would be indispensable to the adjustment of the grip to the friction.

Briefly, there are the "afferent slip responses" in the FA I, SA I and FA II units, the "localized slip responses" principally in the FA I and SA I units, and the "initial responses" most pronounced in the FA I units.

2.10 Answers of the mechanoreceptors during manipulation

When lifting an object using the precision grip, the control system is guided by sensory signals at specific events during the lift. While some mechanoreceptive units are active for static pressure, when the tactile state does not change, the fast adapting units are active when the tactile pressure is changing, e.g., at small vibrations. The four types of skin afferents in the glabrous show different types of responses during manipulative actions. This results in a very functional feedback channel conveying important bits of information about the transitions between the different phases of the lift (table 2.1).

Type I units

The FA I units become highly active during the initial period of grip force increase. This is also true for most SA I units. Accordingly, most of the skin deformation changes take place at low grip forces (below ca. 1 N). The intensive responses in the FA I units and most of the SA I units during the preload phases and early loading phases suggested that the skin deformation changes caused by the increasing grip force are greatest at low grip forces. Later, while the load and grip forces increase in parallel during isometric conditions, the FA I and SA I units continue firing but generally at declining impulsive rates. As long as the object is held in air, the SA I units generally maintained firing with a tendency to adaptation. A minority of the FA I units also discharge, especially during periods of pronounced physiological muscle tremor. The SA I units usually become silent when the grip and load forces in parallel declined to zero during isometric conditions after the object had contacted the table. However,

during the very release of the grip the FA I units and some SA I units show brief burst discharges.

Type II units

The FA II units respond distinctly to the mechanical transients associated with the start of the vertical movement and especially with the sudden cessation of movement at the terminal table contact. Most FA II units also discharge at the initial touch and at the release of the object, albeit less reliably than the type I units. Most FA II units respond at the following four events: the initial touch, the start of the movement, the sudden cessation of movement terminating the replacement phase (contact table), and the release of the object (Westling and Johansson, 1987).

The SA II units are preferentially distributed along the stretch lines of the human hand. Their activations are clearly scaled by the load amplitude (because they need stretching to response). They respond late in the loading phase and reach a maximum of firing rates late in the lifting phase which is sustained throughout the static part of the object manipulation (Johansson, 1978; Johansson and Westling, 1987; Johansson and Edin, 1992; Johnson, 2001; Macefield et al., 1996; Westling and Johansson, 1987). These units show a weak discharge rate during the loading phase and a decline of firing during the phase of unloading. During the last part of the manipulation the SA II units cease firing.

Events	Activated afferent units	Role of the afferent signal
First contact and loss of contact with an object	SA I & FA I	Triggers the following sequence of a multi-phase action
Start of the vertical movement of an object	FA II	Informs CNS of erroneous programming of the anticipatory GF response. May trigger reactive GF response.
Initiation of unloading and loading phases	SA II	Codes an estimate of objects weight. Codes the balance between normal and tangential forces
Frictional slips i.e. local redistribution of strain/stress patterns in the skin contact area	FA I & SA I	Informs CNS of relative orientation of object and contact area. Helps decrease the amount of excess GF used
Localized finger slip	FA I, SA I & FA II	Codes the duration and magnitude of a finger slip. May trigger reactive GF response.
Object's contact table	FA II	Informs CNS that the object has contacted the table during the unloading phase

Table 2.1: Summary of the specific role played by each of the four mechanoreceptors in the control of grip force (GF) during the simple act of lifting an object between index and thumb (Johansson, 1996b; Westling and Johansson, 1987). This table was adapted from Turrell (2000)

2.11 Torque load

Torque loads often develop in natural tasks together with linear load forces due to gravitational and inertial forces. For example, in a precision grip

task tangential torques occur whenever we tilt an object around a grip axis (line joining the fingertips) that does not pass through the object's center of mass and when we lift an object whose center of mass lies off the grip axis while keeping it level (see fig. 2.6 B). These torque loads tend to rotate the object around the grip axis (rotational slip) and in certain circumstances, this may be used to advantage. For example, when we pick up a pencil, rotation during lifting may help to align the pencil appropriately for subsequent writing. However, if instead the intention is to preserve particular geometric relations between hand and object, increases in grip force will be needed to compensate for the torque load as well as for the linear load force when the object's center of mass does not lie on the grip axis. This would occur when we hold a book with its back in a vertical orientation between the fingers and thumb and put it in a slot in a bookshelf. Because we rarely take a book such that the grip axis passes through its center of mass, a torque load is present in relation to the grasp. Torque loads depend on rotational (torsional) friction between the fingertips and the object which arises because the normal force is distributed across the skin-object contact area, rather than focused at a point (Buss et al., 1996; Howe and Cutkosky, 1996). It was originally demonstrated by Kinoshita et al. (Kinoshita et al., 1997) that the minimum grip force required by a fingertip to stabilize a disk subjected to torque load increases approximately linearly with both torque and tangential force, with slopes that depend on the friction within the contact surface. Furthermore, the grip force used by subjects to hold the object was regulated to the tangential torque. Thus, to avoid slips under combined linear force and torque loads, subjects need to apply a grip force that is higher than that required to prevent slips due to the linear load force only (Jenmalm, 2000).

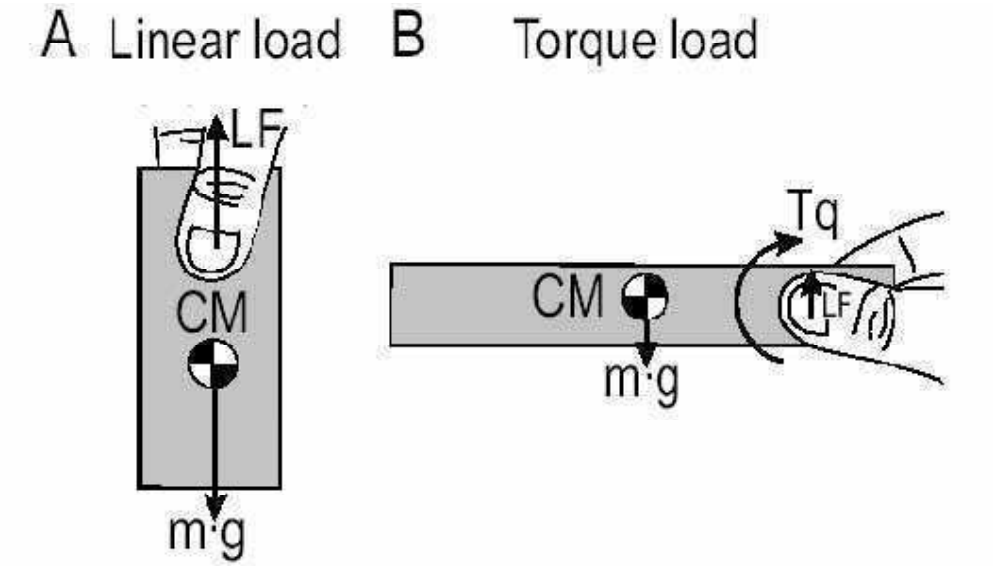

FIG. 2.6: Schematic illustration of two principally different destabilizing fingertip loads, tangential to the grasp surfaces. In A, subjects generate primarily linear load forces (LF) that develop due to gravitational and inertial forces when the object is lifted from its support. The center of mass (CM) is located below the grasp surfaces. In B, subjects hold a lightweight test object whose center of mass (CM) is located in front of the grip axis. They therefore generate tangential torques (Tq) at each grasp surface, i.e., torque loads. The arrows in A-B indicate directions of positive tangential torque and linear load force to counteract object moment and object mass (Jenmalm, 2000).

2.12 Shape adaptation

In this section a survey of the force adaptation to the angle and curvature of the surface (fig. 2.7) is presented.

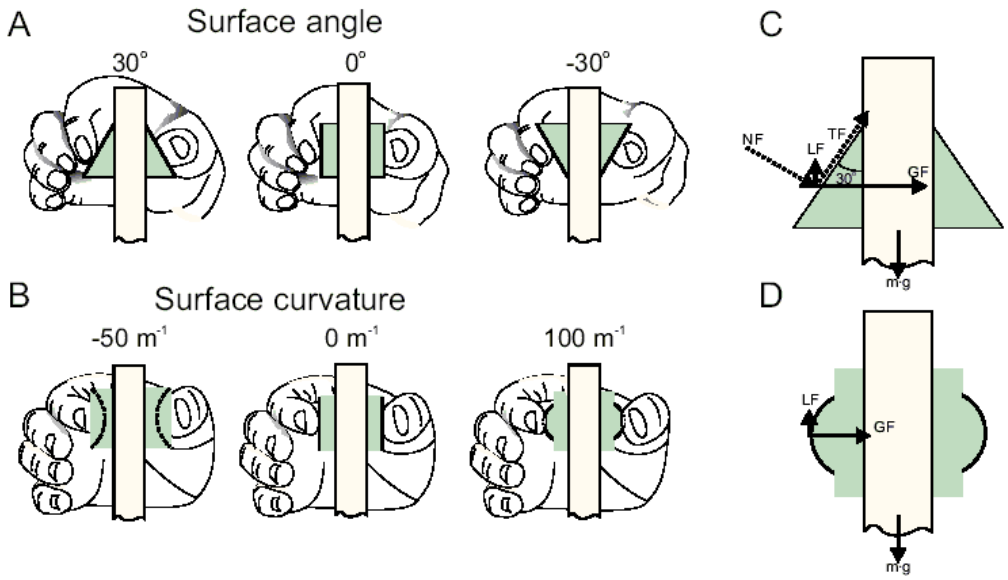

FIG. 2.7: Two different aspects of objects' shape. A: The surface angle between the flat grip surface and the vertical of the object. At zero degrees the grip surfaces are flat and parallel (middle), whereas at positive angles the grip surfaces taper upwards (left; 30° illustrated) and at negative downwards (right; -30° illustrated). B: Spherically curved surfaces, with their curvature expressed as inverse radius ranged from -50 to 200 m^{-1}. Concave curvature(left), flat (middle) and convex (right) are illustrated in the figure. C - D: Schematic illustration of forces measured with the tapered object and the object whose grasp surfaces were spherically curved, respectively. LF - vertical load force; GF - horizontal grip force; NF - force applied normal to the grasp surface; and TF - force applied tangential to the grasp surface (Jenmalm, 1998).

2.12.1 Adjustments to surface angle

Forces normal (NF) and tangential (TF) to the grip surface (fig. 2.8) can be computed for each digit from the measured vertical forces (VFs) and

horizontal forces (HFs) and the known surface angle (α) between the grip surface and the vertical of the object using the following equations: NF = HF $\times$ cos(α) - VF $\times$ sin(α), and TF = HF $\times$ sin (α) + VF $\times$ cos(α) (Jenmalm and Johansson, 1997).

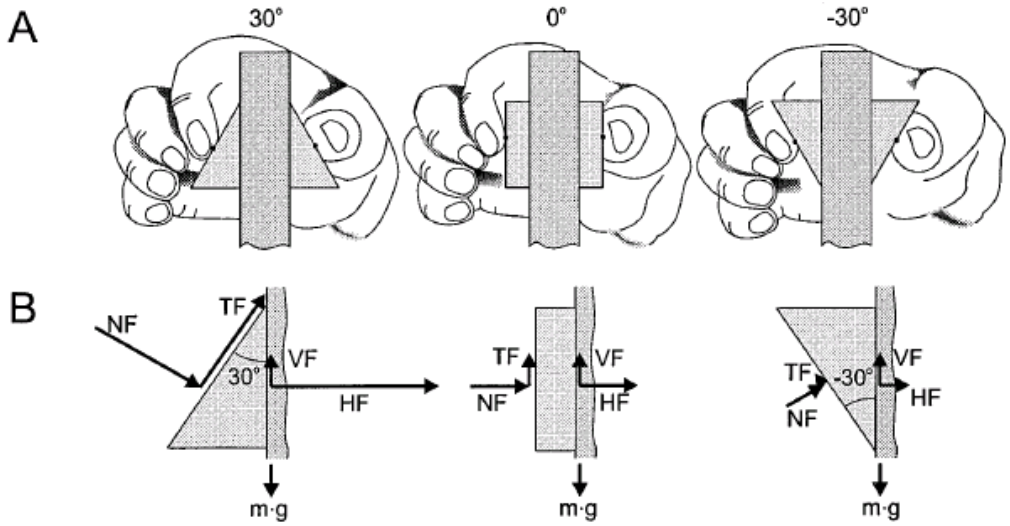

FIG. 2.8: Normal and tangential forces for objects with different surface angles (Jenmalm and Johansson, 1997).

Changes in object tapering give rise to a marked and graded variation of the employed fingertip forces although the object's weight and the surface friction between object and digits is the same. The horizontal grip force increases progressively with surface angle (Figs. 2.9A and C). This effect is present because the angle principally influences the grip force rate; the more positive the angle the higher the rate of force change. The generation of vertical load force and the vertical movement is less influenced by the surface angle; the static vertical force is not influenced at all, since the weight of the object is constant. Consequently, the horizontal grip force at any given vertical load force increases with the surface angle (Fig. 2.9A). As a consequence of the manner in which the subjects change the balance between the horizontal and vertical forces with the geometry of the object, both the normal force and that tangential to the grip surfaces increase progressively as a function of the surface angle (Fig. 2.9B and C). Importantly, the two forces increase in parallel, keeping an approximately constant rela-

tionship regardless of surface angle (Fig. 2.9B, right panel). Thus, despite the extensive variation in force requirements, the safety margin expressed as the difference between the employed static normal force and the corresponding minimum normal force to prevent slip ('slip force') is nearly constant across the different surface angles (Fig. 2.9C, dotted lines in bottom row) (Jenmalm, 1998).

When the subjects can see the object and have normal digital sensibility, the surface angle reliably influences the development of the horizontal grip force already from the initial contact with the object, i.e. before somatosensory information related to the object's surface angle could have influenced the force output. Therefore, subjects use vision to compute the force requirements (Jenmalm, 1998).

2.12.2 Adjustments to surface curvature

The grip force measured along an axis through the centers of the grip surfaces increases in parallel with increasing linear load force, but the relationship between the two forces is hardly affected by the surface curvature(Jenmalm et al., 1998). However, the curvature becomes critical in tasks that involve torques tangential to the grasp surfaces, such as when we tilt objects whose center of mass does not lie on the grip axis. That is, the curvature markedly affects the grip force required to prevent rotational slips under tangential torque loads; the grip force required increases for larger curvatures (Goodwin et al., 1998; Jenmalm and Johansson, 1997; Kinoshita et al., 1997). Accordingly, at any given torque load, subject use a higher grip force with more curved surfaces in a manner matching the effect of the curvature on the rotation friction. This parametric scaling of the grip force results in an adequate safety margin against rotational slips over a wide range of curvatures.

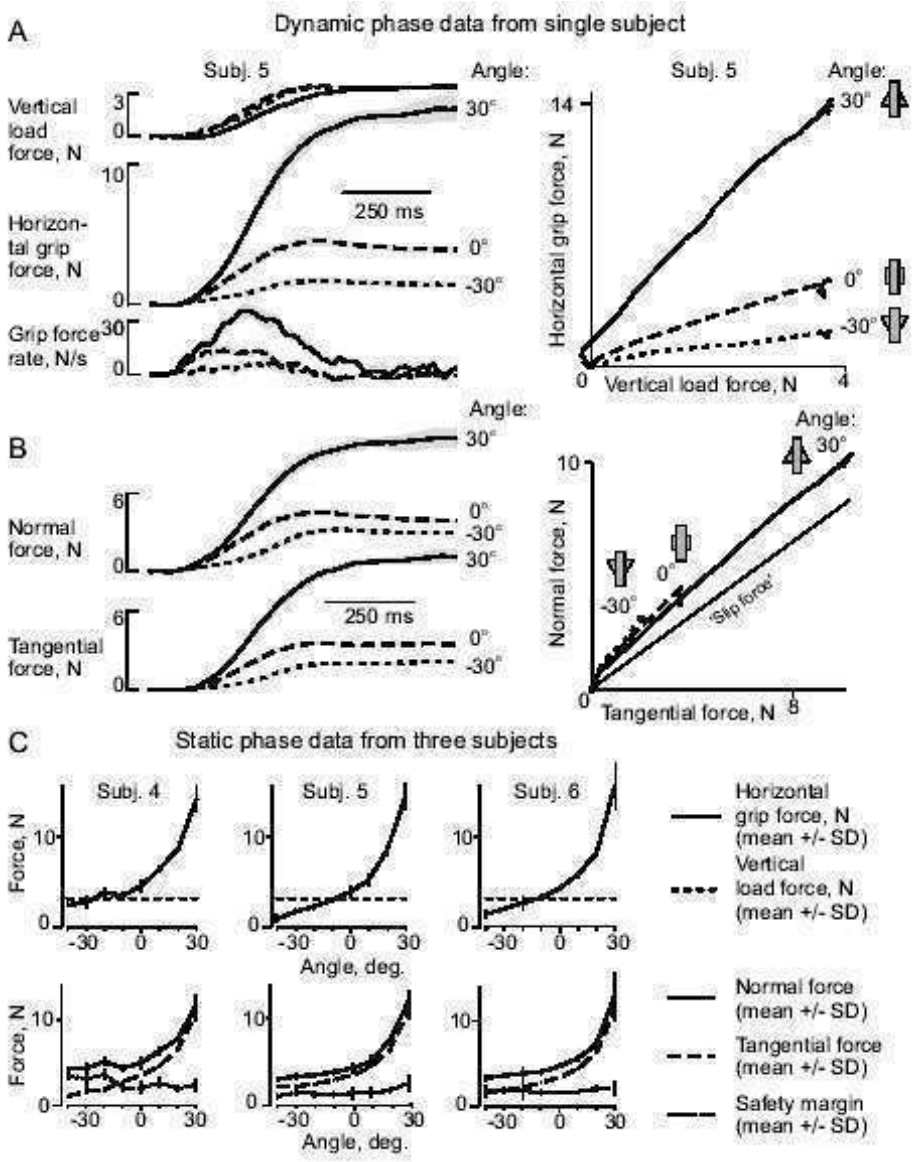

FIG. 2.9: Force development during the initial part of the lifting task in which the subjects lifted tapered objects with different surface angles. A - left panel: Vertical load force, horizontal grip force and grip force rate as a function of time for data averaged across trials; shaded areas give $\pm$ 1 SEM and all trials are synchronized on touch. B: Forces applied normal and tangential to the grasp surfaces for data corresponding to those in A. Right panels in A and B: Coordination between horizontal grip force and vertical load force and between normal force and tangential force. C: Static horizontal grip force and vertical load force (upper ro) w and static normal force, tangential force and safety margin (lower row) shown as function of surface angle for individual subjects. Vertical bars indicate $\pm$ 1 SD (Jenmalm, 1998).

2.13 Grasp development

Precision grip appears at about 10 months of age but the mature patterns do not occur until between ages of six to eight (Forssberg et al., 1991). Young children regularly tend to increase the grip force well before the load force. This behavior might be an expression of feedback strategy since there is an absence of anticipatory weight-related parameter control. At about two years of age there is a coupling between grip and load forces (Werremeyer and Cole, 1997). Children under the age of three do not use visual cues about the size of the object to estimate the weight of the object (Forssberg et al., 1991). They continue to increase the load force in small increments until liftoff occurs. This feedback strategy is similar to that observed when adults underestimate the weight of an object and then have to increase the load force again until liftoff occurs.

Cole et al made a study of the relation between age and fingertip forces (Cole et al., 1999). As a summary, they suggested that older adults tend to use higher forces than younger adults but the skin slipperiness explains this increase between the ages of 50 and 60. Only after age 70 there is also an increase in the safety margin for the rough (non-slippery) surfaces. On an average the grip forces and the safety margins were twice as high for older than for younger adults. Older subjects also showed a longer delay between grasping an object and lifting the same. Even when the experimenters had accounted for skin slipperiness, older adults showed a grip force that was between 33% and 57% higher than for younger subjects. Since the population of FA I units decline the older we get may explain the higher safety margins since it is difficult to observe and adapt the forces due to friction without them. Cole et al found that older subjects used safety margins that were between 41% and 104% higher than younger subjects.

CHAPTER 3

STATE OF THE ART

In this section, we survey the different techniques that have been proposed for the estimation of the friction coefficient, the detection of the incipient slip, the correction of the slip, and the simulation of the human afferent signals.

3.1 Friction coefficient and incipient slip detection

In the field of fine grasp, consistent efforts have been devoted to design sensors able to detect an incipient slip condition. The development of such sensor is very useful in the estimation of the friction coefficient of an unknown object during manipulation. To achieve the above goal, one can outline two main approaches.

The first consists in calculating the friction coefficient by measuring the normal and the tangential forces when the object starts to slide. The main advantage of this approach is that it can be implemented without using dedicated sensors, although the measure is obtained in consequence of a relative movement of the object and the grasping device. This method has been used, for example, in Bicchi et al. (1993); Cicchetti et al. (1995).

The second approach consists in the development of special sensors. These are mainly dedicated devices, designed and realized with the only goal of detecting a slip condition. Mostly, they are based on accelerometers properly placed in elastic materials which start vibrating when slip begins (Howe and Cutkosky, 1989; Tremblay and Cutkosky, 1993). The main ad-

vantage of these sensors is that they provide a robust and a reliable measurement. On the other hand, they are dedicated devices and therefore increase the overall complexity of the sensorial system.

Holweg et al. (1996) presented two techniques for detecting a slip condition with rubber-based tactile sensors. The first technique employs the elasticity of the rubber. Before the object starts to slip, the rubber is stretched. This deformation can be interpreted as a signal of an incipient slip. In fact, it is shown how a slip can be detected by implementing a frequency analysis of the center of the force distribution an by testing the low frequency components. Note that this approach proposes a technique based on the detection of a spatial variation. The second approach is more closely related to the human sensation of slip. It is based on the idea that the normal forces measured by the tactile sensor fluctuate with a certain frequency during slip. This fluctuation is due to vibrations of the rubber during slip of the object. The vibrations can be regarded as a "catch and snap back" effect (Howe and Cutkosky, 1989). During the catch phase the rubber moves along with the object due to the friction between the rubber and the object. Due to this stretching the measured force decreases while, after the rubber snaps back, it increases again. During slip two main contributions of the frequency spectrum have been individuated. A low frequency component, approximately at 10 Hz, is due to the stress of the rubber. It starts immediately when slip occurs, and successively is present only for a short period of time. The second component can be found at about 65 Hz and starts and stops directly with the slip. This seems to be the actual vibration of the rubber, the so called "catch and snap" effect.

Canepa et al. (1998) designed and realized a tactile sensor selectively sensitive to shear and normal stress components generated during frictional contact. A backpropagating neural network is then used to make a comparison of the normal and shear stress, and detect an incipient slip condition. The accuracy reached in the detection is rather high, considering the low resolution of the sensor and the high noise level on the data. Another important feature of the method is the high speed of the network (in particular if it is implemented via-hardware), and the implicit robustness of the design to vibration noise.

Maeno et al. (1998) showed that changes in the stick/slip condition at the surface of an elastic finger when lifting an object can be estimated by the shear strain distribution pattern. When the stick/slip condition is known, the grasping and lifting force can be controlled without producing a com-

plete slip. Furthermore, detection of the friction coefficient between the finger and object is not necessary.

Shinoda et al. (2000) showed that tangential stress/strain at the center of the elastic finger indicates the difference in friction coefficient when the elastic finger is pressed against a planar object.

Hosoda et al. (2002) proposed an internal representation of slip for a soft finger with vision and tactile sensors. They used uncalibrated vision and tactile sensors, and detected the slip by a hebbian neural network connecting the vision and tactile system. At the beginning of learning, only the vision can sense the slip as the movement of the target, but after a while the tactile sensors can sense the slip even if it is so small that the vision sensor cannot sense it. The originality of this proposal is the use of uncalibrated sensors, and the representation of slip inside the agent. However, they cannot distinguish slip from just pressured.

3.2 Simulation of the afferent responses

Israelsson (2002) made a computational simulator of the responses of the afferents from the glabrous skin during human manipulation. The output of the simulation program are spike-trains from each of the simulated afferents (fig. 3.1).

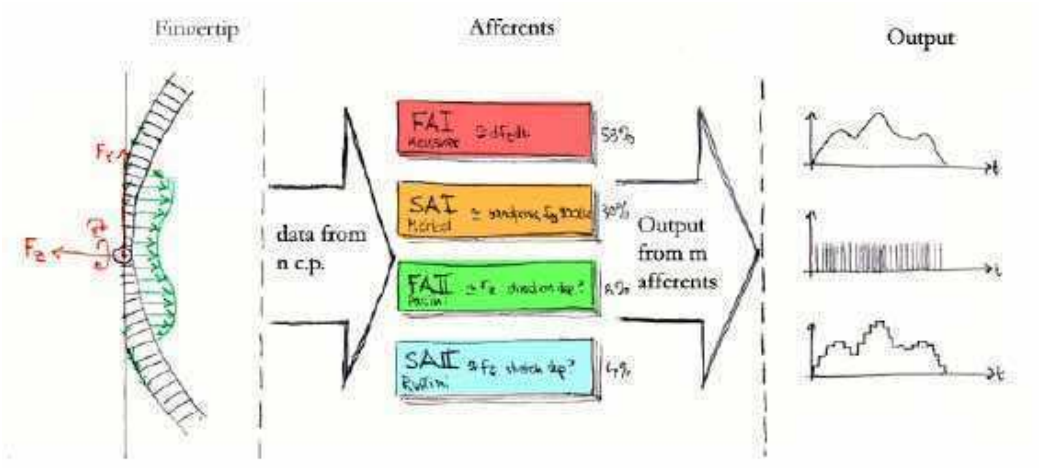

FIG. 3.1: Scheme of the program simulating human afferents (Israelsson, 2002).

To develop the simulation program experimental data were used from a from a not yet published at that time study by Roland Johansson and coworkers at Umeå University. In this study, subjects had their nail of their index finger glued to a support structure. A flat circular contact plate was moved against the fingertip, to a center point located near the center of the approximately flat portion of the fingertip surface, which serves as the primary point when manipulating objects. This point was used as the zero point in a coordinate system of the subjects' fingertip. The movement of the plate towards the fingertip was controlled through position servo control and then pressed against the fingertip under force servo control once the normal force had reached 0.2N up to a total of 4N. Forces were delivered in one of five directions: normal to the surface, in the distal, proximal, radial, and ulnar directions (in addition to the normal force of 4N, there were, in the four tangential directions, force direction components of 1.1N). The contact plate was covered with a 25 μ latex rubber glued to its surface, which would give the objects a surface of rubber i.e. a high frictional value, during the simulated manipulations. In the center of the contact plate there was a hole (diameter 1.2 mm) with a force probe (diameter 1 mm). The flat tip of the force probe was at level with the contact surface and measured the local force in a small skin area (i.e., within about 1 mm^2) in three orthogonal directions, X, Y and Z, representing the local tangential forces and the normal force, respectively. The plate was moved in 1 mm steps across the fingertip in six different subjects and at each site the same total force profile was applied while the local forces were measured. This way, a complete data set for each stimulus direction represented the local forces across the fingertip surface in touch with a contact plate. In parallel experiments, afferent responses to the same type of stimuli were recorded.

Thus, data of two types were used during the simulations: (1) local forces in the plane of the skin and normal to the surface and (2) microneurographical recordings of afferent activity in humans.

Each fingertip profile was translated into a 29×29 large matrix (each cell corresponds to 1 mm^2). To represent the force development at the fingertip, with a resolution close to the one available from the recording equipment, the force distribution across the fingertip (i.e. the 29×29 matrix) was represented at 0.1N steps of total normal force. Because the normal force ranged from 0.0 to 4.0N (41 steps not counting the moment before contact), a complete description of the force development could be obtained by means of a $41 \times 29 \times 29$ matrix. As for the subjects' profiles, the two tangential forces and the normal force were locally distributed across the surface of the model fingertip, i.e. in each cell there were three forces (X,

Y and Z). These three force components were dissimilar in all tangential directions and therefore, in order to get a matrix that holds all of this, i.e. three forces (X, Y, Z) and five stimulus directions (normal, distal, proximal, radial and ulnar), the final matrix became $41 \times 29 \times 29 \times 3 \times 5$. The force at intermediate values was calculated by interpolation.

The same force profile was used during all of the simulations, and was the same as in the empirical data, i.e., a half sinusoidal wave, 125 ms for the loading ramp, 250 ms for the hold phase and 125 ms for the unloading ramp. The afferent responses correspond to different stages in the force profile which means that in order to correctly imitate the afferent responses, all the parts of the force that are deforming the fingertip must be taken into account. Therefore, the afferent responses to the changing forces on the finger were simulated by using the forces applicable to their receptive fields (RF's) projected onto the digit surface. The RF's of type I afferents are located correspondingly to the cells in a matrix model of the surface of the model fingertip i.e. they correspond to 1 mm^2. For the FA II, the RF corresponds to the whole hand and the SA II's RF is calculated in a separate function in the program. This function uses the contact point (cp) in which the center of the SA II is located and from there calculates the total force in related cp's, i.e. each SA II has a field covering 21 cp's.

Generating spike trains similar to those observed in actual neuro- physiological experiments require several steps:

1. For all receptor classes, except the FA II afferent, the response intensity was calculated, at specified time intervals (Δt = 1 ms), as a weighted sum of the forces (X, Y, Z) and first time derivates of the same three orthogonal force directions:

$$\begin{aligned} f(t) &= k_1 \times F_z(t) + k_2 \times \tfrac{dF_z(t)}{dt} \\ &+ k_3 \times F_y(t) + k_4 \times \tfrac{dF_y(t)}{dt} \\ &+ k_5 \times F_x(t) + k_6 \times \tfrac{dF_x(t)}{dt} \end{aligned}$$

   where k_{1-6} represent the weights that differed between the different afferents. F_z represents the force in the normal plane, F_y and F_x correspond to the tangential forces in the Y and X directions, respectively.

   The weights allow to define the simulated afferents with different sensitivity to the dynamic and static components of the force devel-

opment, as well as different sensitivity to forces normal and tangential to the surface. The weights of the table 3.1 were used.

	Z(k_1)	dZ(k_2)	Y(k_3)	dY(k_4)	X(k_5)	dX(k_6)
FA I	0.0	2.5	0.0	1.5	0.0	1.5
SA I	8.0	1.0	5.0	0.5	2.0	0.25
FA II	1.1	0.0	0.0	0.0	0.0	0.0
SA II	6.5	0.2	2.5	0.2	2.5	0.2

Table 3.1: Coefficients used by Israelsson in the simulation of the afferents (Israelsson, 2002)

Accordingly, for FA units the weights of the force derivatives were comparatively large whereas the weights for the static forces were zero. Conversely, adopting non-zero weight for the static components and more modest weights for the force derivatives could simulate the response intensity of SA afferents. Moreover, FA I units are known to be particular sensitive to changes in the tangential forces and accordingly the corresponding weights were larger for FA I units than for, i.e., SA II units. Given that there is no way of figuring out the value of the weights of the table 3.1 from experimental data, they were determined by trial-and-error and qualitative comparisons. When comparing the responses that resulted from 'reasonable' settings with published afferent responses the simulated responses were qualitatively similar with those recorded in neurophysiological experiments.

2. To specifically capture the dynamic responses of FA II units, whose responses are highest between 250-300 Hz (Johansson and Westling, 1987; Westling and Johansson, 1987), a digital recursive band pass filter (245-375 Hz, 12 dB) was applied to the input force (FZ), at each time step (Δt = 1 ms). As a consequence of this, the simulated FA II unit shows similar responses to 'vibration' as a human FA II and responded strongest for signals at 300 Hz and then showed smaller response intensities at higher and lower frequencies.

3. To simulate the irregularity in discharges of natural spike trains, noise was added to the calculated response intensity. All units, except SA I, was assumed to show a normal distribution of their interspike intervals and therefore a simple Gaussian noise (normal distribution) was added to their responses (Edin, 1992). Gaussian noise

could be added using standard randomizing routines. In contrast, SA I units show a distribution of their interspike intervals that resembles a Poisson distribution (Edin, 1992).

Since the force ramp throughout all the simulations is the same, the only thing that changes the afferents responses between simulations is the above strategy to apply noise. This means that the afferents respond differently (although small differences) each time they are stimulated, as do a human afferent, since no indentation i.e. deformation of the fingertip, during human manipulations is exactly the same.

4. Finally, spike trains were generated from the response intensity signals by integration; every time the integration of the signal reached above a specified threshold a spike was 'generated' (similar to the action potential of the human receptors), the integrator was reset and the process repeated for the whole simulation. This model does not have an explicit way to simulate the refractory period, i.e. right after the action potential, the cell is not capable to generate a new action potential in a short period of time. However, since the model integrates in order to generate a 'spike', there is a short delay until the area beneath the analog signal reaches the threshold again, this could in some indirect way count as the receptors refractory period.

3.3 Slip correction

Fagergren et al. identified three factors influencing the efficiency of the slip correction (Fagergren et al., 2003):

1. The time development of the motor command (correction profile).
2. The delay between the onset of the grip and load forces (GF-LF-delay). This delay builds up a safety margin before the onset of the LF and makes the grip less sensitive to changes in frictional condition and to external perturbations in the LF.
3. How fast the lift is performed. If an object is picked up slowly, i.e., the load phase duration is long, the fingers will slip less than in a fast lift. This is because the LF rate is lower for a slow lift and, hence, will cause a slower and shorter movement of the fingers at slip.

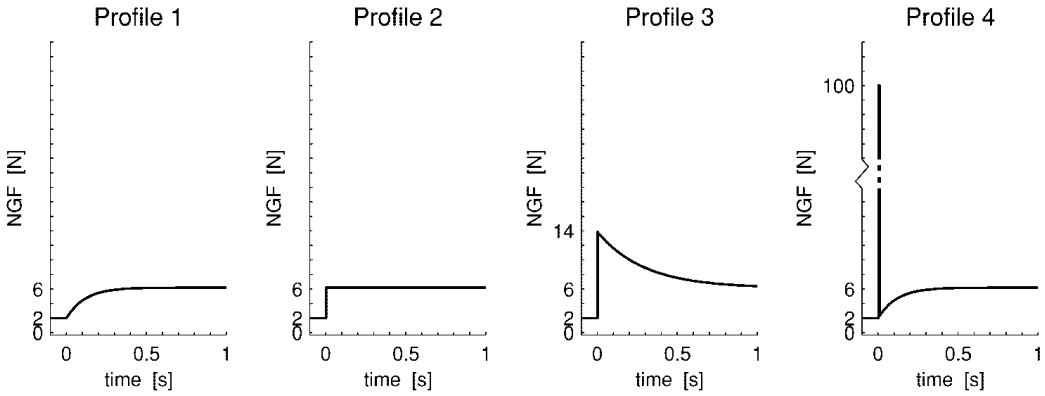

FIG. 3.2: The four correction profiles. Neural grip force (NGF) is the output of the control component of the model, corresponding to the motor commands to the motoneuron pool in the spinal cord. The unit is the Newton (Fagergren et al., 2003).

They tested four correction profiles (fig. 3.2).

It was measured how each parameter affected the ability to stop and prevent a slip. The ability to stop an ongoing slip was indicated by the slip distance when the correction profile was applied. The ability to prevent a slip from occurring was measured by finding the latest time at which the correction profile could be introduced and still preventing slip from occurring. This time defined the *neural correction window* (NCW) as the time window spanning from the first possible moment that the slippery surface could be detected, i.e., at finger contact, to the latest possible time to activate the correction profile and still preventing slip to occur.

Slip stopping

The ability to stop a slip was performed by measuring the slip distance. All three parameters affected the slip distance. The sharper the Correction Profile, i.e., the higher frequencies it contained, the earlier it stopped the slip. Correction Profile 4 was the most efficient because it produced the fastest increase in the GF. It was concluded that the ability to stop an ongoing slip improved with the presence of higher frequency components in the Correction Profile because sharp increase in the input signal resulted in a steeper increase in the output GF. The GF-LF-delay affected the slip

distance. An increase in the GF-LF-delay from 20 to 80 ms increased the slip distance from 3.4 to 6.4 mm. This is because the slip margin is greater for a longer GF-LF-delay. Consequently, for a long GF-LF-delay, the LF and the LF rate were higher when the slip started than for a short GF-LF-delay, which resulted in a greater acceleration of the finger at slip. The Load Phase Duration influenced the slip distance. A slow lift with a Load Phase Duration of 500 ms slipped only 2.0 mm, whereas a fast lift with a Load Phase Duration of 200 ms slipped 8.7 mm.

Slip prevention

The three control parameters influenced the NCW in different ways. As the Correction Profile became sharper, it could be introduced later and still prevent a slip, see Fig. 3.3 A. Profiles 2-4 had a NCW of 46-48 ms, whereas profile 1 only had a 26 ms window, requiring a fast reaction to completely prevent slip. Hence by using Correction Profile 2, 3, or 4, more time for sensory information processing is made available before the correction profile must be introduced. The GF-LF-delay had the strongest influence of all three parameters on the efficiency of slip prevention, see Fig. 3.3 B. A 60 ms increase in the GF-LF-delay (from 20 to 80 ms) increased the NCW by 115 ms (from 7 to 122 ms). Therefore, the longer the GF-LF-delay the greater the probability for preventing a slip. The Load Phase Duration had almost no effect on the NCW as shown in Fig. 3.3 C.

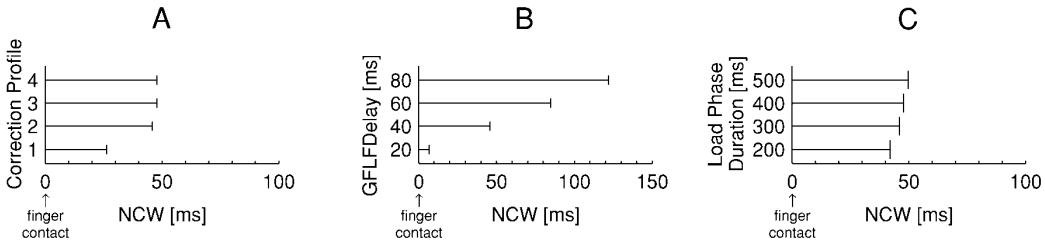

FIG. 3.3: Sensitivity analysis when slip was prevented. The three control parameters' effect on the neural correction window (NCW), indicated by horizontal lines A: Correction Profile is varied. B: GF-LF-delay is varied. C: Load Phase Duration is varied. If a Correction Profile was released within this time window, the slip was prevented. If it was released later, a slip occurred (Fagergren et al., 2003).

The longer the initial slide distance, the greater the probability for pre-

venting a slip. This suggests that the longer the initial slide distance the more evidence is received by the CNS indicating a new friction, and that to delay the LF onset is a strategy that is used to prevent slipping, as proven efficient in the sensitivity analysis. Indeed, the GF-LF-delay decreases during development and is the last parameter (of 8 investigated) to reach the level in adults (Forssberg et al., 1991). For children at 2 years of age, the GF-LF-delay is $\sim$ 120 ms, at 7 years, it is $\sim$ 60 ms, and for adults, it is $\sim$ 40 ms.

In the sensitivity analysis, profile 4 was the most efficient because the slip distance was 30% shorter than the second best profile and it had one of the longest NCWs. In addition, the variance analysis suggested profile 4 as the precision was regained earlier than for profiles 2 and 3. Indeed, the human data confirmed the use of a sharp burst as in profile 4.

CHAPTER 4
THE CONTROL MODEL

We propose a control model and algorithms for each one of the phases of a manipulation process, that emulate the way humans take objects.

4.1 Relevant object's features

The world of possible objects is uncountable. Human beings discriminate objects based on visual and tactile stimuli. Therefore, in order to afford the problem of dexterous manipulation in unknown environments the first step is to identify the features that are useful to discriminate objects. Two relevant features are the *friction* and the *shape* of the object. The friction and the shape of the object at the contact points, influence the slip ratio, which determines the force ratio. Another relevant feature is the *weight*. The weight determines the necessary load force rate to lift the object. Another important feature is the *density*. The density of the object's material is essential to estimate the weight of the object.

4.2 Weight adaptation

The parallel increase in the grip and load forces during the load phase terminates shortly after the object starts to move. Memory information based on previous experiences with the weight of the current object is used to parameterize the force output in anticipation of the weight of the object. Consequently, with an unexpected change to a lighter weight, the load and grip force rates are excessively high when the load force suddenly over-

comes the force of gravity. However, an abruptly triggered termination of the muscle commands driving the load phase takes place some 80-110 ms after lift-off (Johansson and Westling, 1988b). Burst responses in FA II afferents, which effectively indicate that the object has started to move, are most likely used to trigger this. But the delays in the control loop (due to receptor and effector delays, axonal conductances, and CNS processing delays) are still long enough to cause a pronounced position overshoot (a common experience when lifting an unexpectedly light object) (Johansson, 1996b).

If the object is heavier than expected and the lift-off does not occur at the predicted load force, the absence of motion is indicated through the lack of a transient sensory response at the expected moment of lift-off. In this case, the CNS uses the absence of the expected sensory signal to quickly initiate a new control mode. This is characterized by slow, discontinuous increases in force that, in effect, probe for the lift-off. This control mode continues until somatosensory information confirming movement is eventually obtained (Johansson, 1996b).

Hence, whether the object's weight is correctly anticipated or not, somatosensory signals apparently trigger the termination of the load phase and presumably simultaneously update the memory system representation of the weight of the object. Indeed, with erroneous weight anticipation, only one lift is typically required to efficiently update the weight-related memory system (Johansson, 1996b).

Therefore, the human weight adaptation mechanism seems to behave like the following algorithm:

while *(Load Force* $\leq$ *Estimated weight* **and** *FA II = False)* **do**
  `Do in Parallel(`*Fast increase of Load Force* **and** *Test FAII*`);`
end
if *(FA II = False* **and** *Load Force* $>$ *Estimated weight)* **then**
  while *FA II = False* **do**
    `Do in Parallel(`*Little increase of Load Force* **and** *Test FAII*`);`
  end
end

Algorithm 1: Human weight adaptation

With respect to the lifting speed, to get a predictable, smooth and critically

damped vertical lifting movement, the lifting drive must be decreased and appropriately adjusted to match the weight of the object before the moment of lift-off. In fact, with an adequately programmed lift, the first time derivative of the grip and load forces have their maximum when the load force matches about half the weight of the object; the force rates are reduced prior to lift-off to harmonize with the expected weight (Johansson, 1996b). In addition, the desired speed (acceleration) and height of the lifting movement play a significant role in the parametrization of the force output during the isometric load phase (Kinoshita et al., 1993).

The estimation of the object's weight in humans is used to predict the necessary load force rate to lift the object. This estimation increases the velocity of the lifting task. The objective is to place the hand-object system at some reasonable height respect to the subject. In robots there is an important delay in the mechanical execution of a motor command because the mechanical motors are slow. For this limitation, our strategy will be to estimate the weight of the object and apply a load force rate lesser than this estimation, because if the object's weight was underestimated there would be a great overshoot that couldn't be avoided.

4.3 Friction modeling

The first studies on friction can be attributed to Leonardo da Vinci, although it was only with Coulomb in 1785 that a useful formulation of the friction laws was introduced, defining a relationship between the overall friction force f_f opposing the motion of two rigid bodies in contact and the normal force acting between them. The most common and simple description of the friction phenomenon considers two cases, i.e., $static$ and $dynamic$ (or $kinetic$) friction. Let us suppose that an external force f_t parallel to the contact plane is applied to one of the contacting bodies, and that a force f_n perpendicular to the contact plane is present, keeping the bodies in contact. A reaction force f_f due to the friction effect is generated and, in the static case, the following relationship holds between f_f and the normal force f_n:

$$f_f \leq \mu_s f_n$$

where the static friction coefficient μ_s depends on the nature and the smoothness of the surfaces, and with good approximation can be considered independent of the size of the contact area. While the ratio f_t/f_n is less than or equal to the value of μ_s, the force f_f generated by friction is

sufficient to balance any external force f_t and the body does not move. If the external load f_t is increased, the body will eventually start sliding and the friction force f_f, opposing the motion, assumes a new value given by

$$f_f = \mu_d f_n \tag{4.1}$$

where μ_d is the dynamic friction coefficient. In general, $\mu_s > \mu_d$ (Melchiorri, 2000).

Therefore, we assume that the maximum force of friction is μ_sGF, where μ_s is the coefficient of static friction when the relative motion between the hand and the object is zero. When a fingertip slides, the force of friction is μ_dGF in the opposite direction to the velocity. A slip occurs when the force of friction is greater than μ_sGF or when the relative velocity between the hand and object is non-identical. This double condition accounts for the case when the GF is zero (Fagergren et al., 2003). The transition from slip to no slip would occur when the force of friction is less than μ_dGF and the relative velocity is zero, but when the object is moving there is an acceleration, and then although the friction coefficient decreases, more grip force is necessary to counteract the acceleration effect.

The case of rotational friction is more complex than the linear one. In fact, in general, a nonlinear relationship exists between the applied normal force f_n and the torque τ_f. This relationship may be expressed as (Jameson, 1985)

$$\tau_f = 0.59\mu_s\alpha^{1/3}f_n^{4/3} = \beta_s f_n^{4/3} \tag{4.2}$$

where α is a parameter depending on both the geometry and the elastic properties of the contacting bodies, such as the curvatures and the Young and Poisson moduli. Note that the friction coefficient β_s depends on the size of the contact area.

4.4 Shape adaptation

In our model, the force ratio stored in memory, is the force ratio corresponding to an object with parallel flat grip surfaces. When the object is a tapered one, the angle modifies the force ratio.

In section §2.12 it was seen that

NF = HF $\times$ cos(α) - VF $\times$ sin(α)

TF = HF $\times$ sin (α) + VF $\times$ cos(α)

NF = SR $\times$ TF

where SR is the inverse of the friction coefficient (i.e., the slip rate when the object has flat parallel grip surfaces), NF is the normal force, TF the tangential force, HF the horizontal force (grip force), VF the vertical force (load force), and α is the surface angle.

It follows that,

NF = SR $\times$ TF

HF $\times$ cos(α) - VF $\times$ sin(α) = SR $\times$ (HF $\times$ sin (α) + VF $\times$ cos(α))

HF $\times$ cos(α) - VF $\times$ sin(α) = SR $\times$ HF $\times$ sin (α) + SR $\times$ VF $\times$ cos(α)

HF $\times$ cos(α) - SR $\times$ HF $\times$ sin (α) = SR $\times$ VF $\times$ cos(α) + VF $\times$ sin(α)

HF $\times$ (cos(α) - SR $\times$ sin (α)) = VF $\times$ (SR $\times$ cos(α) + sin(α))

$$\Downarrow$$

$$\frac{HF}{VF} = (\text{SR} \times \cos(\alpha) + \sin(\alpha))/(\cos(\alpha) - \text{SR} \times \sin(\alpha))$$

4.5 Initial force ratio

When a human touches an object, he/she increments the grip force during a short time. Depending on the friction coefficient, a different pattern of FA I signals is received (see section §2.8). If the object's material has a great friction coefficient, the FA I signals will have a great frequency. On the contrary, if the object's material has a low friction coefficient, the FA I signals will have a low frequency. At the transitional phase, the required force ratio to lift the object with grasp stability is known. Then, we want to create an association between this force ratio, and the initial pattern of the FA I signals received. To create this association a supervised artificial neural network is used.

To create the initial examples to train the neural network, it is convenient that the objects have parallel plain surfaces, and to take the object by its center of mass. In this way, it is not necessary to care about the curvature effect on the force ratio, or the rotational slips.

At the initial state, the control system has no knowledge about the required force ratio associated to any pattern. After some experiments, the system knows the association between the seen patterns and the corresponding force ratios. When a new pattern is received the system maps

the new pattern into the neural network and gets an initial force ratio. If this force ratio produces slips, then the system will train the neural network to introduce the new pattern and required force ratio association.

4.6 Slip measure

At the loading phase, localized slips are detected by responses in the FA I and SA I units. When the slip is gross there are also answers in the FA II units, because these units respond to vibrations. At the static phase, the presence of a slip is detected by bursts in the FA I and SA I answers. Based on the intensity of these signals, humans graduate the force ratio adjustment. To emulate this mechanism a multilayer perceptron is used, that receives as input simulated afferent signals, and gives as output the percentage of contact nodes that are slipping. The force ratio adjustment is calculated based on the estimation of the percentage of contact nodes that are slipping.

4.7 Vision module

The recognition of materials by computer vision is still a complex and unsolved task. We assume that there is a vision module that can recognize different materials. The vision module must have the following functionalities:

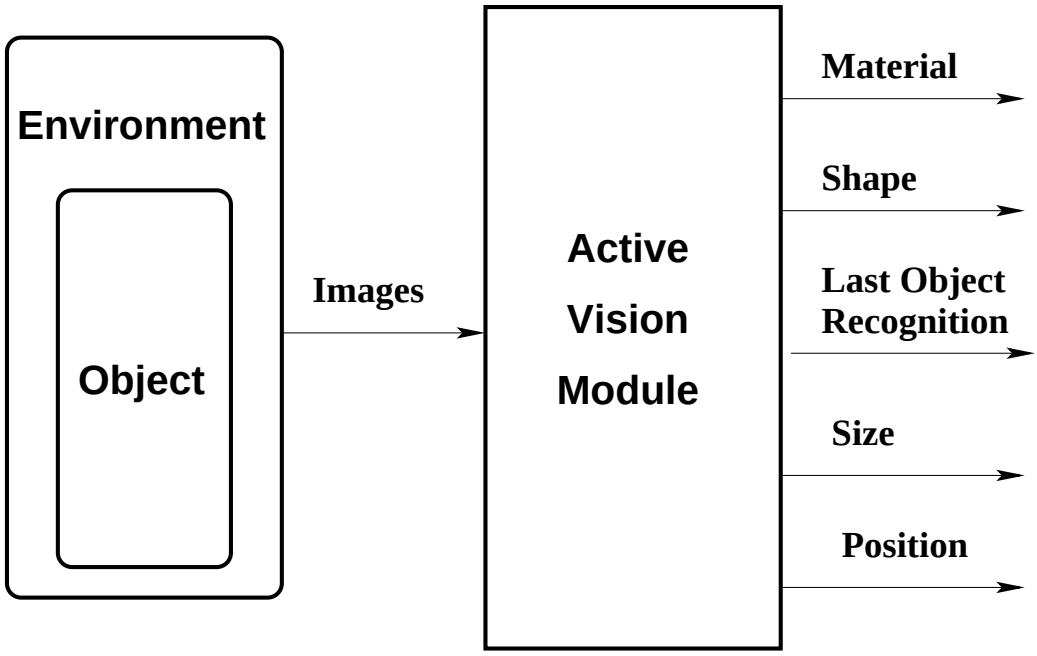

FIG. 4.1: Required functionalities of the Vision Module.

4.8 Memory model

The human memory remembers the force ratio and weight of the last object that has been manipulated (Johansson and Edin, 1993). Thus, in our system, there is a *Short Term Memory*, that stores the information about the force ratio and weight of the last manipulated object. In our system, we include also a *Long Term Memory* whose function is to store a rough estimation of the slip ratio for each known material. The necessary fine adjustments are made during the manipulation process. The whole memory model is seen in fig. 4.2.

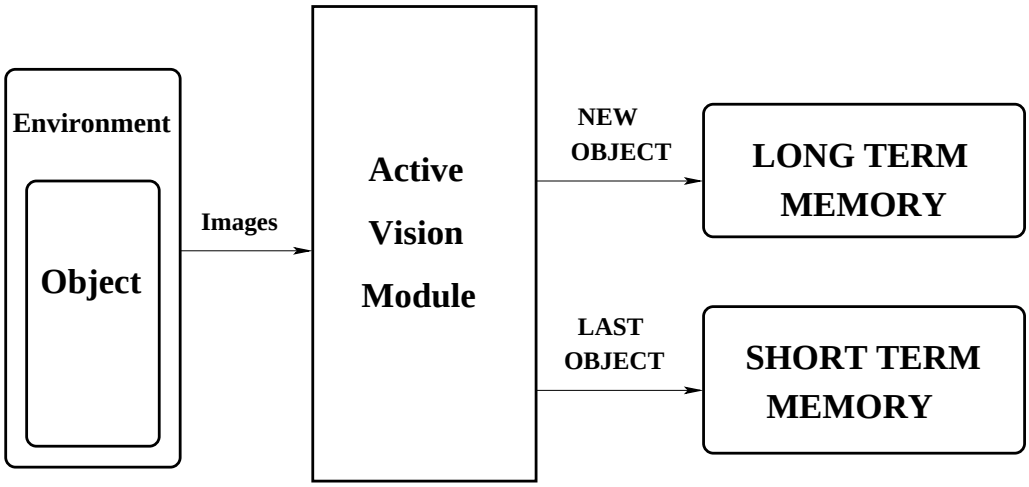

FIG. 4.2: The two memories model.

4.8.1 Short term memory module

The Short Term Memory module keeps the information about the last object that has been manipulated. It is modeled as the following data structure:

- Visual image of the object (for the visual recognition of the object)
- Force ratio
- Object's weight

It is assumed that there is a vision module, that can discriminate if the object to be manipulated, is the same as the last object that has been manipulated.

4.8.2 Long term memory module

The Long Term Memory module is modeled as a growing array of units indexed by the material field. Each unit has 3 fields:

- Material
- Density
- Force ratio

In the presence of an unknown material, a new unit is added to the array memory. The following procedure updates the system to add the new material:

1. Update the Vision Module with the visual features of the new material.
2. Call the control system with a low initial force ratio.
3. Update the Long Term Memory Module with the density and force ratio of the new material.

When the materials are visually undistinguishable, the physical properties stored in memory correspond mainly to the most frequent type of material with those visual characteristics. To achieve this objective, the physical

properties of the materials are updated with a weight factor. For example, to update the friction coefficient of a material m, the following rule is used,

$$friction^m_{new} = k * friction^m_{old} + (1 - k) * friction^m_{last}$$

with $0.9 < k < 1$.

4.9 Control system design

The general design of the control system is shown in fig. 4.3. The object is immersed in an environment. The active vision module takes multiple images of the environment. Then it provides the object's properties needed by the force control module. If the object to be taken is the last object that has been manipulated, the force control module asks for information to the short term memory, else it asks to the long term memory. Note that the proposed control system does not pretend to emulate exactly the human manipulation system. Instead, it is a simplified model of the human manipulation system designed for engineering applications to robotics.

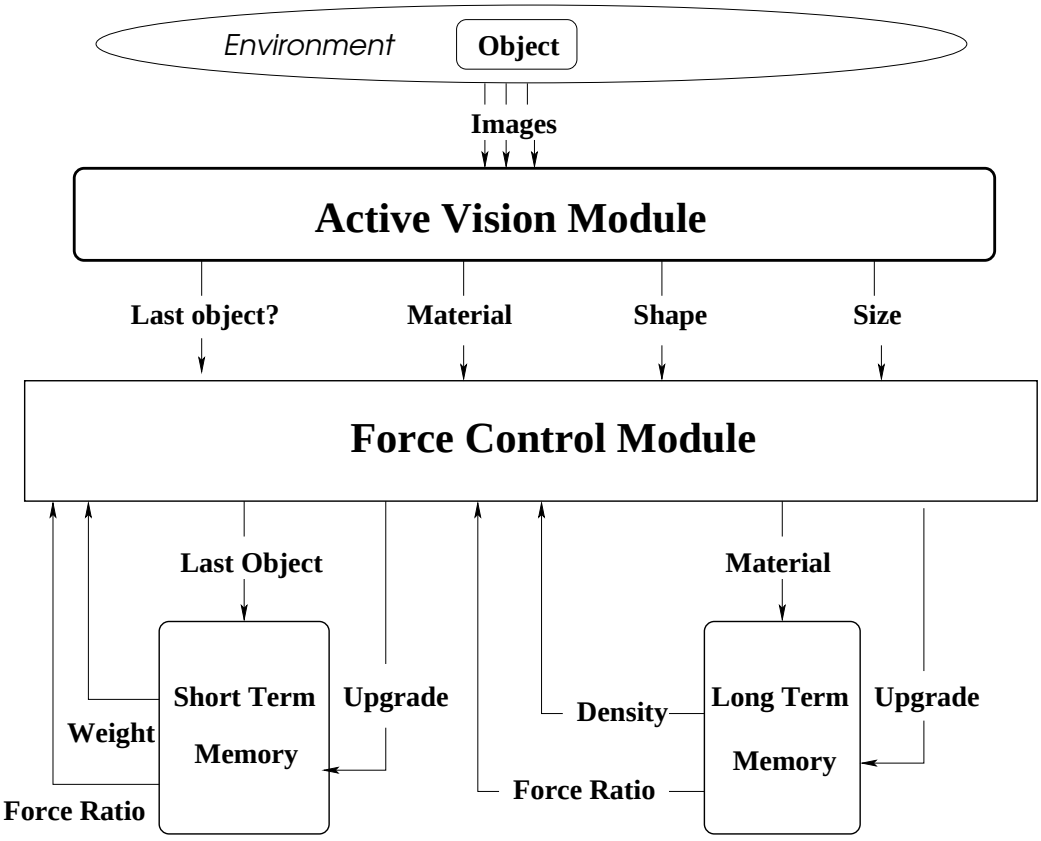

FIG. 4.3: General design of the control system.

The system is a state-dependent control system. In a state-dependent control system the same sensory events, here mechanoreceptor activation caused by small slips, can be used to elicit different actions appropriate for the accomplishment of each phase. The phenomena of state dependent corrections in precision grip tasks was first described by Johansson and Westling (Johansson and Westling, 1984c). When subjects lifted an object with a precision grip, the grip and lift force corrections, in response to a slip between the object and the fingertips, differed between the different phases of the lift. For example, during the load phase the slip correction was a combination of increasing the grip force rate and decreasing the load force rate, but when holding the object in the air the correction was only seen as a fast increase in the grip force.

4.10 The force control module

The module is divided in sections that correspond to the different phases observed in human dexterous manipulation (section §2.4).

Force Control Module:

Input: Force ratio on the thumb's side ρ_t^{memory}, force ratio on the opposing fingers' side ρ_o^{memory}, material density on the thumb's side $density_t$, material density on the opposing fingers' side $density_o$, estimated size of the object $Size$, acceleration of gravity g, surface angle *SurfaceAngle*, initial deformation of the finger *Significant deformation*.

1. ***Initialization***

$GF \leftarrow 0$; $LF \leftarrow 0$;
if $density_t = NULL$ ***or*** $density_o = NULL$ **then**
  $Weight \leftarrow Size$ * $LowDensityValue$ * g;
else
  $Weight \leftarrow Size$ * $\frac{density_t + density_o}{2}$ * g;
end

Algorithm 2: Initialization

First, the grip and load forces are initialized to zero. Then, the weight of the object is estimated based on the size and the density returned

by the vision module. If the object has an unknown material a low value is used as the density of the material.

2. ***Preload phase***

while *Finger deformation* $\leq$ *Significant deformation* **do**
  `Do in Parallel(`*Increase GF, Record FA I signals*`)`
end
if $\rho_t^{memory} = NULL$ ***or*** $\rho_o^{memory} = NULL$ **then**
  $k \leftarrow 1$;
end
$\rho_t \leftarrow k$ * ANN(FA I history)$_t$ + $(1-k)$ * ρ_t^{memory};
$\rho_o \leftarrow k$ * ANN(FA I history)$_o$ + $(1-k)$ * ρ_o^{memory};
`Shape adaptation(`ρ_t, *Surface angle*`);`
`Shape adaptation(`ρ_o, *Surface angle*`);`

Algorithm 3: Preload phase

First, in order to get a representative set of FA I signals, the grip force is increased until a significant deformation of the finger is reached.

Next, the force ratio ρ is estimated as a function of the FA I signals history and the recorded force ratio of the object's material. As seen in section §2.8, the initial responses in the FA-I afferents are considered responsible for the initial adjustment to a new frictional condition because they are influenced by the surface material. The more slippery the material, the higher the FA I discharge rate is at the preload phase (Johansson and Westling, 1987). Thus, based on the intensity of the responses in the FA I afferents, the value of the force ratio can be estimated. This estimation will be improved with the slip events in the next phase. To estimate the force ratio an artificial neural network (ANN) is used that receives as input the FA I signals history (see section §4.5). A weight $0 < k < 1$ is assigned to the ANN force ratio estimation, and the complement weight $(1-k)$ to the force ratio recovered from memory. The current force ratio is estimated as the addition of the former values. If there is no record in the memory for that material, the force ratio estimation is based only on the initial responses of the FA I afferents.

Finally, the Shape Adaptation function adapts the force ratio ρ to the shape of the grip surface. The Shape Adaptation function uses the equation described in section §4.4.

3. ***Loading phase***

while $LF_t \leq \frac{GF}{2}/\rho_t$ ***and*** $LF_o \leq \frac{GF}{2}/\rho_o$ ***and*** *Lift Off = False* **do**
  `Do in Parallel(`*Test Lift-off, Test Slip, Increase* LF_t*, Increase* LF_o`)`
end
while $(LF_t+LF_o) \leq k_{mec}$**Weight* ***and*** *Lift Off = False* **do**
  if $(LF_t+LF_o) \leq (k_{mec}*Weight)/2$ **then**
    `Do in Parallel(`*Test Lift-off, Test Slip, Parallel increase of GF and LF at increasing velocity*`)`
  else
    `Do in Parallel(`*Test Lift-off, Test Slip, Parallel increase of GF and LF at decreasing velocity*`)`
  end
end
while *Lift Off = False* **do**
  `Do in Parallel(`*Test Lift-off, Test Slip, Burst increase of GF and LF*`)`
end

Algorithm 4: Loading Phase Algorithm

At this phase, the forces are increased in parallel preserving the force ratio estimated at the preload phase (i.e., $LF_t \leq \frac{GF}{2}/\rho_t$ and $LF_o \leq \frac{GF}{2}/\rho_o$), until the object lifts off. First, the load force is increased to make it proportional with the grip force. Next, the grip and load forces are increased in parallel, until the load force reaches the estimated weight of the object, or the object lifts off. The constant k_{mec} < 1 is a factor introduced to lower the value of the weight, in order to avoid a force overshoot, due to the delay of the robot's mechanical motors to stop the arm. Finally, if the estimated weight is lesser than the actual object's weight, the third loop is entered. At this loop, burst parallel increases of the grip and load forces are made until the object lifts off, as seen in humans.

To detect the lift-off and slip events, we follow closely the methodology observed in the human tactile system. In our model, the lift-off and slip events are signalled by simulated afferent responses, that correspond with the afferent responses that signal these events in humans.

The lift-off is detected by the presence of FA II responses and the absence of FA I and SA I responses. Thus, the lift off event is detected in the following way:

Test FA II, SA I, FA I Signals;
if *Strong FA II signals* ***and*** *FA I and SA I signals near null* **then**
  Lift Off $\leftarrow True$
end

Algorithm 5: Test Lift-off

In humans, the slips are signalled by sudden changes in the load force between the thumb and the opposing fingers, and by discharges of FA I, SA I, and eventually FA II mechanoreceptors. The slip events fire force ratio corrections. If there are responses of the FA I, SA I and FA II afferents, then the force ratio upgrade will be larger than if there were only responses of the FA I and SA I afferents (i.e., a localized slip). If there are only responses of the FA II units, then the vibration will not be recognized as slip, and therefore it will not trigger upgrades of the force ratio (Johansson and Westling, 1987). In our model, an artificial neural network is used to estimate the intensity of the slip. The neural network receives as input the FA I, SA I, and FA II signals, and gives as output the intensity of the slip. The intensity of the slip indicates the percentage of contact nodes that are slipping, and it is measured as a number in the interval $[0...1]$. The test slip function checks if there are slip events. If there were significant slip events it calls the slip correction function:

Slip Intensity $\leftarrow$ ANN (FA I, SA I, FA II);
if *Slip Intensity* $>$ *Threshold* **then**
  Call Slip Correction (GF, LF_t, LF_o, ρ_t, ρ_o, *Slip Intensity*);
end

Function: `Test Slip`

The function *Slip Correction* adjusts the force ratio based on the intensity of the slips. Slips are stopped with a burst increase of the grip force as in Fagergren, Ekeberg, and Forssberg (2003). A factor $0.75 \leq k_{SlipIntensity} \leq 1$ that depends on the slip intensity multiplies the grip force adjustment. After the burst increase of the grip force, the grip force is decreased to an appropriate value. When grasping objects, humans readily identify the minimum force required to prevent slipping and maintain a safety margin of 10% - 30% (Johansson and Westling, 1984a). In our model, a safety margin is added to the force ratio also. The safety margin will depend on the sensor system (i.e., if it is a good sensor system, a margin of 20% could be enough, but if it is a poor sensor system, a larger safety margin should be used).

GF $\leftarrow$ 2.0 * $k_{SlipIntensity}$ * GF;
GF = GF * (1 + Slip Intensity + Safety Margin);
$\rho_t \leftarrow \frac{GF}{2}/LF_t$;
$\rho_o \leftarrow \frac{GF}{2}/LF_o$;

Function: `Slip Correction(`GF, LF_t, LF_o, ρ_t, ρ_o, *Slip Intensity*`)`

4. ***Transitional phase***

while *Height of Hand* $<$ *Desired Height* **do**
  `Do in Parallel(`*Test Slip under Gravity, Parallel increase of the GF and LF at low velocity*`)`
end
$GF_{old} \leftarrow GF$;
$GF \leftarrow k * GF$;
Stop upward movement of the arm;
$GF \leftarrow GF_{old}$;

Algorithm 6: Transitional phase

At the transitional phase, the hand moves vertically until it reaches the desired height. First, the grip and load forces are increased in parallel until the desired height is reached. In humans there is a grip

force increase at the end of the parallel coordination of the forces during manipulation (see section §2.5, Fig. 2.3). Thus, just before stopping the upward movement, the grip force is increased by a factor $k > 1$, to prevent that the object slips out by the sudden stop of the upward movement. Then, the arm is stopped. Finally, the original value of the grip force is restored.

At the transitional phase the hand is in an upward movement towards the desired height. As the object is no more on the table, if there is a slip, only the grip force should be modified (see section §2.9). To estimate the slip intensity an artificial neural network (ANN) is used, that receives as input the FA I and SA I signals, and gives as output the slip intensity.

Slip Intensity ← ANN (FA I, SA I);
if *Slip Intensity* > *Threshold* **then**
  Call Slip Correction (GF, LF_t, LF_o, ρ_t, ρ_o, *Slip Intensity*);
end

Function: `Test Slip under Gravity(`GF,LF,ρ_t,ρ_o, *FA I, SA I*`)`

5. ***Static phase***

   In the static phase the object is held in the air and it is moved horizontally towards the new position.

while *Goal position arrival = False* **do**
  `Do in Parallel(`*Test Slip under Gravity, Translate object*`)`
end

Algorithm 7: Static phase

6. ***Replacement and Unloading phase***

   At this phase the object is moved downward until it contacts the table top. Then it is released. First, the load force value is saved into the $Weight$ variable. The weight is saved at this moment, and not at the moment of lift-off, because at this phase the object is held in the air and there is a stable load force (at the moment of lift-off there is an increasing load force value caused by the acceleration). Next,

the arm goes down until the object contacts the table. The contact table event is detected by a burst signal of the FA II afferents. Then, there is a sudden reduction of the load force, to set the object on the tabletop. In human manipulation, this reduction of the load force is about 80%. In humans, there is a short delay between the contact table event and the parallel decrease of the forces. We incorporate a short delay too, whose goal is to stabilize the object on the table. After this wait follows a parallel decrease of the forces, that causes the release of the object. Finally, the memory is updated. The *slip condition* parameter is a measure of the number and intensity of the slips.

$Weight \leftarrow LF$;
repeat Go down the arm at slow velocity **until** *Contact Table = True*;
LF $\leftarrow$ k*LF;
Wait a time t;
repeat Parallel decrease of GF and LF at great velocity **until** *Object Release*;
if $Material_t$ = $Material_o$ **then**
  Density $\leftarrow$ $\frac{Weight}{g}$ / Size;
else
  Density $\leftarrow$ Null;
end
`Update memory` ($Material_t$, $Material_o$, Density, ρ_t, ρ_o, Slip condition, Fragility);

Algorithm 8: Replacement and Unloading phase

4.11 Discussion

The control algorithms presented in section §4.10 are strongly inspired in neurophysiological studies of the human dexterous manipulation presented in chapter 2. Algorithms for each one of the human manipulation phases are given. These algorithms are sufficient algorithms, designed to follow as nearly and simply as possible the human way to manipulate objects.

However, a future work is to implement the algorithms on a real robot with strong real time constraints. Therefore, it would be a critical and

very important future analysis to study what are the most sensitive parameters of the proposed algorithms, if there were simplest algorithms for a robotic implementation, and to see how the algorithms would perform under partial failure or ambiguous information.

The general design of the control system of fig. 4.3 summarizes neurophysiological studies of the human dexterous manipulation from a computer science perspective. The proposed control system does not emulate exactly the highly complex human manipulation system. Instead, it is a simplified model of the human manipulation system designed for engineering applications. However, it has a very strong biological inspiration, and it's designed to achieve a dexterous manipulation in unknown environments, very closely as humans do. Recall from section §2.6 that in humans vision provides information on object position, object size, object shape, and object material, and based on visual estimates of weight and friction, a set of tactile responses is predicted to guide planning for the application of initial grip force to the object. Tactile perceptions of weight and texture are fed back and compared to the predicted weight and texture. The mismatch is used to update memory representations of weight and texture for a specific object appearance. This memory is assumed to be retrieved on later occasions to guide anticipatory application of forces (Gordon et al., 1993). Thus, the proposed computational model of fig. 4.3, is very similar to a human dexterous manipulation model. Also, it has a memory of the previous lift, as humans, and a long-term memory.

The recognition of objects by computer vision is a well-developed field, but the recognition of materials has been studied rather little. The proper recognition of the material by the vision module of section §4.7, is an essential information to estimate visually the weight and friction of an object. However, the proposed model would work the same in the absence of vision. Let's suppose that the weight and the friction of the object can't be estimated visually. The force control module of section §4.10 is robust in the absence of vision, because in the face of an unknown material, the algorithm starts with a null force ratio in memory, and uses only the FA I signals to set the force ratio. The slip signals will adjust later the force ratio. And in the absence of weight information, the algorithm starts with a low weight value, and increases the forces until it receives the FA II signal of lift-off.

CHAPTER 5

SIMULATION

THe estimation of the friction coefficient and the detection of the incipient slipping were simulated. These are the two crucial events behind the dexterous manipulation in unknown environments.

5.1 Finite element modelling

The part of the finger to be modeled is shown in fig. 5.1. Contact between an elastic finger with a curved surface and an object with a flat surface was analyzed using the finite element method (FEM). Finite element code MSC.Marc 2005 release 2 was used to create a 3-D model of the finger. First, a finite element plane model of the finger of radius 100 and lateral edge height of 36.6 as in Maeno et al. (2004) was generated (fig. 5.2). Then, the model was expanded in the Z-axis direction, and a 3-D model of a generic fingertip was obtained (fig. 5.3).

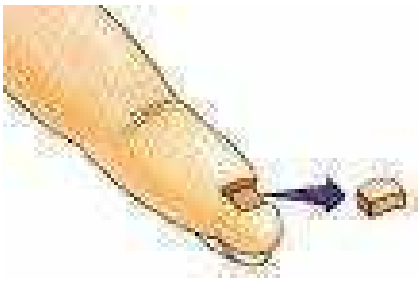

FIG. 5.1: Part of the finger to be modeled by the finite element method (picture extracted from Israelsson (2002)).

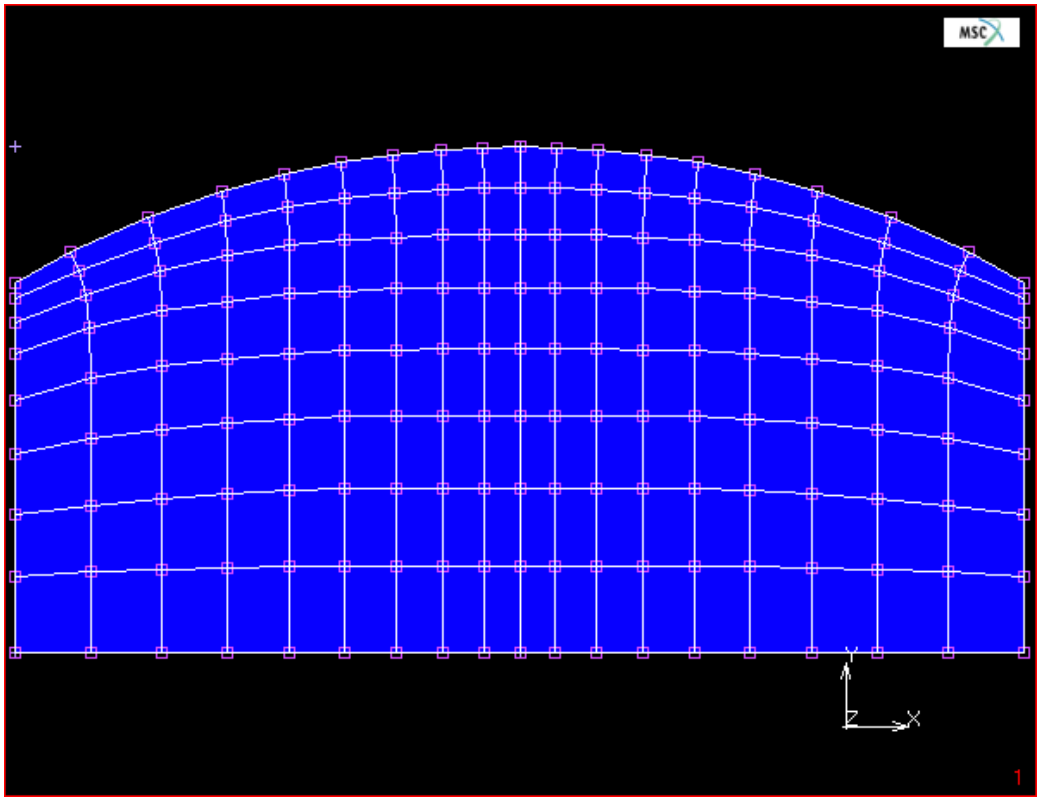

FIG. 5.2: Planar model of the fingertip.

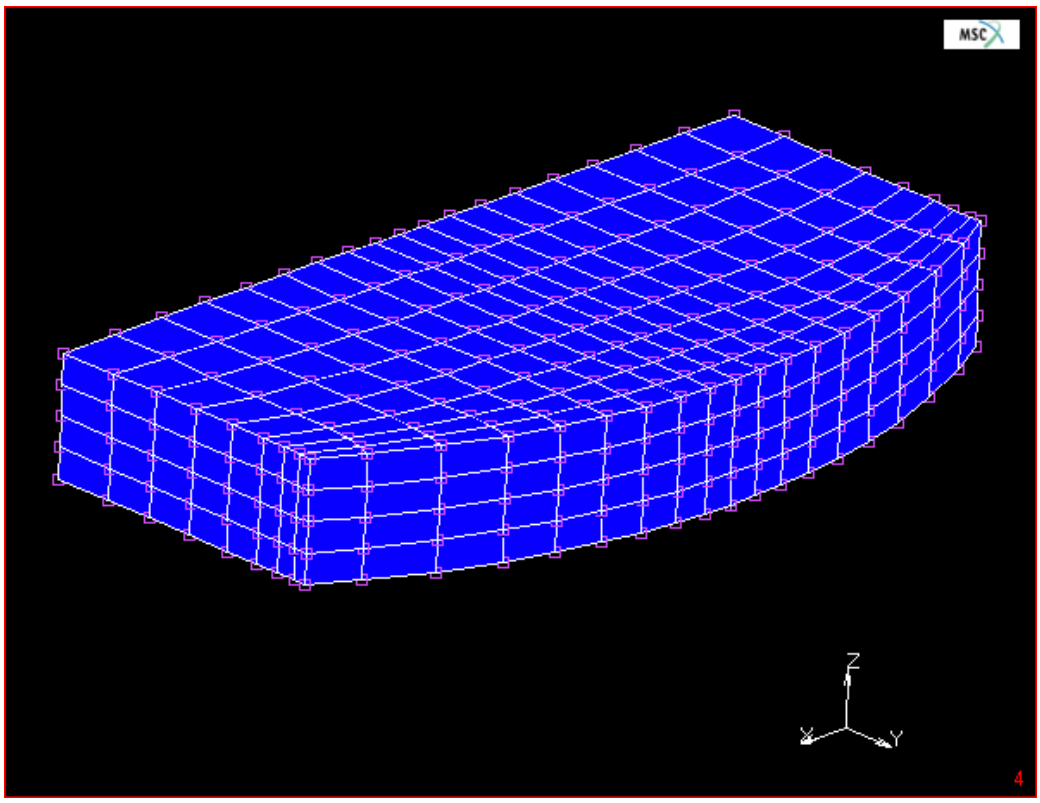

FIG. 5.3: 3-D model of a generic fingertip.

The skin was modeled as a linear isotropic elastic material, for which two constants (elastic modulus and Poisson's ratio) need to be specified. Since soft tissues are generally considered incompressible owing to their predominant fluid content, the Poisson's ratio was assumed to be 0.48, close to the theoretical limit of 0.5 (North and Gibson, 1978; Srinivasan et al., 1992; Vossoughi and Vaishnav, 1979). The elastic modulus was assumed to be 0.18 MPa (Dandekar et al., 2003).

5.2 Friction coefficient estimation

The afferent responses were obtained adapting software code of the Israelsson's human afferent simulator program. *Matlab 7* modules were programmed to process the output of the *MSC.Marc*, and artificial neural networks were programmed to process the output of the Israelsson's afferents simulator. Thus, our software contribution consists of designing the FEM model, programming the simulated experiments using the FEM model, formatting the output of the FEM model to be feeded to the Israelsson's afferent simulator program, and processing the output of the Israelsson's afferent simulator program with artificial neural networks to obtain the friction coefficient (Fig. 5.4).

FIG. 5.4: Block diagram of the software modules.

As seen in Sect. §2.8, the initial responses in the FA I afferents are considered responsible for the initial adjustment to a new frictional condition. As humans estimate the friction coefficient pressing their fingers against the object of interest (Johansson and Westling, 1987; Westling and Johansson, 1987), in this work the friction coefficient was estimated pressing the simulated finger against the surface of the object. The grip force is increased until a representative proportion of the finger is deformed. In this way, there will be a sufficient amount of afferent signals to infer the friction coefficient. This experiment was repeated for various friction coefficients. The force sensors of the finger return the values of the normal and tangen-

tial forces. These force values are used to simulate the afferent responses as seen in section §3.2. Thus, as the grip force of the finger against the object is raised incrementally, simulated FA I responses are obtained. A supervised artificial neural network is then used to estimate the friction coefficient, analyzing the simulated FA I responses for the different friction coefficients.

The input pattern for the neural network was built joining the simulated FA I afferent answers obtained for all the normal force increments. The input pattern is built only with the afferent answers of the sensors situated along one half of the central longitudinal line of the fingertip, because when the object is flat similar outputs are generated on the other rows, and the same values in modulus are obtained on the other half (fig. 5.12 and 5.13). The friction coefficient was used as target of the neural network. To improve the learning capacity of the neural network the patterns of the spike answers of the FA I afferents were compressed. The compression step consisted of choosing a compression factor c, dividing each one of the afferent answer patterns of size s obtained for each node of interest, where s is the number of grip force increments, in $\lceil \frac{s}{c} \rceil$ consecutive intervals, and adding the spike responses at each interval.

A multilayer perceptron with 1 hidden layer was trained, which received as input the compressed pattern of FA I spike signals, and gave as output the estimated friction coefficient. It must be remarked that the input signal is a compressed spike train, and the output, the friction coefficient, is a continuous value. The activation function in the hidden layer was chosen to be a sigmoidal function in the form of a hyperbolic tangent for its convenient antisymmetric property. The output layer activation function was chosen to be linear, because the friction coefficient could be in principle any positive value.

For its fast convergence, the Levenberg-Marquardt algorithm was chosen as the minimization method to train the network. The training parameters for the Levenberg-Marquardt algorithm in the Neural Networks package of *Matlab 7.0* are `epochs`, `show`, `goal`, `time`, `min_grad`, `max_fail`, `mu`, `mu_dec`, `mu_inc`, `mu_max`, and `mem_reduc` (Demuth et al., 2007). The training status is displayed for every `show` iterations of the algorithm. The other parameters determine when the training stops. The training stops if the number of iterations exceeds `epochs`, if the performance function drops below `goal`, if the magnitude of the gradient is less than `mingrad`, or if the training time is longer than `time` seconds. The `max_fail` parameter, which is associated with the early stopping

technique, was not used. The parameter `mu` is the initial value for the learning rate. This value is multiplied by `mu_dec` whenever the performance function is reduced by a step. It is multiplied by `mu_inc` whenever a step would increase the performance function. If `mu` becomes larger than `mu_max`, the algorithm is stopped. The parameter `mem_reduc` is used to control the amount of memory used by the algorithm . The following parameters were used: `epochs=100`, `show=5`, `goal=1e-5`, `time=Inf`, `min_grad=1e-10`, `mu=0.001`, `mu_dec=0.7`, `mu_inc=1.05`, `mu_max=1.04`, and `mem_reduc=1`.

Maeno et al. (Maeno et al., 2004) used finite element analysis to calculate the deformation of an elastic finger, contact forces, and strain distribution inside the elastic finger for various friction coefficients between the finger and the surface. Their results show that the shear strain differs when the friction coefficient differs. Then they used strain sensors to estimate the friction coefficient. In this work, we use finite element analysis as in Maeno's work to simulate a finger and an object, but we don't estimate the friction coefficient based on the shear strain. Instead, we estimate the friction coefficient based on simulated human afferent signals because we intend to follow a bio-inspired approach.

The width of the finger was only of 2 elements (fig. 5.5) because when the object is flat transversal planes of the finger generate similar signals. The FEM model consisted of 288 elements and 513 nodes.

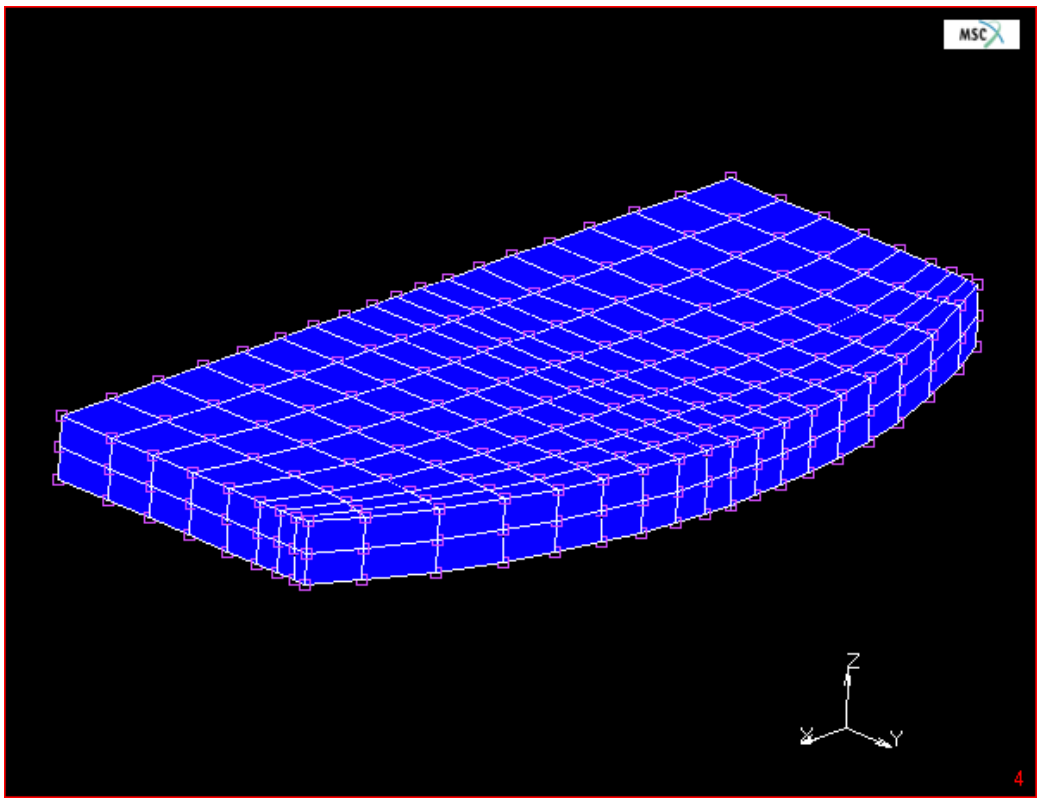

FIG. 5.5: 3-D finite element model of the finger.

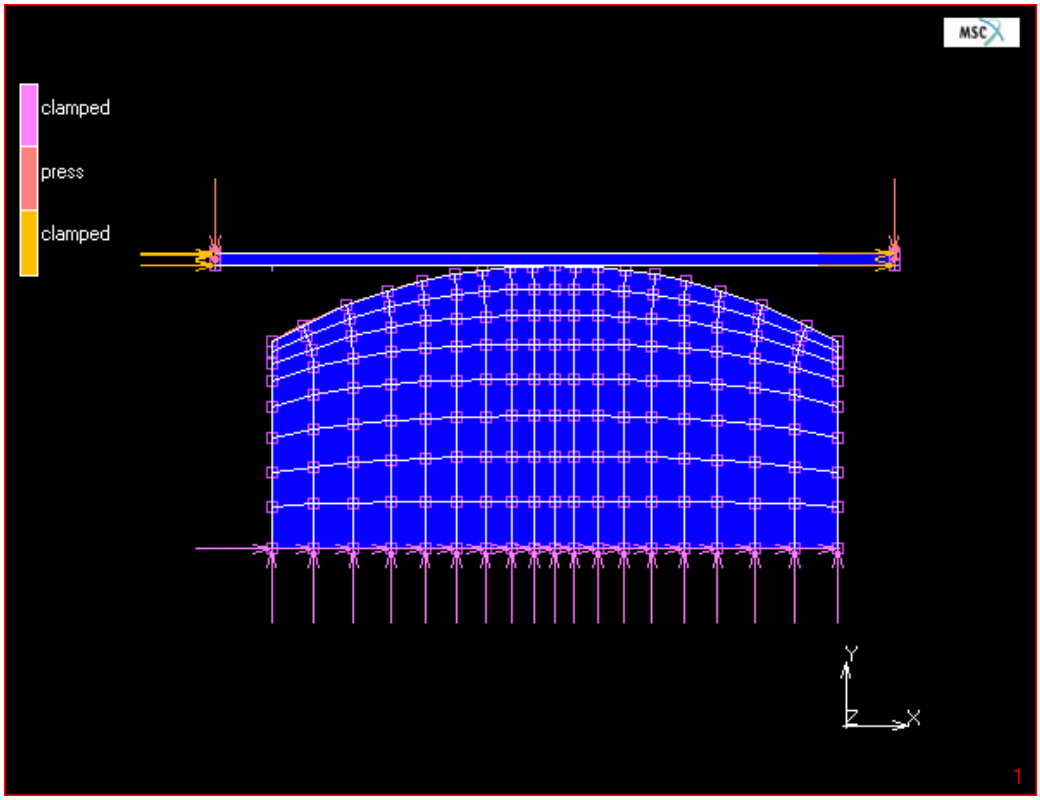

FIG. 5.6: Boundary conditions and initial state.

The experiment to estimate the friction coefficient consisted of moving down the object 10 units along the y-axis, while recording the nodal stress tensors at the surface of the fingertip. The nodes of the finger at y=0 (i.e., the nodes situated at the finger's base) were constrained in the $x-$, $y-$ and $z-$directions, to avoid the displacement of the finger. The nodes of the object were constrained in the $x-$ and $z-$directions (fig. 5.6). Thus, normal load was increased moving the object towards the finger. The object was displaced 0.1 units along the y-direction until the total displacement reached 10 units (Figs. 5.8, 5.9, 5.10, and 5.11). In this way, data for 100 increments was obtained. The stress tensor has 9 components (fig. 5.7). In the designed experiment, the normal force is F_y (σ_y - 2nd. component of stress) and the tangential forces are F_x (τ_{yx} - 4th. component of stress) and F_z (τ_{yz} - 5th. component of stress). The normal and tangential forces were then obtained from the stress tensors.

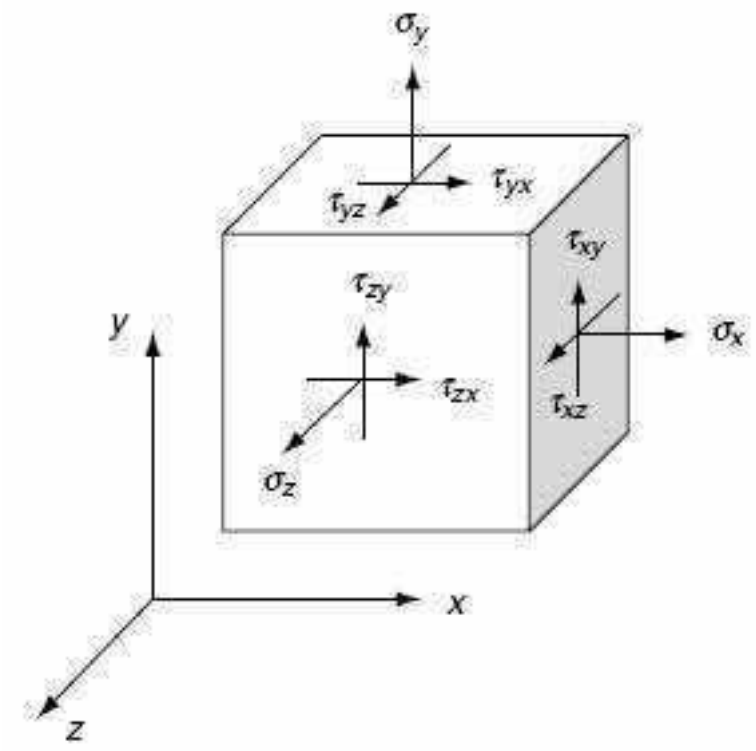

FIG. 5.7: Components of the stress.

In the fingertip there are 3 rows of 19 nodes (fig. 5.5). As shown by fig. 5.8, 5.9, 5.10, 5.11, 5.12, 5.13 and 5.14 the signals are symmetrical. Therefore,

only the signals of the 10 nodes that are on the right half of the central line of the finger in contact with the object were recorded.

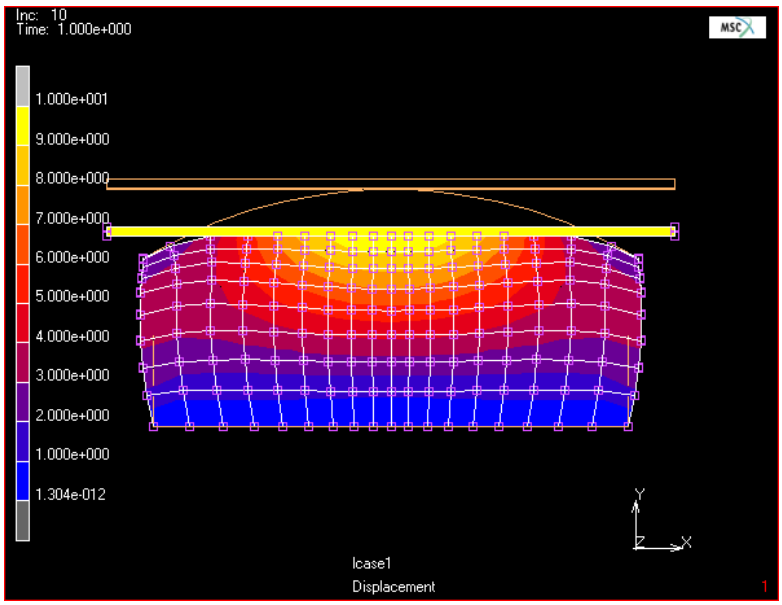

FIG. 5.8: Contour bands of the displacements at the final state. The image shows the original and final shapes of the finger and the object.

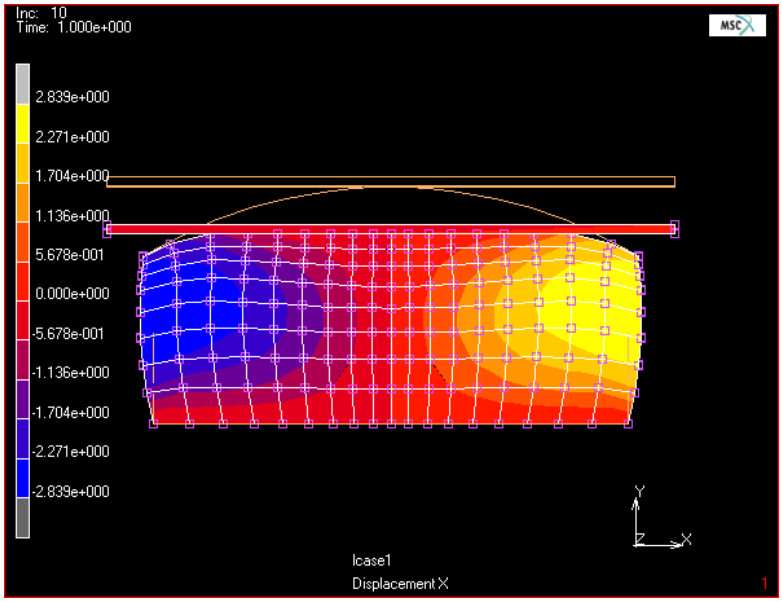

FIG. 5.9: X-Displacements at the final state.

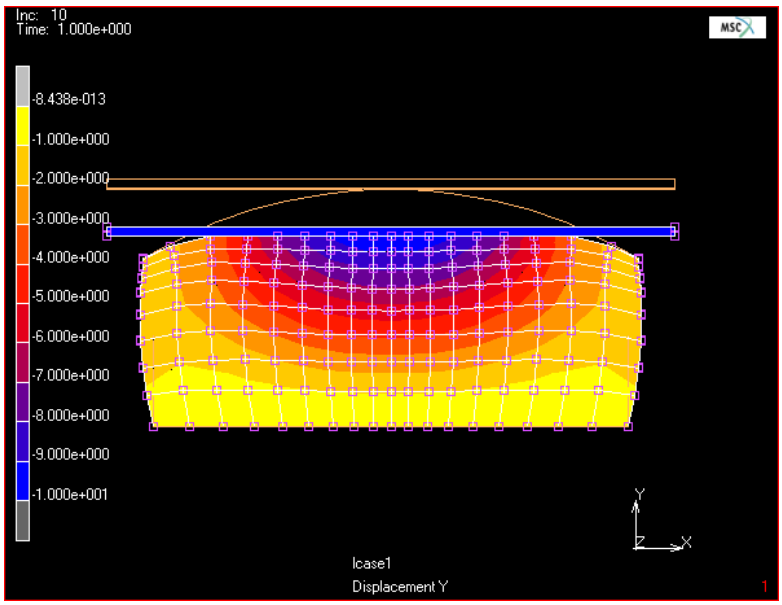

FIG. 5.10: Y-Displacements at the final state.

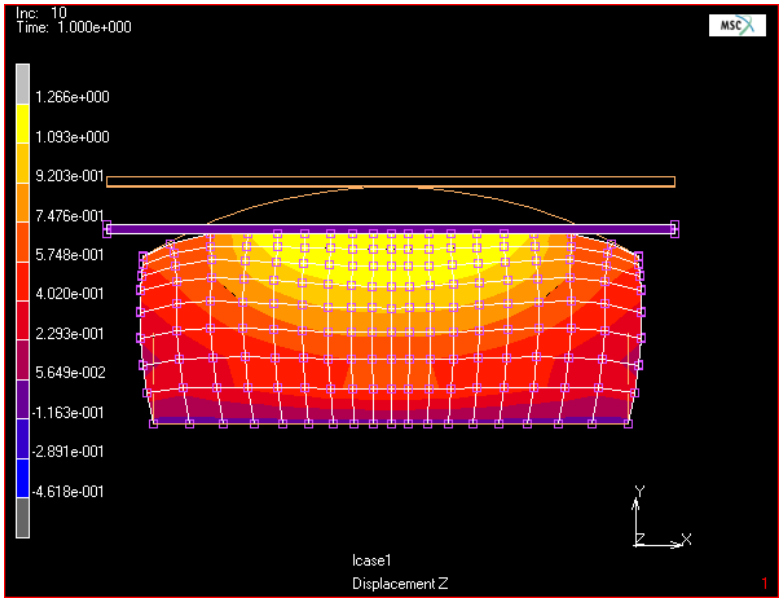

FIG. 5.11: Z-Displacements at the final state.

The whole experiment was repeated increasing the friction coefficient μ of the object's material in the FEM model from 0.01 to 1.00 (with a step size of 0.005). The F_x, F_y and F_z values were measured for each friction coefficient at each increment step. The obtained force values at the final state for different friction coefficients are shown in Figs. 5.12, 5.13 and 5.14. The normal force distribution F_y is always semi-circular because the finger is curved. The obtained curves for the normal force are similar (Fig. 5.12). The tangential reaction forces, i.e. the friction forces, have a local minimum and a local maximum. The sum of the tangential force F_x is always zero because no movement of the surface in the x-direction is applied (Fig. 5.13). However, the shapes of the curves change as the friction coefficient is increased. These results are in accordance with the results obtained by Maeno et al. (Maeno et al., 2004) for their 2-D FEM model of the finger. Finally, the sum of the tangential force F_z is always zero because no movement of the surface in the z-direction is applied. The slope of the curves of the tangential force F_z decreases as the friction coefficient increases (Fig. 5.14).

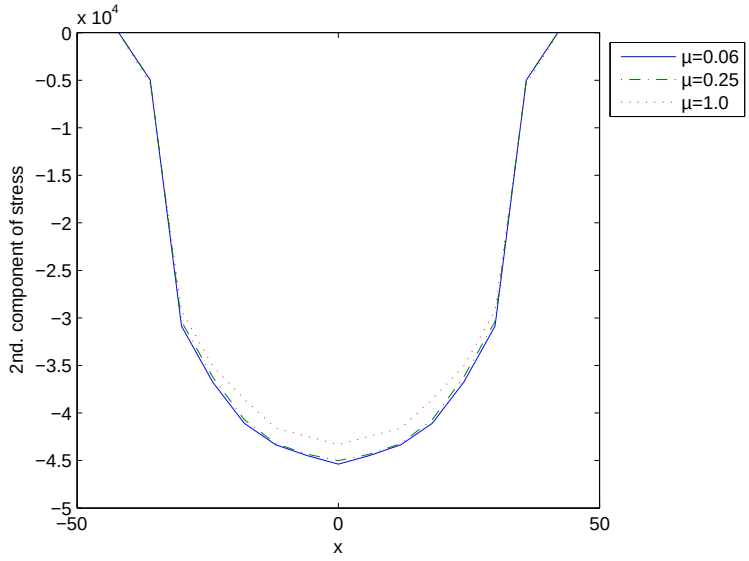

FIG. 5.12: Normal force F_y (2nd. stress component) in the final state along the central longitudinal line of the fingertip's surface.

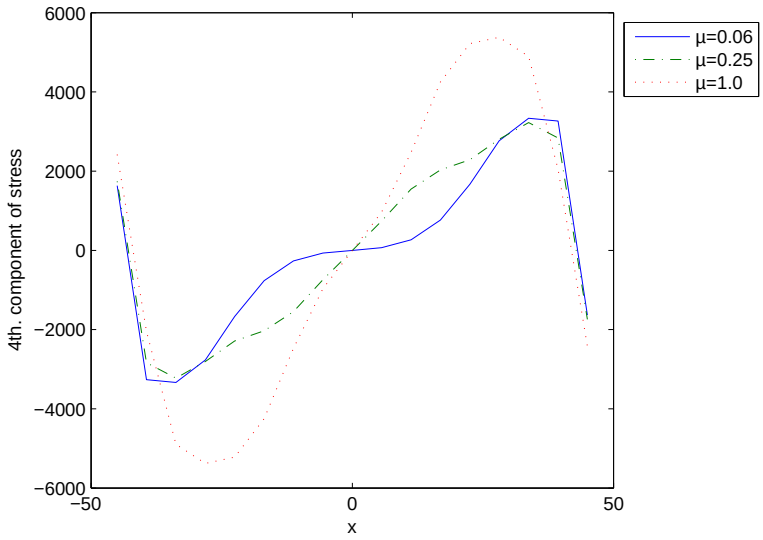

FIG. 5.13: Tangential force F_x (4th. stress component) in the final state along the central longitudinal line of the fingertip's surface.

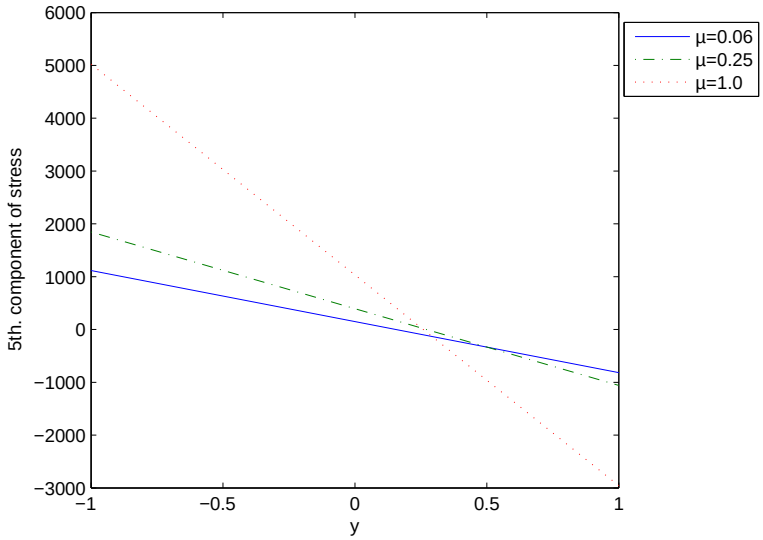

FIG. 5.14: Tangential force F_z (5th. stress component) in the final state along the central transversal line of the fingertip's surface.

Therefore, for each simulated friction coefficient, measures of the F_x, F_y and F_z force values at each increment were obtained. The values of the FA I signals at each node and at each increment were then simulated using the method explained in section §3.2. For each simulated friction coefficient, a vector of dimension 100 (because there were 100 grip force increments) with 0 and 1 values (0 if there was not spike and 1 if there was a spike) corresponding to the FA I answers was obtained for each node of interest. The obtained spike patterns were compressed with a 10:1 compression ratio. The patterns were then preprocessed to normalize their mean and standard deviation in order to improve the training's performance of the neural network. The friction coefficient was used as target of the neural network.

As the experiment was repeated changing the friction coefficient from 0.01 to 1.00, with a step size of 0.005, 200 input patterns were generated. A random partition of this set was done, in which the 90 percent of the patterns was chosen as training set and the remaining 10 percent as testing set. Multilayer perceptrons with different numbers of units in the hidden layer were trained and tested, and a multilayer perceptron with 1 hidden layer of 3 neurons obtained the best performance (Fig. 5.15). At the final state, the mean squared error of the training set was 0.0025 and its mean absolute error was 0.0373. The mean squared error of the testing set was 0.0118 and its mean absolute error was 0.0853. The obtained performance of the neural network for the training and testing sets is shown in Fig. 5.15. The regression analysis between the network response and the corresponding targets is shown in Fig. 5.16. The m and b correspond to the slope and the y-intercept of the best linear regression relating targets to network outputs.

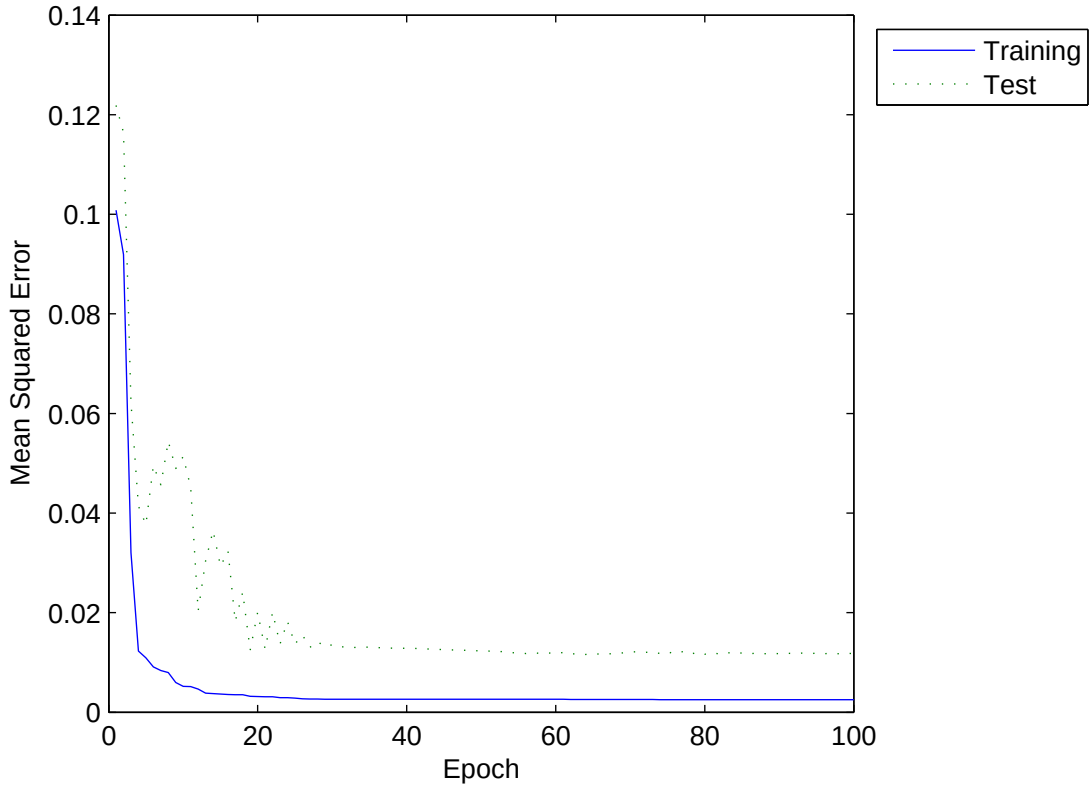

FIG. 5.15: Performance of the multilayer perceptron (the shown results are the values obtained from the second epoch).

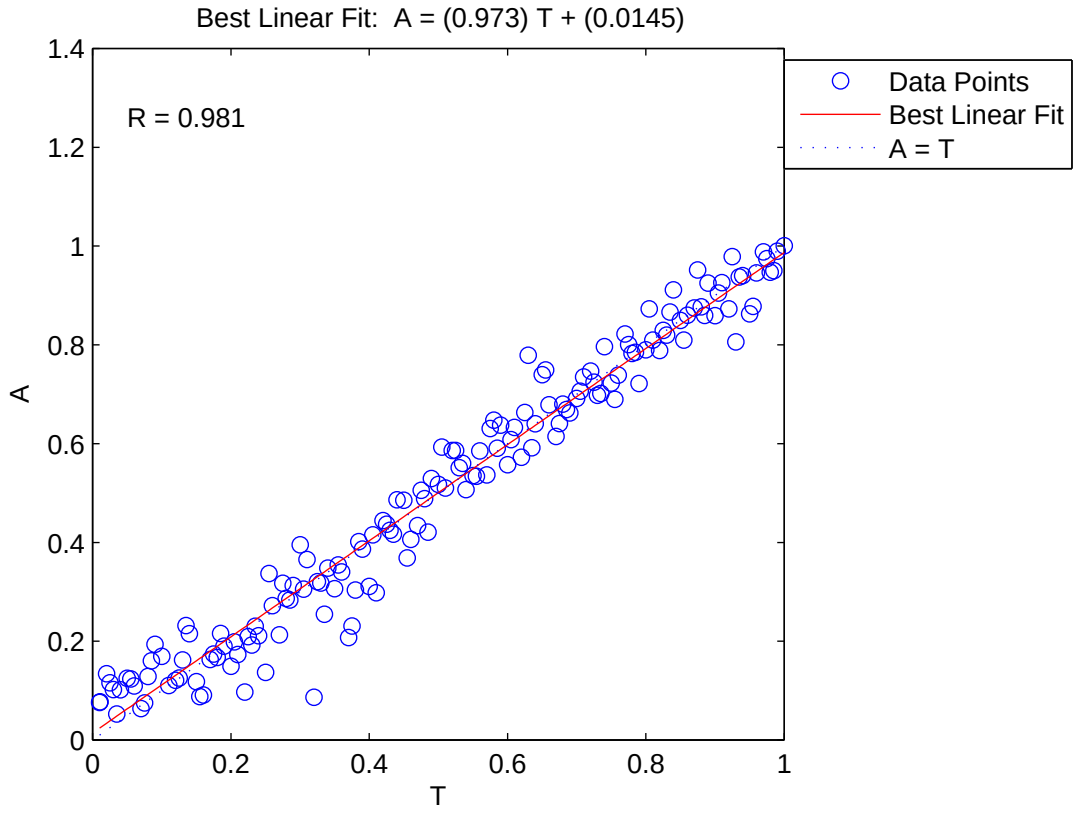

FIG. 5.16: Regression analysis corresponding to the friction coefficient estimation between the network response (A) and the corresponding targets (T). The best linear fit is indicated by a dashed line. The perfect fit (output equal to targets) is indicated by the solid line. In this figure is difficult to distinguish the best linear fit line from the perfect fit line because the fit is so good.

5.3 Incipient slip detection

Contact between an elastic finger with a curved surface and an object with a plane surface was analyzed using the finite element method (FEM). Finite element code *MSC.Marc release 2* was used to create a 3-D model of two fingers and an object. To simulate the FA-I afferent responses, we adapted software code provided by Anna Theorin (f. Israelsson), Lars Rådman, Benoni Edin and Roland Johansson of Umeå University. Israelsson Israelsson (2002) designed a computational simulator of the responses of the afferents from the glabrous skin during human manipulation. Thus, the afferent responses were obtained adapting software code of the Israelsson's human afferent simulator program. *Matlab 7* modules were programmed to process the output of the *MSC.Marc*, and artificial neural networks were programmed to process the output of the Israelsson's afferents simulator. Thus, our software contribution consists of designing the FEM model, programming the simulated experiments using the FEM model, formatting the output of the FEM model to be feeded to the Israelsson's afferent simulator program, and processing the output of the Israelsson's afferent simulator program with artificial neural networks (Fig. 5.4).

FIG. 5.17: Block diagram of the software modules.

Three deformable contact bodies were modeled: left finger, right finger and object (fig. 5.18, 5.19 and 5.20). The table was modeled as a rigid body at the bottom. The object was modeled as a unique block element. The Poisson's ratio of the object was set at 0.48 and the Young modulus at 0.72 MPa. Therefore the object was almost incompressible and harder than the finger.

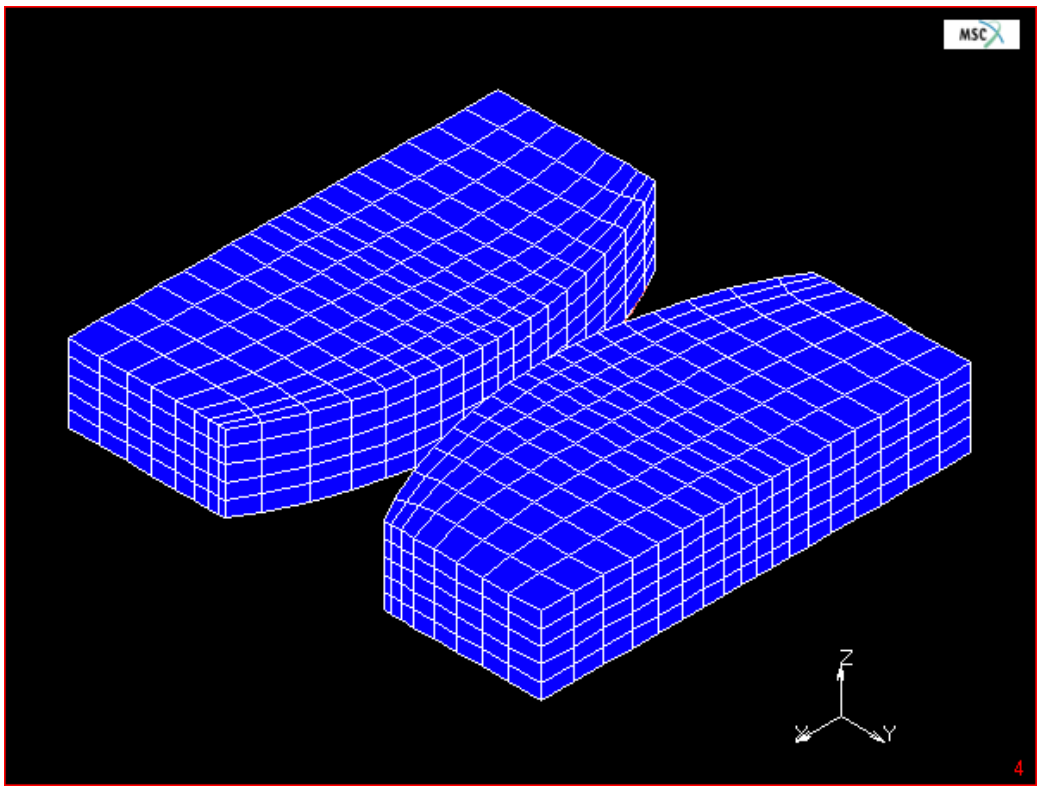

FIG. 5.18: Fingers without object.

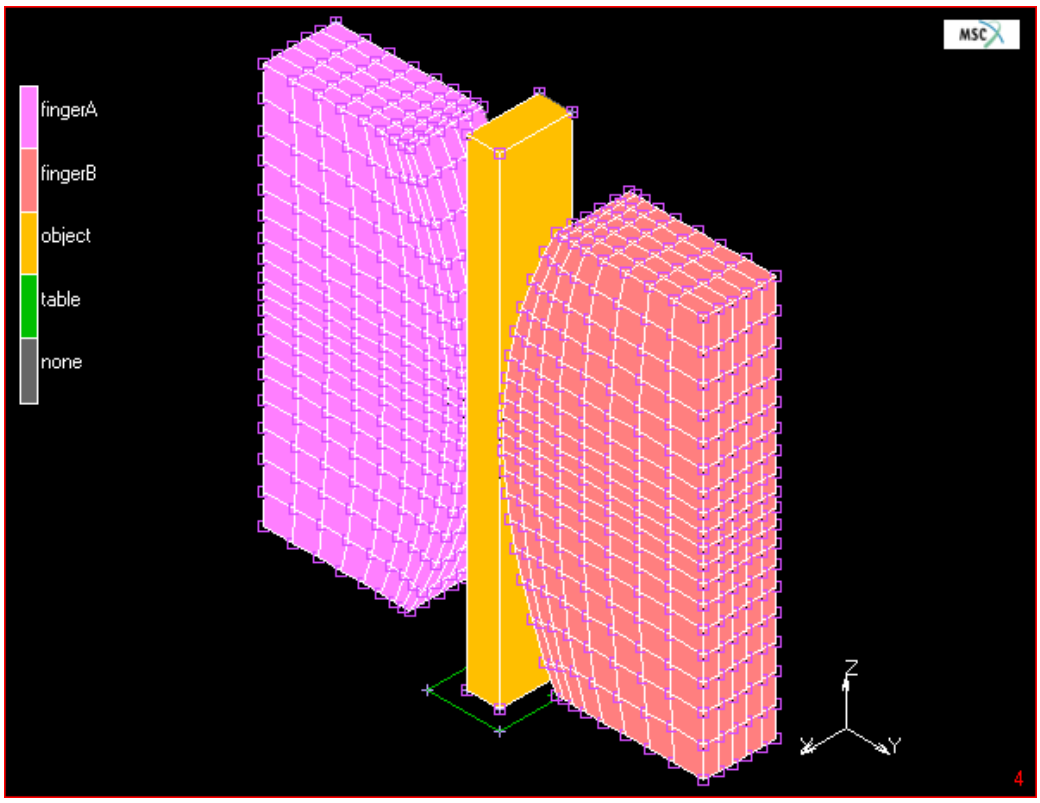

FIG. 5.19: Fingers with object at the initial state.

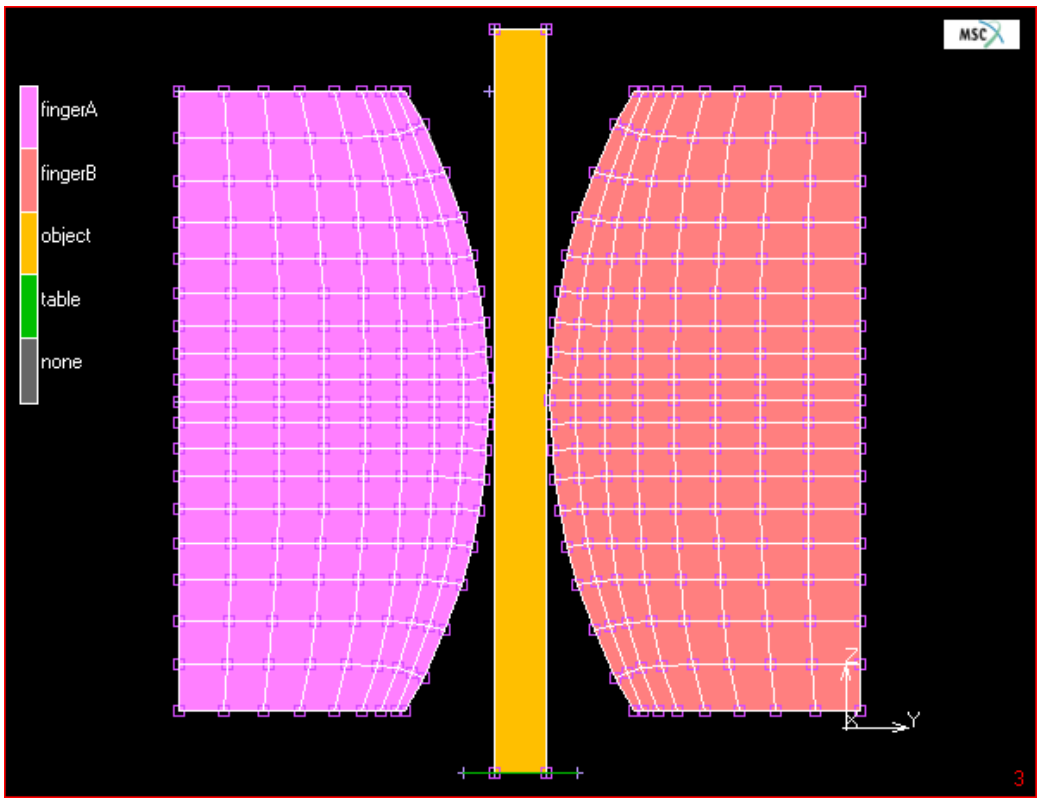

FIG. 5.20: Fingers with object at the initial state.

Nodes at the surface of the elastic finger should satisfy the following equations (adapted from Maeno et al. (2004)):

1. non contact nodes: $w_n \neq w_{nobject}, f_n = 0$
2. contact nodes: $w_n = w_{nobject}, f_n > 0$
3. sticking nodes: $w_t = w'_t + (w_{tobject} - w'_{tobject}), |f_t| < \mu |f_n|$
4. slipping nodes: $|f_t| = \mu |f_n|$

where, w_n and w_t are the nodal locations in the normal and tangential directions, f_n and f_t are the nodal forces in the normal and tangential directions, $w_{nobject}$ is the normal location of the object, $w_{tobject}$ is the tangential location of the object, and μ is the friction coefficient. Although the static friction coefficient is usually larger than the kinetic friction coefficient, these values are assumed the same in the fundamental calculations to simplify the argument. The prime represents values in the previous time frame.

When an incipient slip occurs at the preload phase, there are signals of the SA I and FA I mechanoreceptors (see section §2.8). The experiment to detect the incipient slip consisted of applying a normal force to grip the object, and then applying a load force to lift the object. The grip and load force were raised incrementally. The preceding equations were used to know if the nodes were sticking or slipping, and to know if the nodes were in contact with the object or not. The goal was to create an association between the state of the nodes at each force increment (i.e., number of sticking/slipping nodes, number of contact/non contact nodes) and the FA I and SA I responses. The FA II responses were not considered to calculate the incipient slip intensity, because the lift was done at a slow velocity and therefore FA II responses were not expected at the slip events.

The boundary conditions are shown in fig. 5.21. The object was restricted to move on the z-axis. The table was fixed in all axis. The initial position of the fingers and the object is shown in fig. 5.22. First, the displacement of the fingers was fixed on the x-axis and a grip force was applied (fig. 5.23). Afterwards, a vertical load force was applied. Depending on the friction coefficient of the object's material, when the same amount of grip and load force was applied on an object of the same weight, the object may lift off or not (fig. 5.24 and 5.25).

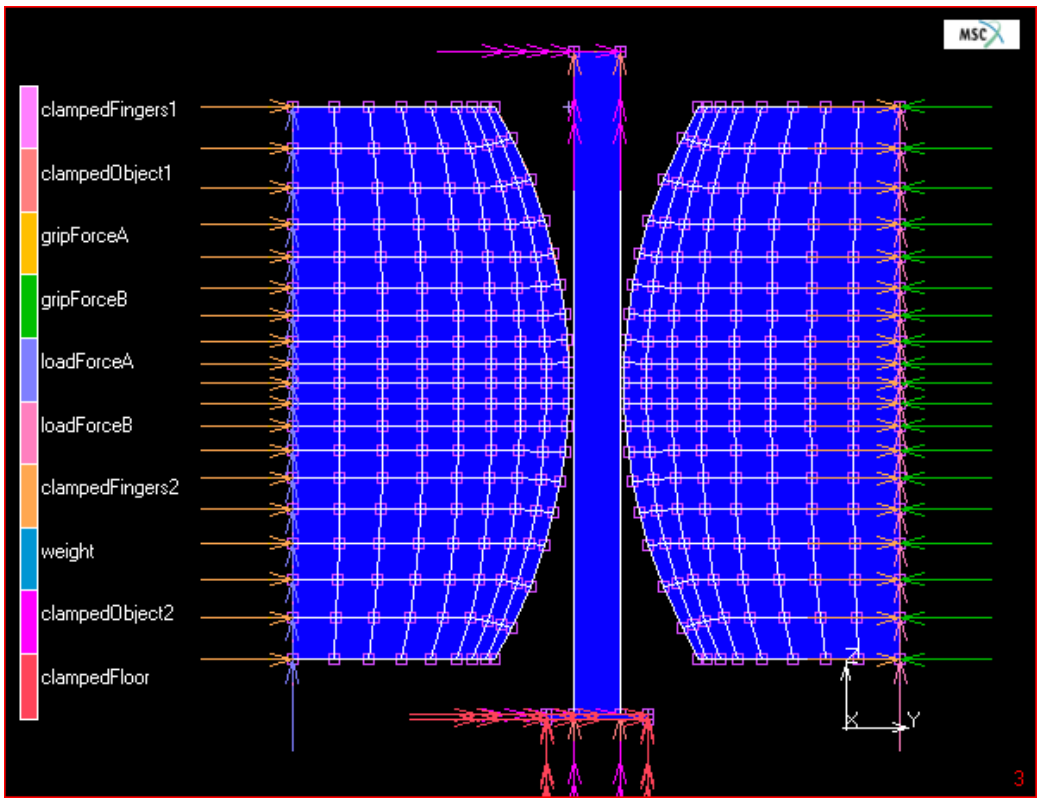

FIG. 5.21: Boundary conditions.

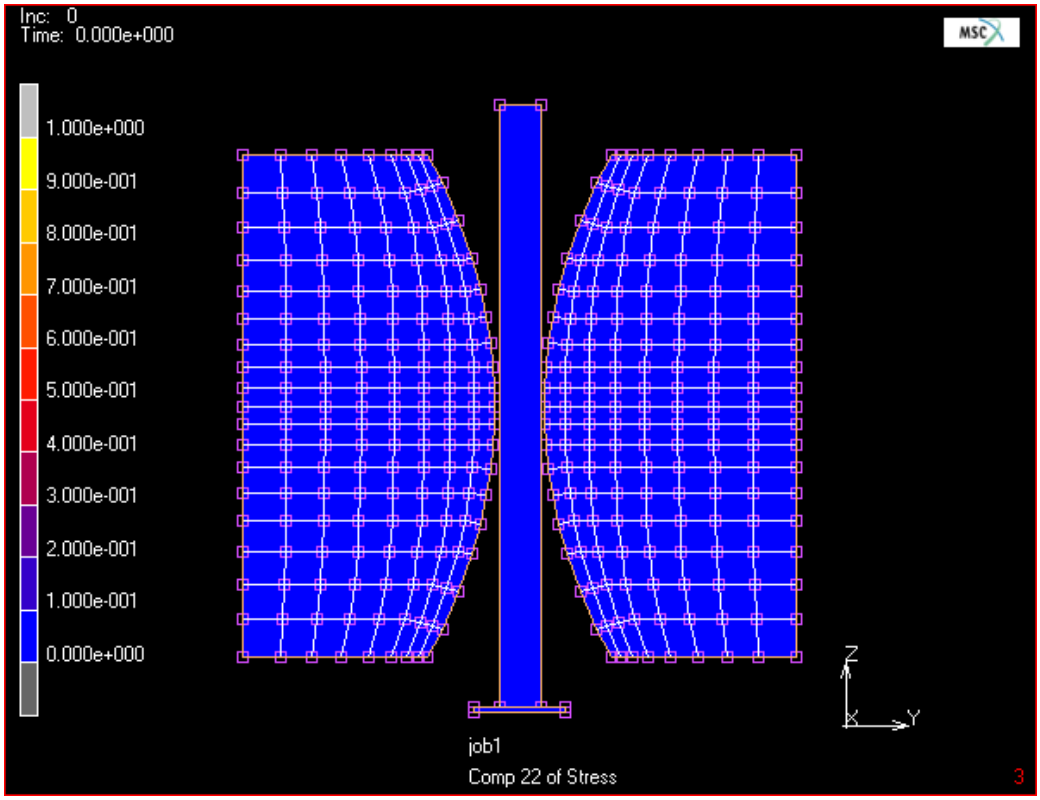

FIG. 5.22: Fingers with object at the initial state.

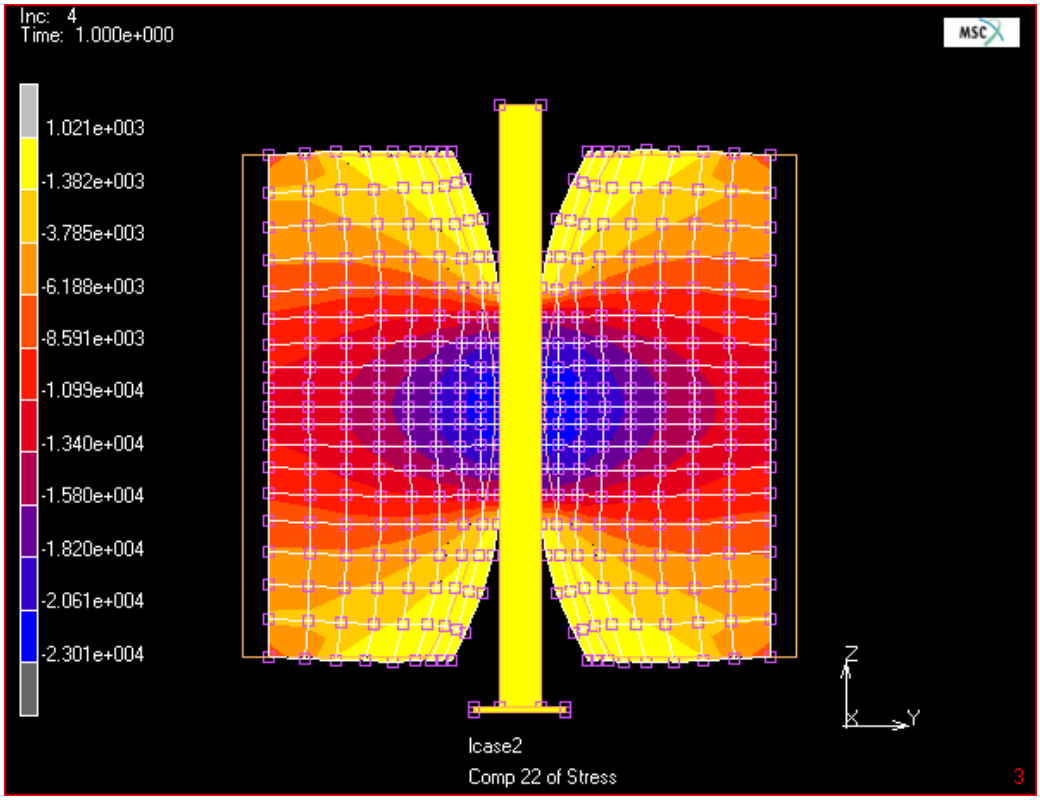

FIG. 5.23: Normal force contour bands of the fingers and the object after applying the grip force.

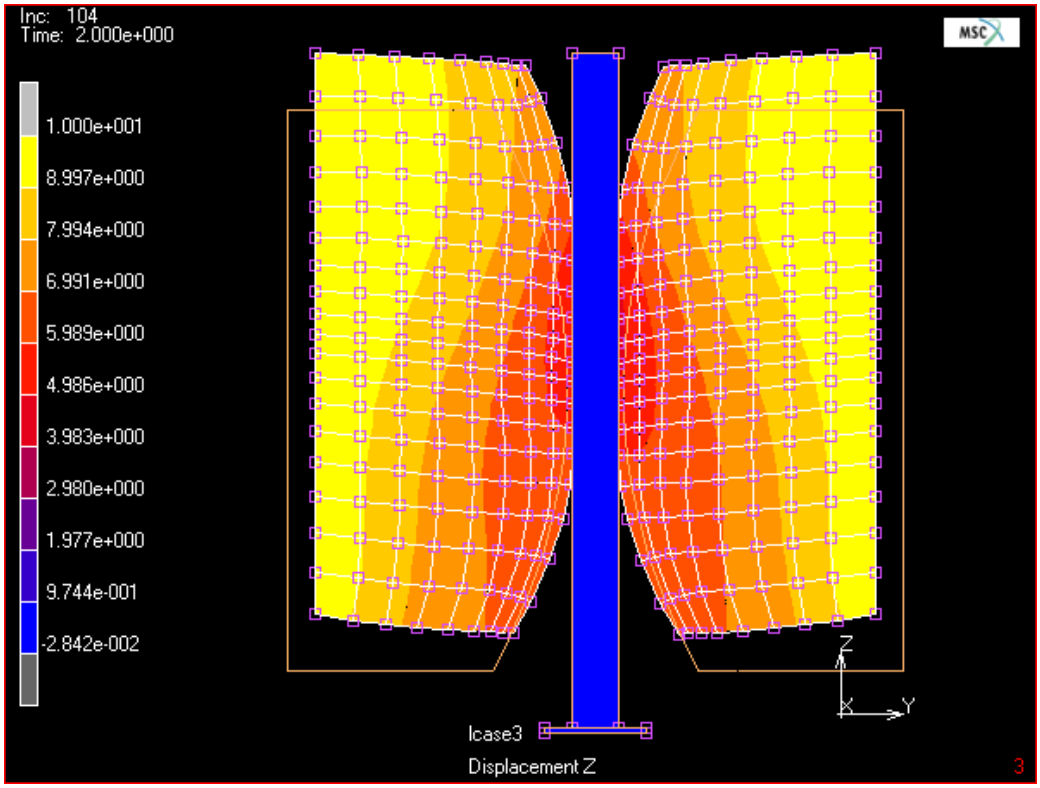

FIG. 5.24: Fingers with object at the final state after applying the grip and load forces. The friction coefficient is $\mu = 0.5$. The contour bands correspond to the total displacement on the Z-axis. The fingers have slipped and the object has not been lifted.

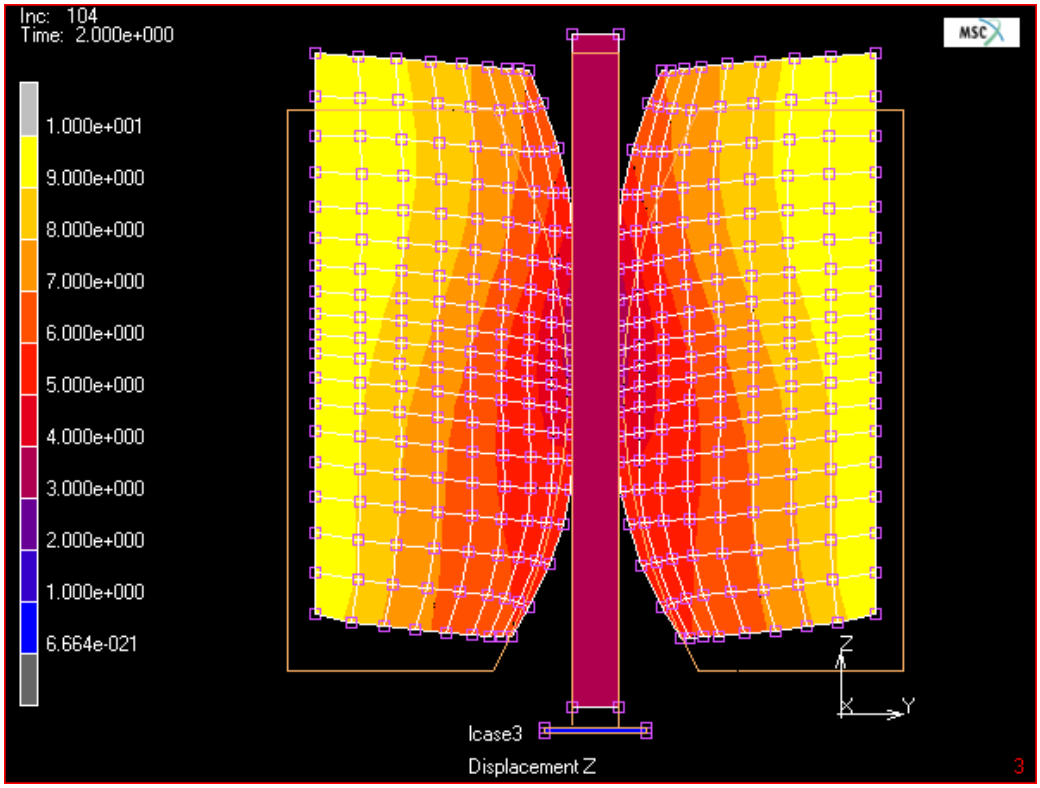

FIG. 5.25: Fingers with object at the final state after applying the grip and load forces. The friction coefficient is $\mu = 0.7$. The contour bands correspond to the total displacement on the Z-axis. The object has lifted off.

Due to the symmetry of the afferent responses, only the afferent responses of the 19 nodes situated along the central line at the front of the finger were recorded. The input patterns were built joining the FA I and SA I signals (i.e., a pattern of dimension 38 was obtained for each force increment). To build the target the number of contact nodes cn and slip nodes sn were counted, and the value $\frac{sn}{cn}$ was used as target (i.e., the proportion of contact nodes that were slipping). The patterns were preprocessed to normalize their mean and standard deviation in order to improve the performance of the training of the neural network. A multilayer perceptron was designed to associate the SA I and FA I patterns at each force increment, with the percentage of contact nodes that were slipping. It must be remarked that the input signal is a spike train, and the output, the percentage of contact nodes that were slipping, is represented as a continuous value into the interval $[0..1]$. The activation function in the hidden layer was chosen to be a sigmoidal function in the form of a hyperbolic tangent for its convenient antisymmetric property. The output layer activation function was chosen to be logsig, because the proportion of contact nodes that were slipping could only be a value into the interval $[0..1]$. For its fast convergence, the Levenberg-Marquardt algorithm was chosen as the minimization method to train the network. The following parameters were used: `epochs=100`, `show=5`, `goal=1e-5`, `time=Inf`, `min_grad=1e-10`, `mu=0.001`, `mu_dec=0.7`, `mu_inc=1.05`, `mu_max=1.04`, and `mem_reduc=1`.

Experiments with an object of weight 200 were made. Several simulated experiments were done changing the friction coefficient of the object from 0.50 to 0.90, and a total of 2100 input patterns were generated. A random partition of the input patterns set was done, in which the 90 percent of the patterns was chosen as training set and the remaining 10 percent as testing set. Multilayer perceptrons with different numbers of units in the hidden layer were trained and tested, and a multilayer perceptron with 1 hidden layer of 3 neurons obtained the best performance. Thus, the final architecture of the neural network consisted of an input layer of 38 units, a hidden layer of 3 units, and an output layer of 1 unit. The neural network was trained, and at the final state (46th. epoch), the mean squared error of the training set was 5.5617e-004 and its mean absolute error was 0.0135. The mean squared error of the testing set was 0.0016 and its mean absolute error was 0.0178. The performance for the training and testing sets is shown in Fig. 5.26. The regression analysis between the network response and the corresponding targets is shown in Fig. 5.27. The m and b correspond to the slope and the y-intercept of the best linear regression

relating targets to network outputs. In this picture the targets are discrete because they represent the percentage of contact nodes that were slipping. As only the afferent responses of 19 nodes were considered, the percentage of contact nodes that were slipping can only take 20 values as maximum.

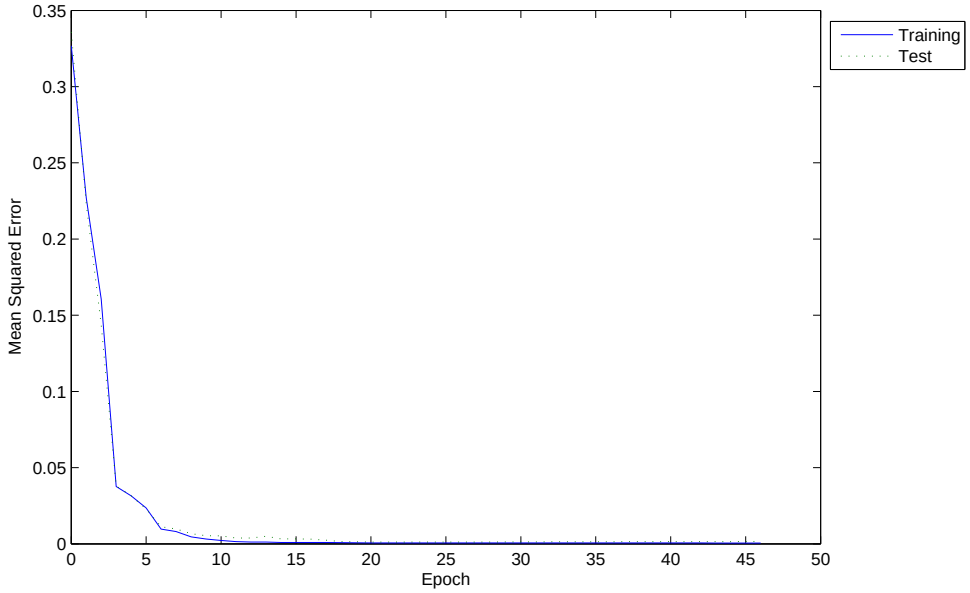

FIG. 5.26: Performance of the neural network.

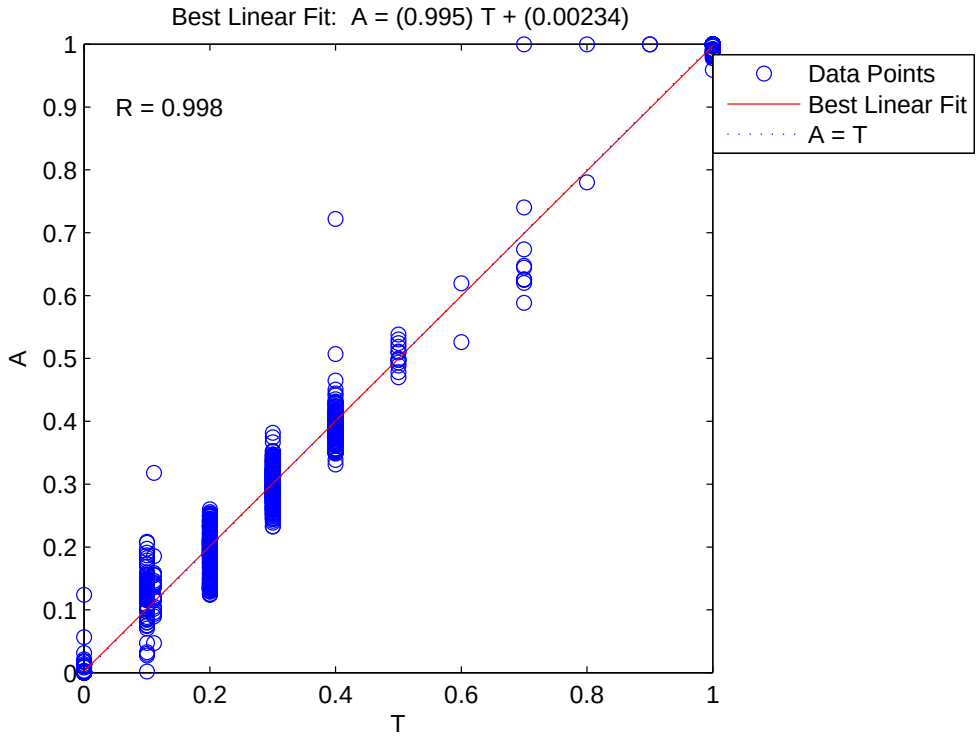

FIG. 5.27: Regression analysis corresponding to the incipient slip detection between the network response (A) and the corresponding targets (T). The best linear fit is indicated by a dashed line. The perfect fit (output equal to targets) is indicated by the solid line. In this figure is difficult to distinguish the best linear fit line from the perfect fit line because the fit is so good.

Fig. 5.28 shows a histogram of the percentage of slipping contact nodes. It is seen that the percentages are distributed mainly in the $[0\%, ..., 40\%]$ range, and the 100%. In the $[50\%, ..., 90\%]$ range there are only a few values. This result shows that 40% seems to be the maximum allowed value before the object starts to slide.

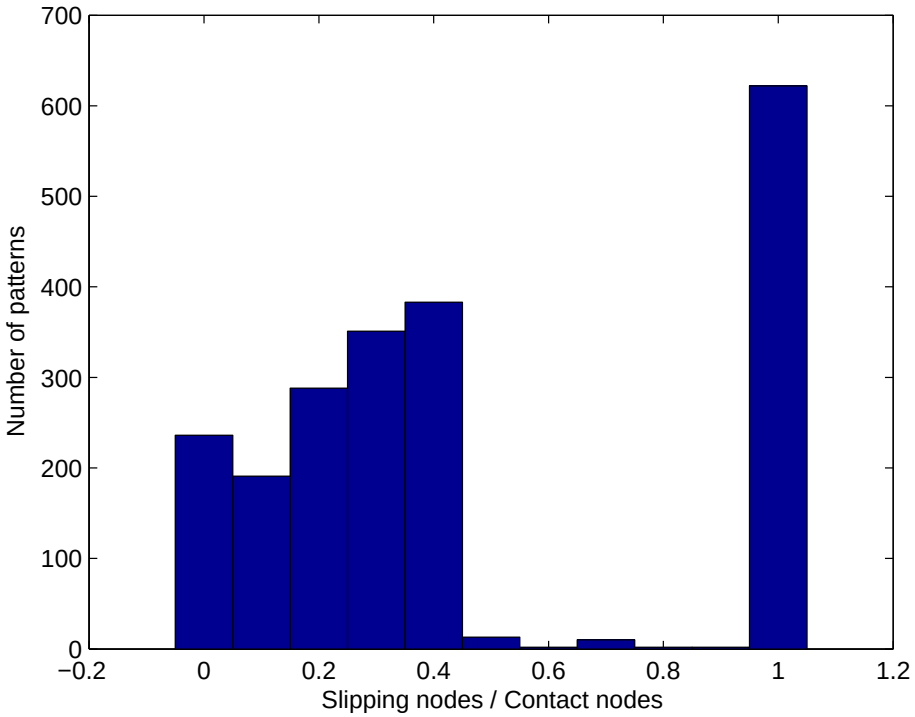

FIG. 5.28: Histogram of the percentage of slipping contact nodes for all the 2100 input patterns.

In order to analyze the relation between the proportion of slipping contact nodes and the grasp stability, the same grip:load force ratio was applied on an object of weight 200 changing the friction coefficient (fig. 5.29, 5.30 and 5.31). When $\mu = 0.5$ the object slid and did not lift off; when $\mu = 0.7$ or $\mu = 0.9$ the object lifted off (fig. 5.29).

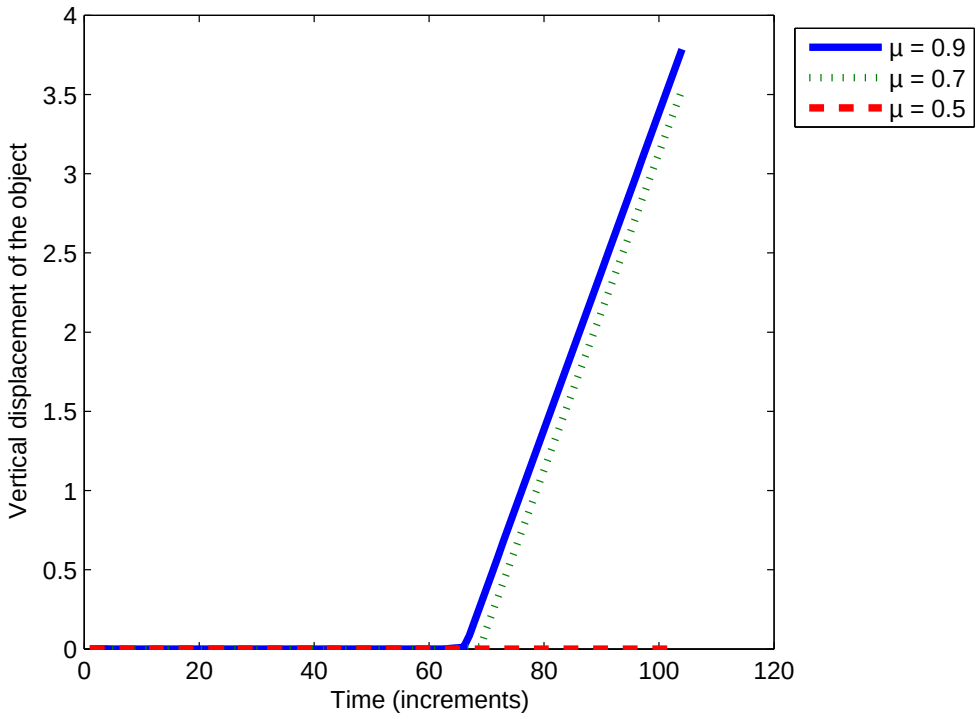

FIG. 5.29: Vertical displacement of an object of weight 200 for different μ when the same grip:load force ratio was applied.

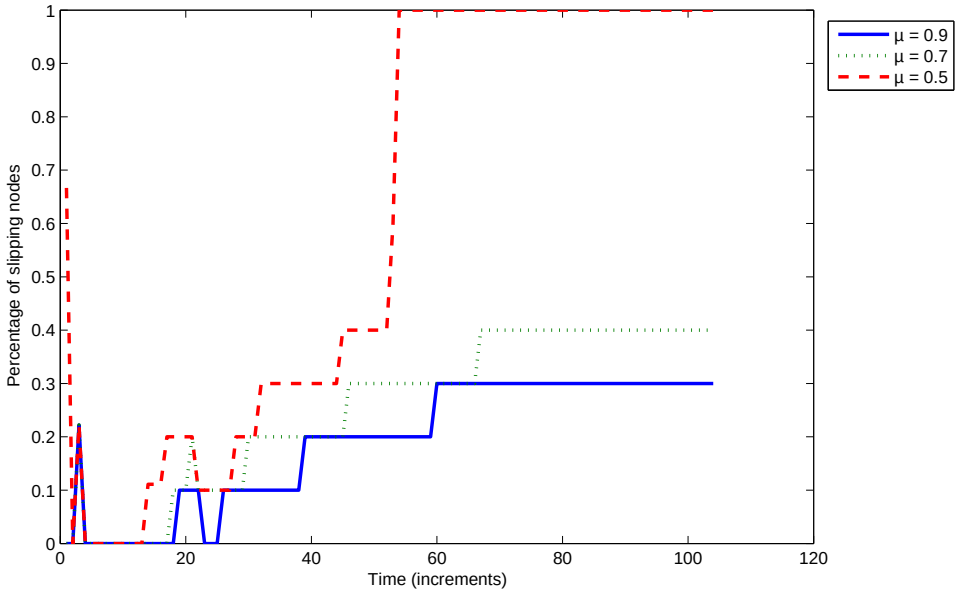

FIG. 5.30: Slipping nodes:contact nodes for different μ when the same grip:load force ratio was applied on an object of weight 200.

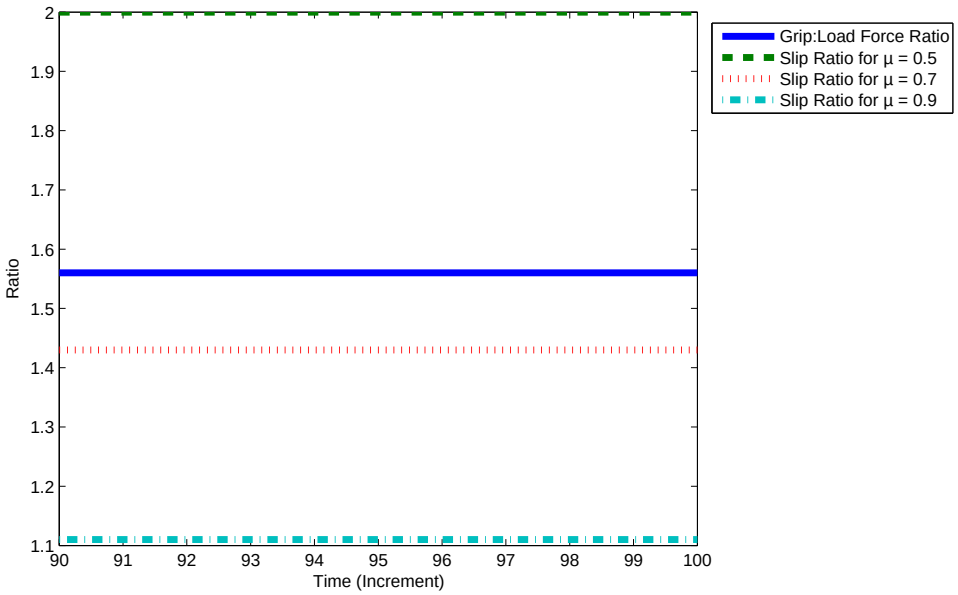

FIG. 5.31: Relation between the applied force ratio and the slip ratio for different μ when the same grip and load forces are applied on an object of weight 200.

5.4 Discussion

As changing the friction coefficient produces different shapes for the curves of the tangential forces (fig. 5.13 and 5.14), and the afferent answers are estimated based on values of these forces, it is expected to obtain different afferent answers for different friction coefficients. Therefore, it seems consistent a method that estimates the friction coefficient based on the afferent answers. At the friction estimation experiment, the neural network was trained with 180 patterns and tested with 20 patterns. At the final state, the mean squared error of the training set was 0.0025 and its mean absolute error was 0.0373. The mean squared error of the testing set was 0.0118 and its mean absolute error was 0.0853. As the maximum value of the target test set was 1.0, this result gives a relative error for the testing set of only 8.53%. The regression analysis between the network response and the corresponding targets is shown in fig. 5.16. The m and b correspond to the slope and the y-intercept of the best linear regression relating targets to network outputs. If there was a perfect fit (outputs exactly equal to targets), the slope would be 1, and the y-intercept would be 0. In fig. 5.16 it is seen that $m = 0.973$ and $b = 0.0145$ that are very close to 1 and 0 respectively. The R-value is the correlation coefficient between the outputs and targets. It is a measure of how well the variation in the output is explained by the targets. If this number is equal to 1, then there is a perfect correlation between targets and outputs. In fig. 5.16 it is seen that the R-value is 0.981, which is very close to 1 and indicates a good fit. As the input patterns were generated adding noise to the simulated afferent answer, this result shows a good performance for the friction coefficient estimation. We believe that this performance can be improved enlarging the set of input patterns used to train the neural network.

At the incipient slipping experiment, the final mean squared error of the test set was 0.0016 (Fig. 5.26). The mean absolute error of the test set was 0.0178. As the maximum value of the target test set was 1.0, this result gives a relative error for the testing set of only 1.78%. The regression analysis between the network response and the corresponding targets is shown in Fig. 5.27. In Fig. 5.27, it is seen that $m = 0.995$ and $b = 0.00234$ are very close to 1 and 0 respectively, and then the regression is very near to a perfect fit. The R-value is 0.998 that is very close to 1 and indicates a good fit.

To analyze the relation between the proportion of slipping contact nodes and the grasp stability, in Figs. 5.29, 5.31 and 5.30 we compare the effect of applying the same grip:load force ratio on an object of weight 200 for

different friction coefficients. When the material had a friction coefficient of value $\mu = 0.5$, the object slipped and it did not lift off. When the friction coefficient was enlarged (i.e., the object's material was less slippery) the object lifted off (Fig. 5.29). Analyzing the percentage of contact nodes that were slipping it is observed that when the friction coefficient was enlarged the percentage of slipping nodes decreased (Fig. 5.30). Comparing the grip:load force ratio with the slip ratio (slip ratio = $\frac{1}{\mu}$), it was seen that when the object did not lift off ($\mu = 0.5$), the force ratio was lesser than the slip ratio, and when the object lifted off ($\mu = 0.7$ and $\mu = 0.9$) the force ratio was greater than the slip ratio (fig. 5.31). These results are in accordance with the mechanical law that establishes that must be $|LF| < \mu|GF|$ for the object to lift off (see Sect. §2.2). Comparing Fig. 5.29 and Fig. 5.30 it is seen that when the percentage of slipping contact nodes is less or equal to 40% the object lifts off. On the other side, in Fig. 5.27 and 5.28 it is observed that the percentage of slipping nodes goes abruptly from 40% to 100%. These results show that 40% is the limit before the gross slip. Then, still an estimation of the percentage of slipping nodes without a perfect precision can be useful as the support of a grasp stability mechanism (i.e., if a 30% of slipping can be detected with a 10% of precision, a gross slip can be avoided). Therefore, as the proposed method estimates the incipient slipping with a relative error of only 1.78%, this result shows an excellent performance for the incipient slipping detection.

CHAPTER 6

CONCLUSIONS AND FUTURE WORK

6.1 Conclusions

Few years old children lift and manipulate unfamiliar objects more dexterously than today's robots. The aim of this thesis was to take inspiration in neurophysiological studies about the human dexterous manipulation, to design a computational control system for the dexterous manipulation in unknown environments. The architecture of the proposed control model is described in chapter four, and it is outlined in fig. 4.3. In section §4.10 algorithms were proposed for each one of the manipulation phases. The force ratio adjustments are driven by simulated human afferent signals. The proposed control model and algorithms were designed based on neurophysiological observations of the human dexterous manipulation.

Methods were proposed for the estimation of the friction coefficient and the percentage of contact nodes that are slipping. These methods follow closely the human way to detect the friction coefficient and to detect the incipient slip. Finite element analysis was used to simulate two 3-D fingers and planar objects of different friction coefficients. Artificial neural networks were used to estimate the friction coefficient and to detect the incipient slip, using as input simulated human afferent signals. The friction coefficient and the percentage of slipping nodes were estimated with very high precision. To the best of our knowledge, this is the first time that simulated human afferent signals are combined with finite element analysis and artificial neural networks, to estimate the friction coefficient and to detect the incipient slipping.

Figure 6.1 shows a global view of the force control in our model. First, the object is pressed following the algorithms of section §4.10. Next, simulated human afferent signals are generated. The friction coefficient is estimated with the method of section §5.2. It must be remarked, that the estimation of the friction coefficient is absolutely necessary. On one hand, humans estimate the friction coefficient with the initial responses of the FA-I afferents as seen in section §2.8, and we want to emulate the human way of manipulating objects very closely. On the other hand, this initial friction estimation is necessary to set an initial force ratio, and begin the parallel increase of the forces (see section §2.5). The parallel increase of the forces is done following the algorithms of section §4.10. Next, the incipient slipping is detected with the method of section §5.3. The force ratio is adjusted with the algorithms of section §4.10. As seen in fig. 6.1, the estimation of the friction coefficient and the detection of the incipient slipping are two crucial events that support our dexterous manipulation control model. Grasp stability, i.e., the prevention of accidental slips as well as of excessive fingertip forces, is a fundamental requirement in a dexterous manipulation process. Grasp stability is derived by tuned grip force and in humans is based on the detection of the incipient slips. In figure 6.1, it is clear that our model implies grasp stability. In figure 6.1, it is clear too that our model follows closely the neurophysiological studies of the human dexterous manipulation surveyed in chapter 2.

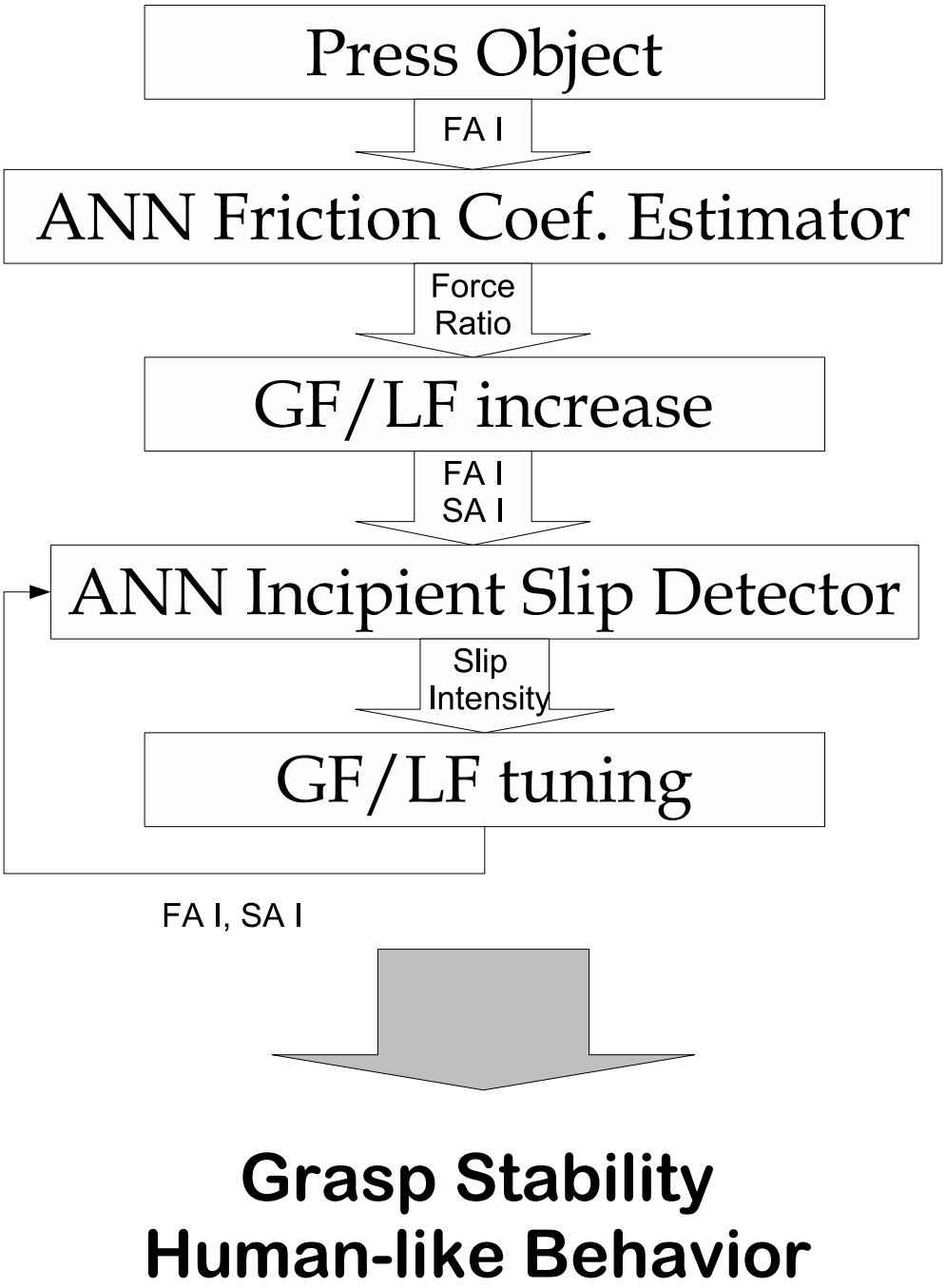

FIG. 6.1: A global view of the force control.

The conjunction between robotics and human neurophysiology can give fruitful and interesting results. The obtained results show that simulations of human afferent signals, can be used by artificial intelligence techniques to estimate the friction coefficient and to detect the incipient slipping with high precision. As shown by neurophysiological studies, these are crucial events for a dexterous manipulation process with grasp stability. Therefore, a control model architecture driven by simulated afferent signals like the one proposed in this work, seems to be a promising way to afford the dexterous manipulation problem in unknown environments.

6.2 Further work

The research that has been undertaken for this thesis has highlighted a number of topics on which further research would be beneficial.

The simulated experiments in chapter 5 have been made using objects with parallel flat sides. As seen in sections §2.12 and §4.4, the force ratio is influenced by the shape of the object. Thus, experiments with tapered objects of different angles would be illuminating.

Another important point is the torque with which the object has been taken. The simulated experiments in chapter 5 have been made taking the objects by its center of mass. As seen in section §2.11 a great amount of complexity is involved in the dexterous manipulation of objects with different torque loads. Adapting the proposed model, algorithms and methods to take objects with different torque loads is required to reach more flexibility.

An implementation of the proposed model and algorithms in a real robotic hand with miniaturized tactile sensors, will give insights about the robustness of the model under strong real time constraints. In particular, a future critical analysis is to study what are the most sensitive parameters of the proposed control algorithms presented in section §4.10, if there were simplest algorithms, and to see how the algorithms would perform under partial failure or ambiguous information.

The model and experiments have been designed for 'passive objects', i.e., mechanically predictable objects with a certain mass and mass distributions, and with stable viscous and elastic properties. However in everyday life, we may also interact with 'active abject', i.e., objects that are subjected to unpredictable external forces. This occurs when we, for example restrain a lively kid by holding her hand when taking a walk. Depend-

ing on whether object is 'active' or 'passive', the control of grasp stability is achieved by partly different mechanisms. Thus, an interesting future work is to extend the proposed model and algorithms to manipulate active objects.

BIBLIOGRAPHY

Bicchi, A. 2000. Hands for dexterous manipulation and robust grasping: a difficult road toward simplicity. *IEEE Transactions on robotics and automation* 6:652–662.

Bicchi, A, JK Salisbury, and D Brock. 1993. Experimental evaluation of friction characteristics with an articulated robotic hand. In *Exp. rob. ii*, ed. R Chatila and G Hirzinger. Springer-Verlag.

Birznieks, I. 2003. Tactile sensory control of dexterous manipulation in humans. Doctoral Dissertation, Department of Integrative Medical Biology, Physiology Section, Umeå University, Sweden.

Burstedt, MKO, I Birznieks, BB Edin, and R Johansson. 1997. Control of forces applied by individual fingers engaged in restraint of an active object. *Journal of Neurophysiology* 78:117–128.

Buss, M, H Hashimoto, and JB Moore. 1996. Dextrous hand grasping force optimization. *IEEE Transactions on Robotics and Automation* 12:406–418.

Cadoret, G, and Smith AM. 1996. Friction, not texture, dictates grip forces used during object manipulation. *Journal of Neurophysiology* 75:1963–1969.

Canepa, G., R. Petrigliano, M. Campanella, and D. Derossi. 1998. Detection of incipient object slippage by skin-like sensing and neural network processing. *IEEE Transactions on Systems, Man, and Cybernetics, Part B: Cybernetics* 28:348–356.

Cicchetti, A, A Eusebi, C Melchiorri, and G Vassura. 1995. An intrinsic tactile force sensor for robotic manipulation. In *Proc. 7th. Int. Conf. on Advanced Robotics, ICAR'95*.

Cole, KJ, and R Johansson. 1993. Friction in the digit-object interface scales the sensorimotor transformation for grip responses to pulling loads. *Exp Brain Res* 95:523–532.

Cole, KJ, D Rotella, and J Harper. 1999. Mechanisms for age.related changes of fingertip forces during precision grip and lifring in adults. *Journal of Neuroscience* 19:3238–3247.

Cutkosky, MR. 1985. *A mathematical introduction to robotic manipulation*. Kluwer Academic Publishers.

Dandekar, K, B Raju, and MA Srinivasan. 2003. 3-d finite-element models of human and monkey fingertips to investigate the mechanics of tactile sense. *Transactions of the ASME* 125:682–691.

Demuth, H, M Beale, and M Hagan. 2007. *Neural network toolbox 5 usert's guide*. The MathWorks, Inc.

Edin, BB. 1992. Quantitative analysis of static strain sensitivity in human mechanoreceptors from hairy skin. *Journal of Neurophysiology* 1105–1113.

Edin, BB, G Westling, and R Johansson. 1992. Independent control of fingertip forces at individual digits during precision lifting in humans. *Journal of Physiology* 450:547–564.

Elliott, JM, and K Junge. 1984. A classification of manipulative hand movements. *Developmental Medicine and Child Neurology* 26:283–296.

Fagergren, A. 2003. A multidisciplinary system identification of the human precision grip. Doctoral Dissertation, Karolinska Institutet, Stockholm.

Fagergren, A, O Ekeberg, and H Forssberg. 2003. Control strategies correcting inaccurately programmed fingertip forces: model predictions derived from human behavior. *Journal of Neurophysiology* 89:2904–2916.

Forssberg, H, AC Eliasson, H Kinoshita, RS Johansson, and G Westling. 1991. Development of human precision grip i: Basic coordination of force. *Exp Brain Res* 85:451–457.

Forssberg, H, AC Eliasson, H Kinoshita, G Westling, and RS Johansson. 1995. Development of human precision grip iv: Tactile adaptation of isometric finger forces to the frictional condition. *Exp Brain Res* 104:323–330.

Goodwin, AW, P Jenmalm, and Johansson RS. 1998. Control of grip force when tilting objects: effect of curvature of grasped surfaces and of applied tangential torque. *The Journal of Neuroscience* 18:10724–10734.

Gordon, A, H Forssberg, G Westling, and R Johansson. 1991. Integration of sensory information during the programming of precision grip: comments on the contributions of size cues. *Exp Brain Res* 85:226–229.

Gordon, A, G Westling, K Cole, and R Johansson. 1993. Memory representations underlying motor commands used during manipulation of common and novel objects. *Journal of Neurophysiology* 69:1789–1796.

Holweg, EGM, H Hoeve, W Jongkind, L Marconi, C Melchiorri, and C Bonivento. 1996. Slip detection by tactile sensors: Algorithms and experimental results. In *Proc. 1996 IEEE Int. Conf. Robotics and Automation*, ed. IEEE.

Hosoda, K, Y Tada, and M Asada. 2002. Internal representation of slip for a soft finger with vision and tactile sensors. In *Proc. 2002 IEEE International Conference on Intelligent Robots and Systems*.

Howe, RD, and MR Cutkosky. 1989. Sensing skin acceleration of slip and texture perception. In *Proc. IEEE Int. Conf. Robotics and Automation*, volume 1, 145–150.

Howe, RD, and MR Cutkosky. 1996. Practical force-motion models for sliding manipulation. *International Journal of Robotics Research* 15:557–572.

Israelsson, A. 2002. Simulation of responses in afferents from the glabrous skin during human manipulation. Master's thesis, Master thesis in Cognitive Science, Umeå University, Umeå, Sweden.

Jameson, JW. 1985. Analythic techniques for automated grasp. Doctoral Dissertation, Stanford University, Stanford, CA.

Jeannerod, M. 1997. Neural substrates for object-oriented actions. In *The cognitive neuroscience of action*, ed. M Jeannerod, 31–35. Blackwell Publisher.

Jenmalm, P. 1998. Control of grasp stability in man: Effects of objects' shape. Master's thesis, Department of Physiology, Umeå University, Umeå, Sweden.

Jenmalm, P. 2000. Dexterous manipulation in humans: Use of visual and tactile information about object shape in control of fingertip actions. Doctoral Dissertation, Department of Integrative Medical Biology, Physiology Section, Umeå University, Sweden.

Jenmalm, P, AW Goodwin, and R Johansson. 1998. Control of grasp stability when humans lift objects with different surface curvatures. *Journal of Neurophysiology* 79:1643–1652.

Jenmalm, P, and R Johansson. 1997. Visual and somatosensory information about object shape control manipulative fingertip forces. *The Journal of Neuroscience* 17:4486–4499.

Johansson, R. 1978. Tactile sensibility in the human hand: receptive field characteristics of mechanoreceptive units in the glabrous skin area. *Journal of Physiology* 281:101–123.

Johansson, R. 1996a. Sensory and memory information in the control of dexterous manipulation. In *Neural bases of motor behaviour*, 205–260. Kluwer Academic Publishers.

Johansson, R. 1996b. Sensory control of dexterous manipulation in humans. In *Hand and brain: The neurophysiology and psychology of hand movements*, ed. A Wing, P Haggard, and J Flanagan, 381–414. Academic Press.

Johansson, R, and BB Edin. 1993. Predictive feed-forward sensory control during grasping and manipulation in man. *Biomedical Research* 14:95–106.

Johansson, R, and G Westling. 1984a. Factors influencing the force control during precision grip. *Exp Brain Res* 53:277–284.

Johansson, R, and G Westling. 1984b. Influences of cutaneous sensory input on the motor coordination during precision manipulation. In *Somatosensory mechanisms*, ed. C von Euler, O Franze, U Lindblom, and D Ottoson, 249–260. Macmillan Press, London.

Johansson, R, and G Westling. 1984c. Roles of glabrous skin receptors and sensorimotor memory in automatic control of precision grip when lifting rougher or more slippery objects. *Exp Brain Res* 56:550–564.

Johansson, R, and G Westling. 1987. Signals in tactile afferents from the fingers eliciting adaptive motor responses during precision grip. *Exp Brain Res* 66:141–154.

Johansson, R, and G Westling. 1988a. Coordinated isometric muscle commands adequately and erroneously programmed for the weight during lifting task with precision grip. *Exp Brain Res* 71:59–71.

Johansson, R, and G Westling. 1988b. Programmed and triggered actions to rapid load changes during precision grip. *Exp Brain Res* 71:72–86.

Johansson, R, and G Westling. 1990. Tactile afferent signals in the control of precision grip. In *Attention and performance*, ed. M Jeannerod, volume XIII, 677–713. Erlbaum, Hilldale, NJ.

Johansson, RS. 1998. Sensory input and control of grip. In *Sensory guidance of movement*, ed. Novartis Foundation Symposium 218, 45–59. Wiley & Sons, Chichester.

Johansson, RS, JL Backlin, and MKO Burstedt. 1999. Control of grasp stability during pronation and supination movements. *Experimental Brain Research* 128:20–30.

Johansson, RS, and KJ Cole. 1992. Sensory-motor coordination during grasping and manipulative actions. *Current Opinion in Neurobiology* 2:815–823.

Johansson, RS, and BB Edin. 1992. Mechanisms for grasp control. *Restoration of Walking for Paraplegics Recent advancements and trends* 57–63.

Johansson, RS, and AB Vallbo. 1979. Tactile sensibility in the human hand: relative and absolute densities of four types of mechanoreceptive units in glabrous skin. *J Physiol (London)* 286:283–300.

Johnson, K. 2001. The roles and functions of cutaneous mechanoreceptors. *Curr Opin Neurobiol* 11:455–461.

Kinoshita, H, L Bäckström, JR Flanagan, and RS Johansson. 1997. Tangential torque effects on the control of grip forces when holding objects with a precision grip. *Journal of Neurophysiology* 78:1619–1630.

Kinoshita, H, K Ikuta, S Kawai, and M Udo. 1993. Effects of lifting speed and height on the regulation of forces during lifting tasks using a precision grip. *Journal of Human Movement Studies* 25:151–175.

Lee, M.H. 2000. Tactile sensing: new directions, new challenges. *The International Journal of Robotics Research* 19:636–43.

Macefield, V, C Häger-Ross, and R Johansson. 1996. Control of grip force during restraint of an object held between finger and thumb: responses of cutaneous afferents from the digits. *Exp Brain Res* 108:155–171.

Maeno, T, S Hiromitsu, and T Kawai. 2000. Control of grasping by detecting stick/slip distribution at the curved surface at an elastic finger. In *Proc. IEEE International Conference on Robotics and Automation*, 3896–3901.

Maeno, T, T Kawai, and K Kobayashi. 1998. Analysis and design of a tactile sensor detecting strain distribution inside an elastic finger. In *Proc. IEEE/RSJ International Conference on Intelligent Robotics Systems*, 1658–1663.

Maeno, T, T Kawamura, and S Cheng. 2004. Friction estimation by pressing an elastic finger-shaped sensor against a surface. *IEEE Transactions on Robotics and Automation* 20:222–228.

Melchiorri, C. 2000. Slip detection and control using tactile and force sensors. *IEEE Trans. on Mechatronics, Special Issue on Advanced Sensors for Robotics* 5:235–243.

Murray, RN, Z Li, and SS Sastry. 1994. *A mathematical introduction to robotic manipulation*. CRC Press, Inc.

North, JF, and F Gibson. 1978. Volume compressibility of human abdominal skin. *J. Biomech.* 203–207.

Pfeifer, R, M Lungarella, and F Iida. 2007. Self-organization, embodiment, and biologically inspired robotics. *Science* 318:1088–1093.

Purves, D, G Augustine, D Fitzpatrick, L Katz, A-S LaMantia, and J McNamara. 1997. *Neuroscience*. Sinauer Associates.

Shinoda, H, S Sasaki, and K Nakamura. 2000. Instantaneous evaluation of friction based on artc tactile sensor. In *Proc. IEEE Int. Conf. on Robotics and Automation*, 2173–2178.

Smith, AM. 1993. Some shear facts and pure friction related to roughness discrimination and the cutaneous control of grasping. *Can J Physiol Pharmacol* 72:583–590.

Spong, MW, FL Lewis, and CT Abdallah, ed. 1993. *Robot control: Dynamics, motion planning and analysis*. IEEE Press.

Srinivasan, MA, RJ Gulati, and K Dandekar. 1992. In vivo compressibility of the human fingertip. *Adv. Bioeng.* 573–576.

Tegin, J, and J Wikander. 2005. Tactile sensing in intelligent robotic manipulation Ű a review. *Industrial Robot: An International Journal* 32:64Ű–70.

Tremblay, MR, and MR Cutkosky. 1993. Estimation friction using incipient slip sensing during a manipulation task. In *Proc. IEEE Int. Conf. Robotics Automation*, volume 1, 429–434.

Turrell, Y. 2000. Grip force adjustments in collisions. Doctoral Dissertation, University of Birmingham.

Vossoughi, J, and RN Vaishnav. 1979. Comments on the paper 'volume compressibility of human abdominal skin'. *J. Biomech.* 481.

Werremeyer, M, and K Cole. 1997. Wrist action affects precision grip force. *Journal of Neurophysiology* 78:271–280.

Westling, G, and R Johansson. 1987. Responses in glabrous skin mechanoreceptors during precision grip in humans. *Exp Brain Res* 66:128–140.

Wing, A. 1996. Anticipatory control of grip force in rapid arm movement. In *Hand and brain: The neurophysiology and psychology of hand movements*, ed. A Wing, P Haggard, and J Flanagan, 301–324. Academic Press.